The Simulation of the Effect of Rigid Bank Vegetation on the Main Channel Flow

Mohammad Hosein Masouminia

Submitted to the
Institute of Graduate Studies and Research
in partial fulfillment of the requirements for the degree of

Master of Science
in
Civil Engineering

Eastern Mediterranean University
September 2015
Gazimağusa, North Cyprus

Approval of the Institute of Graduate Studies and Research

_____
Prof. Dr. Serhan Çiftçioğlu
Acting Director

I certify that this thesis satisfies the requirements as a thesis for the degree of Master of Science in Civil Engineering.

_____
Prof. Dr. Özgür Eren
Chair, Department of Civil Engineering

We certify that we have read this thesis and that in our opinion it is fully adequate in scope and quality as a thesis for the degree of Master of Science in Civil Engineering.

_____
Assoc. Prof. Dr. Umut Türker
Supervisor

Examining Committee
_____

1. Assoc. Prof. Dr. Mustafa Ergil   _____

2. Assoc. Prof. Dr. Umut Türker   _____

3. Asst. Prof. Dr. Bertuğ Akıntuğ   _____

ABSTRACT

A series of computational hydraulic analyses are applied for the open channels with vertical and inclined banks. During the analyses, riverbank vegetation density on inclined surface were increased to measure the flow hydrodynamic effects of the flow for both, in the inclined riverbank and main channel. The study not only covers the relationship of open channel with vegetated bank, and also proves some of the previous determined results. Additionally, the gathered results illustrate the impacts of vegetation density on riverbank to the entire channel. The longitudinal velocity, turbulence intensity (TI), turbulent kinetic energy and Reynolds stress were presented by figures, to help the outcomes of the results be more readable. The preliminary results are presented in terms of plots, based on the mean velocity along the main flow directon across the channel for ease of comparison between different configurations. The main outcome of the study despicts that, as the river bank vegetation density increases, the mean velocity in the main channel increases, while mean velocity on the river bank decreases. Reynolds stress is an essential part of shear stress in turbulent flows, and the measured Reynolds stresses show that, the stress is higher near bed of the main channel close to the vertical riverbank whereas it shifts to mid flow depths at the region close to the interface of main channel and the inclined riverbank. The turbulence intensity and the turbulence kinetic energy profiles were also showing similarity and parallel behavior with the simulated results of streamwise flow velocities and Reynolds stresses in the main channel and at the inclined riverbank.

Keywords: Velocity profile, Reynolds shear stress, Vegetation, Turbulence intensity, Secondary current, Turbulent kinetic energy.

ÖZ

Bir kenarı dik diğer kenarı ise eğimli şev olan açık kanal sisteminde bir dizi nümerik hesaplamalar gerçekleştirilmiştir. Ana kanal içerisindeki hidrodinamik hareketlerin davranışını inceleme amaçlı yapılan bu çalışmada eğimli kenar üzerine rijid elemanlar yerleştirilerek yapay bitki örtüsü yaratılmış ve bu bitki örtüsünün yoğunluğu sürekli artırılmıştır. Açık kanal kenarında yerleştirilen bitkilerin ana kanal içerisindeki etkileri üzerine daha önce deneysel olarak yapılan çalışmaları nümerik olarak modelleme ve etkileri daha detaylı gözlemleme şansı bulunmuştur. Boyuna hız, türbülans yoğunluğu (TI), çalkantılı kinetik enerji ve Reynolds gerilme sonuçları modellenmiş ve çıktılar şekiller aracılığı ile daha okunabilir hale getirilmiştir. Ilk sonuçlar kanal genelinde akım hız profillerinin çıkartılması ve bu profillerin farklı bitki örtüsü yoğunluklarında uğradıkları farklılıkları inceleme amaçlı kullanılmıştır. Ana kanal içerisinde hız profilleri artarken, eğimli kenar yüzeyleri ile bu yüzeylerin kanal ile yaptığı birleşme noktalarında akım hızı azalma göstermiştir. Reynolds gerilmeleri türbülanslı akımlarda kayma gerilmesi tanımlamaları için önem arzetmektedir. Sonuçlar göstermiştir ki ana kanal içerisinde maksimum gerilmeler tabana yakın bölgelerde meydana gelirken, eğimli kenara yaklaşıldığı durumlarda maksimum gerilmeler akım derinliğinin ortalarına doğru kaymaktadır. Türbülans yoğunluğu ve çalkantılı kinetik enerji profilleri akım içerisindeki hız ve gerilme dağılımlarını destekleyen sonuçlar vermiştir.

Anahtar Kelimeler: Hız profili, Reynolds kayma gerilmesi, Bitki Örtüsü, Türbülans şiddeti, İkincil akım, Çalkantılı kinetik enerji

To Whom I Love the Most

ACKNOWLEDGEMENT

At first, I wish to convey my gratitude to the Department of Civil Engineering for providing the facilities, especially research computers laboratory through the study at Eastern Mediterranean University.

I would like to express my sincerest gratitude to Associate Professor Dr. Umut Turker, for his guidance, advice, and supervision from the beginning stage of this thesis.

Last but not the least, my honest acknowledgments are addressed to my family. I am grateful to my dad, Naser, for providing all I ever wanted or dreamed and his constant inspiration and guidance kept me on my way and also motivated me. It is beyond my power to express my gratitude to my mom, Sedigheh, in words, whose unconditioned love has been my ultimate strength. The endless love and support of my elder sister, Maryam, his husband, Behnam, and their child Baran are sincerely acknowledged. I convey special acknowledgement to my younger sister, Mahtab, who always cares and pushes me to be best of myself. I would like to dedicate this thesis to my family, for being the most important ones in my entire life.

TABLE OF CONTENTS

LIST OF TABLES

LIST OF FIGURES

xv

LIST OF SYMBOLS/ABBREVIATIONS

Symbol	Unit	Property
L	m	Length scale
B	---	Integration constant
B_s	---	Integration constant
C_{TKE}	---	Turbulent kinetic energy constant
D	m	Diameter of the constant cylindrical element
F	---	Blending function
k	m^2/s^2	Turbulence kinetic energy per unit of density
K_s	m	Roughness height
n	$s/m^{1/3}$	Gauckler–Manning coefficient
p	Pa	Peressure
P_k	---	Turbulence production
p_m	Pa	Modified pressure
S	m	Distance between two individual elements
S_r	---	Invariant measure of the strain rate
T	s	Sample time
t	s	The time
TI	---	The turbulence intensity
TKE	N/m^2 , Pa	Turbulent kinetic energy
Tr	---	Transpose operation
U	m/s	Time averaged velocity
u, v, w	m/s	Velocity components in X, Y, Z direction

u_*	m/s	Shear velocity
u'	m/s	Represent fluctuating velocity
$\bar{u}$	m/s	Represent the time average of the velocity
wk	---	The wake function
y	m	Vertical distance
y_0	m	Hypotetical bed level
Δt	s	Physical time step
δ	---	The kronecker delta (δij = 1 if i=j; δij = 0 if i≠j)
ζ	---	The normalized distance from the bed
η	---	Vegetation porosity
κ	---	The von-Karman constant
λ	m^{-1}	Vegetation density
μ	kg/sm	Dynamic viscosity
μ_{eff}	kg/sm	Effective dynamic viscosity
μ_t	kg/sm	Dynamic eddy viscosity
ρ	kg/m^2	Fluid density
σ_k, β'	---	Constants in k-equation
$\sigma_\omega, \alpha, \beta$	---	Constants in ω-equation
τ	$kg/ms^2, Pa$	Shear stress
υ	m^2/s	Kinematic viscosity
υ_T	m^2/s	Kinematic eddy viscosity
φ	---	Solid volume fraction
ω	s^{-1}	Turbulent frequency
Π	---	The Coles wave strength constant

CAE	---	Computer-aided engineering
CFD	---	Computational fluid dynamics
LES	---	Large eddy simulation
RANS	---	Reynolds Averaged Navier-Stokes
RMS	---	Root Mean Square
SST	---	Shear stress transport
TKE	---	Turbulent kinetic energy

Chapter 1

INTRODUCTION

1.1 Background, Definition of the Problem

Vegetation along open channels like rivers, streams and creeks always disturbs the flow direction, speed and behavior. As a result, they have the ability to change the hydraulic properties and morphodynamics of open channels. For this reason, the effect of vegetation cover along the river bed and bank or at bay shores is an important engineering problem and is always required for the calibration and validation of river hydraulic models.

For many years before, vegetation is defined by their effects on resistance forces and the friction in main channel which causing decrease in the channel discharge capacity and increase of the water depth (Liu, Diplas, Fairbanks, & Hodges, 2008). Hence to overcome these weaknesses they have been removed. However, in recent decades, their benefits likes controlling erosion and stream recovery were observed (Simon, Bennett, & Neary, 2004). For example, they have reduction effect on flow turbidity and erosion, they are stabilizing the river bank and giving new nutrition habitat for wildlife. They as well reduce the water pollution by providing oxygen due turbulence (Liu et al., 2008).

Recently, there has been increasing interest and research in bank vegetation management of rivers for a wide range of civil, water resource and ecological engineering

activities. In areas where flow occurs through either submerged or emergent vegetation cover at the bank of the rivers, the properties of the flow are mainly defined by the density and rigidity of the vegetation as well as the depth and velocity of the bank flow.

The vegetation along the main channel of the rivers consumes the energy and momentum of the flow and generally believed that it slowdowns the flow properties. On the other hand, recently, researchers found out that the effect of bank vegetation is not similar to the effects of main channel vegetation. The argument that vegetated banks significantly increase the main channel flow is based mostly on the momentum transfer issue within the main channel and the bank. Nevertheless, while these new arguments at river banks may or may not affect the flow in the main channel, several laboratory studies (Valyrakis, Liu, Mcgann, Turker, & Yagci, 2015) were already performed to initiate the early works regarding to the above argument. In all such studies, the effect of bank vegetation on streamwise velocity, turbulence intensity, turbulence kinetic energy and Reynolds shear stresses were evaluated and analyzed.

So, as recommended the concept of bank vegetation and its effects on main channel flow properties must be developed and several more studies should be carried out in order to understand and clarify the concept of hydraulics.

1.2 The Study Context

This study is conducted at Eastern Mediterranean University. The tools used in this study are the detailed research studies and results of work presented at 36th IAHR World Congress, titled: "Characterizing the effect of increasing riverbank vegetation

on the flow field across the channel", Computational Fluid Dynamics module of AN-SYS software, and the computer laboratory of the Civil Engineering Department of Eastern Mediterranean University. The study, presented at the 36th IAHR World Congress was conducted at the University of Glasgow Water Engineering Laboratory. The supervisor of this thesis was one of the members of the team of laboratory works and analyses of the results. Therefore, most of the details of that study are used in this thesis in order to extend the research studies on bank vegetation one more step.

1.3 Aims and Objectives of the Research

The main goal of this study is to quantify the changes of mean streamwise velocity, stresses, turbulence intensity, turbulent kinetic energy and the secondary currents across a main channel while increasing the density of the riverbank vegetation. The vegetation density will be altered gradually by increasing the number of individual vegetation elements. The change in the pattern of the vegetation will be either staggered or linear to cover a range of representative vegetation densities found naturally in considering environments. This aim will be achieved by using computer based software called ANSYS. The open channel was modelled and different runs were achieved with the help of a computational fluid dynamics module. The results of the computer based study was compared with the results of laboratory works to ensure that the outcomes of the model were reliable.

The computational approach will help to bring the analysis down to a more fundamental level. The previous investigations done on bank vegetation by laboratory studies resulted in a series of relationships with only a very limited range of application and data gathering (e.g. lack of data computing for different physical behaviors simultaneously). However, the modelling in software will help to extend the findings of the

research, such as observing the necessary parameters not point by point but all along the cross-section of the channel.

1.4 Research Questions

The research mainly goes over the following questions:

"What is the effect of bank vegetation on the … in the main channel?"

- Streamwise velocity

- Reynolds shear stresses

- Turbulence intensities

- Turbulence kinetic energy

- Secondary current

1.5 The Proposed Methodology

Within the scope of this study, in order to reach reliable, accurate and physically possible results, the main methodology is proposed as a quantitative study. This was because the objectives and aims of the study were specific and previously well defined by other studies. Putting out the quantitative answers of research questions through mathematical and numerical approaches with the help of computer based software and comparing the results with previous laboratory based measurements were specific and well defined.

The method of works initiated with designing the open channel that will be used for the analysis of the work. The channel was reflecting the mainstream and its bank as similar as the one used in laboratory studies at the University of Glasgow. The width, length and slope of the channel, the slope of the bank were all fixed and then the water depth and underlying sand properties were arranged accordingly.

Later, the ambient flow conditions were performed to match the hydraulic properties of the model with the laboratory model. Next step was to increase the cylindrical vegetation elements gradually, and observe the changes in the hydraulic properties of the main channel flow.

All the necessary hydraulic parameters like streamwise velocity, turbulence intensity, turbulence kinetic energy and Reynolds shear stresses were evaluated, plotted, analyzed and discussed.

The methodology of the study is summarized in Figure 1.1. The flow chart shows the order of the process and clearly, delineates the decision making steps.
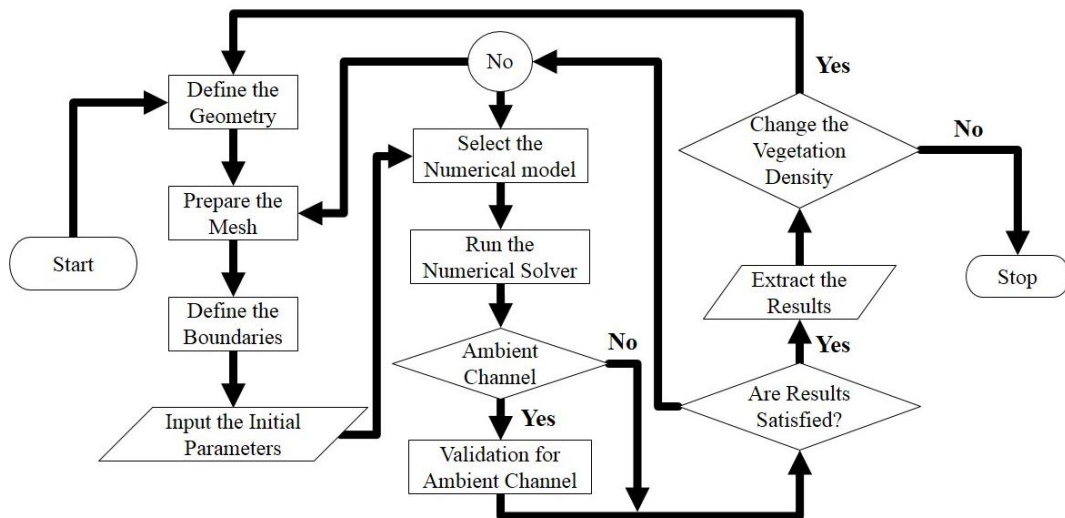
Figure 1.1: Methodology Flow Chart

1.6 Outline of the Study

This study consists of five different chapters. The first part is the introduction where the objectives of the study, information about the contribution of the research to the literature, and target methodology are presented. In the second chapter, the explanation of fundamentals of hydraulics in open channels is discussed. Chapter 3 is consisting

of information about the methodology, sampling issues, initial conditions, numerical calculations, and assumptions. Chapter 4 goes over validating the model with experimental data and the results of the study by focusing on the streamwise velocity, Reynolds shear stress, turbulence intensity and turbulent kinetic energy; and also discussion of the findings is brought in this chapter. The final chapter contains the conclusions and recommendation for further studies.

1.7 Limitations of the Study

There exist several limitations, drawing clear boundaries for the model study. The first one is related to the property of the vegetation cover; and that is the rigidity of the elements, allowing zero flexibility under the action of drag forces. The second limitation was the size of the vegetation elements; and that is the emergent vegetation property in which all the vegetation elements were extended far above the water surface in the channel. The third was the cross section of the channel; the bank slope, main channel width. The width occupied by the vegetation cover was always constant and was never altered.

Regarding to the hydraulics of flow, the flow discharge was kept constant to reach the uniform flow, where no incipient sediment motion within the channel was observed. This was one of the main limitations for assuring constant discharge everywhere within the main channel.

The accuracy and time management of each run of simulation was also the limitation of the work. These two limitations were mainly based on the computer's random memory (RAM) and the speed of central processing unit (CPU). The capacity of the RAM was effective on the total number of nodes that is needed for meshing, and the

CPU strength was directly related to the simulation time. Also, it should be noted that while increasing the number of vegetation cover, the number of nodes were increasing. This further increases the time necessity to calculate the required parameters at these nodes.

1.8 Literature Review

1.8.1 Hydrodynamics of Vegetation

When flow passes through vegetation, flow characteristics are changing. The drag forces and Young's modulus cause the stem of vegetation to change its location via bending or vibrating. On the other hand, depending on the roughness and shape of the body and the configuration of the population of vegetation, the drag force changes which will change the velocity around them. Shape, rigidity, configuration and the height of the vegetation cover have significant effect on the flow properties.

The vegetation changes the flow structure and the sediment transport and act as a treatment facility by helping to purify the polluted water and maintain a good environment.

The physical interaction of vegetation with water is usually considered at three different positions. Sometimes the height of the vegetation is above the water surface and the stem of the plant has totally interfered to the velocity profile. These vegetation is, generally, considered as "emergent vegetation" (Nepf, 1999).

Another type of vegetation is the one that is totally submerged in the water and they create an interface for velocity profiles. Above the vegetation the flow is similar as there is no friction or drag, whereas within the vegetation velocity profile totally changes (Wu, Shen, & Chou, 1999).

The last type is the floating type of vegetation that is generally effective when the waveforms are in concern. They have the wave attraction effect, which can also be considered as a type of energy observer (Plew, 2010).

It is very well known that during flooding (fast flow) the re-suspension of sediment particles are unavoidable, especially when the vegetation cover is sparsely distributed. On the other hand, dense vegetation will help to minimize the erosion of river banks and beds; thus keeping river morphology as stable as possible.

The structure of flow around the vegetation was widely studied by laboratory and field experiments (Gambi, Nowell, & Jumars, 1990; Hu, Liu, Zeng, Cheng, & Li, 2008; Liu et al., 2008; Sand-Jensen & Pedersen, 1999). Hu et al. (2008) and Pujol et al. (2010) show in their experiment that the vegetation can considerably decrease the water flow velocity and the turbulence, respectively, as compared with that in non-vegetation zones (Ackerman & Okubo, 1993; Gambi et al., 1990; Hu et al., 2008; Pujol, Colomer, Serra, & Casamitjana, 2010).

For open channels like rivers and streams with both smooth and rough beds, the power and/or logarithmic velocity distribution with different forms agrees well with the real cases in most of the studies. Mostly, the vertical velocity distribution is connected directly to the bed shear stress for non-vegetation stream, while for vegetated stream, it's mainly defined by the vegetation drag force since the vegetation roughness is much more than river bed roughness (Huai, Zeng, Xu, & Yang, 2009; Klopstra, Barneveld, Van Noortwijk, & Van Velzen, 1996; Righetti, 2008; Wilson, 2007).

The resistance to flow due to vegetation cover has been studied by many researchers.

The initial studies were based on adapting the manning roughness coefficient, *n*, to the flow parameters and attaining a value to "*n*" for representing the vegetation resistance (Petryk & Bosmajian, 1975).

Later, further studies on the effect of resistance or drag on flow structures are performed. Most of these studies were experimental and were focused to analyze the effect of both rigid and flexible vegetation elements of flow structures (Cameron et al., 2013; Carollo, Ferro, & Termini, 2002; Hu et al., 2008; Stone & Shen, 2002; Türker, Yagci, & Kabdaşlı, 2006).

In the most of these studies the resistance to flow and the variations on velocity profile is defined by the help of drag coefficient via the empirical relationships. On the other hand, the flow characteristics of vegetal regions are also described by using the velocity and turbulent intensity profiles at a single point or at average of several points (Nepf, 1999).

1.8.2 Bank Vegetation

Except the artificial channels used for experimental works or water conveying systems, the natural channels like rivers and streams with bed sand inclined banks possesses vegetation at their inclined bank. The velocity of water above the channel bed generally is faster than the velocity at the bank.

The effect of bank vegetation on channel flow is recognized to be confusing hydrodynamics since the lateral exchange of momentum from banks to main stream generates interface flow between flow in the main channel and lateral effect of flow from banks (Shiono & Knight, 1991). The impact of bank vegetation changes with respect to the flow discharge, bank slope, vegetation density and etc.

Afzalimehr and Subhasish (2009) work out the interaction of bank vegetation and gravel bed on the flow velocity and the Reynolds stress distribution. They finally found an average of Von Karman constant as 0.16. Later in 2011, Afzalimehr, Moghbel, Gallichand, and Jueyi (2011) improved this channel roughness for the bank vegetation. Hirschowitz and James (2009) tried to assign a composite resistance coefficient to represent the effect of bank vegetation on open channels.

Recently, Valyrakis et al. (2015) carried out experimental studies to quantify the effect of bank vegetation on flow velocity in the main channel and inside the vegetation, while increasing the density of bank vegetation.

All the above achievements are based on experimental studies, leaving a gap on numerical analysis of effect of bank vegetation on stream flow.

1.8.3 Computational Hydraulics on Flow through Vegetation

Modeling and simulation of interaction of fluid flow through vegetation are generally based on the Navier-Stokes theorem and its generalized equations (Neary, 2003). A depth integrated flow model is developed by Struve, Falconer, and Wu (2003), where large eddy simulation (LES) analysis of fluid flow through vegetation was conducted by Choi and Kang (2004).

In all above studies, the boundary conditions were the main design concerns which, directing effect the outcomes of studies. In most of the studies the computed results show that, the increase in vegetation density leads to increase in water depth and decrease in the flow velocities in the main channel. Although, several computational research has been conducted on vegetation on open channel flows, the effect of bank vegetation on main stream flow has not been investigated.

Chapter 2

FUNDEMENTAL OF VELOCITY BASED FLOW
CHARACTERISTICS

2.1 General

The overall analysis on evaluating the three dimensional structure of velocity in open
channel is based on several physical definitions. The turbulence characteristics of flow
are one of the main indications of defining the effects of bank vegetation on main
channel. Therefore, it is necessary to characterize the velocity based flow parameters,
turbulence intensities, average turbulent kinetic energy and Reynolds stresses for eval-
uating the vegetation effects within a hydraulic system. A depth-averaged models are
usually successful to simulate the velocity profiles of the free surface flow in channels
which are covered by emerging and submerged vegetation (Chao, Zheng, Wang, &
Jun, 2015).

It is clearly known that, the time average velocity based profile of the flow in a vege-
tated channel is a valuable input for the accurate measurements of flow discharge in
the channels. These profiles are also important when the research is detailed on the
prediction of morphological changes (erosion and deposition) are vital (Chao et al.,
2015).

2.2 Time Average Velocity Based Distribution

The flow velocity in a channel section varies from one point to another. This is due to
shear stress at the bottom and at the sides of the channel and due to the presence of

free surface.

Time average velocity distribution can be divided into two regions as inner and outer regions. The height of the inner region, which is totally described at boundary layer is much smaller than the outer region. This layer is usually considered to have different behavior for smooth walls and rough walls. When smooth walls are under consideration, the inner region is divided into three sub layers; viscous sub-layer which is next to the wall, the intermediate region, and the fully turbulent region. The viscous forces are always dominating the flow when the flow is within the viscous region. This results in low Reynolds numbers in which the mean velocity distribution can be given as,

$$\frac{U}{u_*} = \frac{u_* y}{\upsilon} \tag{2.1}$$

where y is the vertical distance from the bottom boundary, u_* is the shear velocity, U is the time averaged velocity in the flow direction and υ is the kinematic viscosity depending on the temperature of the pervading fluid. On the other hand, the vertical velocity profile in the fully turbulent region can be described with the help of logarithmic law and defined as,

$$\frac{U}{u_*} = \frac{1}{\kappa} \ln \frac{u_* y}{\upsilon} + B \tag{2.2}$$

where κ is the von-Karman constant and B is integration constant. The von-Karman constant is usually accepted to be equivalent to 0.41. The integration constant on the other hand is defined by many researchers depending on the flow characteristics. The

suggested B values are varying between 5.1 to 5.5, (Bradshaw, Cebeci, & Whitelaw, 1981; Cardoso, Graf, & Gust, 1989; Nezu & Rodi, 1986; Nikuradse, 1950; Steffler, Rajaratnam, & Peterson, 1985).

In the case of rough wall the logarithmic velocity profile close to the wall is described by von Karmen-Prandtl equation and is given as (Townsend, 1976),

$$\frac{U}{u_*} = \frac{1}{\kappa} \ln \frac{y}{y_0} \tag{2.3}$$

where y_0 is the roughness height of the surface (hypothetical bed level).

In the outer region, the velocity profile is defined by Jiménez (2004) as,

$$\frac{U}{u_*} = \frac{1}{\kappa} \ln \frac{y}{k_s} B_s + wk(\xi) \tag{2.4}$$

in which, k_s is maximum height of bed roughness and $wk(\xi)$ is known as the wake function and is generated for an additive correction to the log law by Coles (Coles, 1956). According to Coles, the wake function can be given as,

$$wk(\xi) = \frac{2\Pi}{\kappa} \sin^2 \left(\frac{\pi}{2} \xi \right) \tag{2.5}$$

where Π is the Coles wave strength and ζ is the normalized distance relative to the location of the occurrence of the dip phenomena from the bed of the channel.
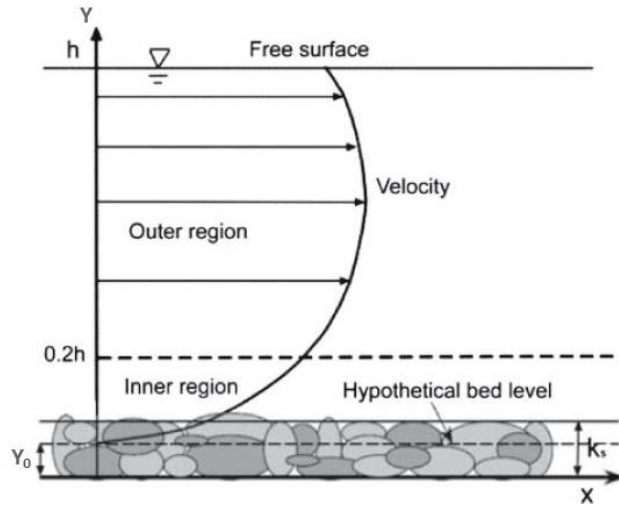
Figure 2.1: Representative velocity profile, consisting of two different parts, inner region and outer region. (Bonakdari, Larrarte, Lassabatere, & Joannis, 2008)

2.3 Reynolds Shear Stress

In a shear flow, the momentum (ρU) is transferred from the region of high velocity to that of low velocity, where ρ is the fluid density. The fluid tends to resist the shear associated with the transfer of momentum. Therefore, the shear stress is proportional to the rate of transfer of momentum. In laminar flows, the shear stress is defined as,

$$\tau_{lam} = \mu \frac{\partial u}{\partial y} \tag{2.6}$$

where τ_{lam} is the shear stress per unit area, μ is the dynamic viscosity of the pervading fluid, and u is the velocity of flow in X-direction. As long as the shear stresses get larger, the viscosity effects are losing their dominant effects on flow and turbulence spots develop within the flow. This turbulence changes the behavior of shear forces and the apparent shear stress in turbulent flow can be expressed as,

$$\tau_{turb} = \rho(\upsilon + \upsilon_T) \frac{\partial u}{\partial y} \tag{2.7}$$

Here the terms in parenthesis represent the viscosity terms, first labeled as kinematic viscosity and the later one the eddy viscosity. The eddy viscosity is also known as the momentum exchange coefficient in turbulent flows. Generally, the magnitude of eddy viscosity is always much greater than the kinematic viscosity that the magnitude of kinematic viscosity becomes negligible. As a result the shear stress equation for turbulent flows is given as,

$$\tau_{turb} = \rho \upsilon_T \frac{\partial u}{\partial y} \tag{2.8}$$

It is also possible to estimate the turbulent shear stresses by the development of the so called Reynolds stress turbulence models. These models do not use eddy viscosity formulations for the turbulent transport quantities, but use the vertical momentum transport of velocity due to the velocity fluctuations. Whenever the velocity profile of a turbulent flow in a horizontal plane is under consideration, the upward eddy motion of fluid particles are observed from a lower velocity layer to the upward adjacent higher velocity layer as a result of the velocity fluctuations v' as given in Figure 2.2. This momentum transfer causes the horizontal velocity of the fluid particles to increase by u'. Any increment in horizontal velocity of the fluid particles results in an increase in momentum in the horizontal direction. It is very well known that, force in a given direction is equal to the rate of change of momentum in that direction. Therefore, the shear force per unit area due to the eddy motion of fluid particles can be accepted as the instantaneous turbulent shear stress per unit area. Then, the turbulent (Reynolds) shear stress can be expressed as,

$$\tau_{turb} = -\rho \overline{v'u'} \tag{2.9}$$

15

where $\overline{v'u'}$ is the time average of the product of the fluctuating velocity components u' and v'.
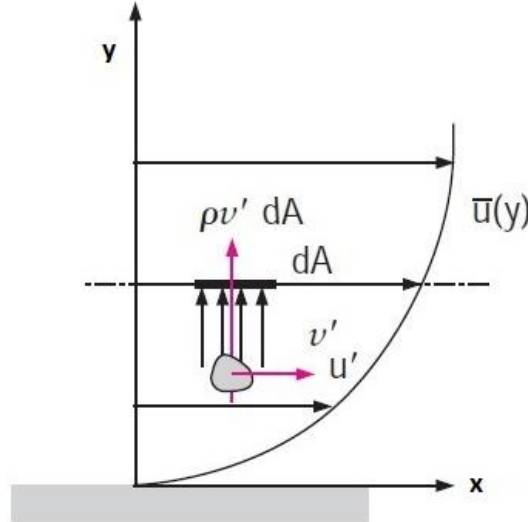
Figure 2.2: The upward eddy motion of fluid particles from a lower velocity layer to the upward adjacent higher velocity layer as a result of the velocity fluctuations (Cimbala & Çengel, 2008)

The turbulent stress produces an effect similar to that of laminar stresses. The difference is that, the laminar stresses are formed due to the fluid viscosity and velocity gradient, while the turbulent shear stress (Reynolds stresses) occurs due to the results of the fluctuating nature of the velocity field.

One of the problem is to find a way to evaluate the Reynolds stresses written in terms of velocity fluctuations. Many semi-empirical, empirical and analytical formulations have been developed that model Reynolds stresses to the mean flow. These models are turbulence models and in most of them turbulent shear stress is expressed in terms of a gradient formulation.

$$\tau_{turb} = -\rho\overline{v'u'} = \rho\upsilon_T \frac{\partial u}{\partial y} \qquad (2.10)$$

The magnitude of the momentum exchange coefficient (eddy diffusivity) depends on flow conditions which mean that it is not a fluid property like kinematic viscosity. Same as the velocity in flow direction, the magnitude of the momentum exchange coefficient reduces when gets close to the wall and becomes zero at the wall.

2.4 Turbulence Models

There are many turbulence models. Among them the classical models which have wide application are generally based on Reynolds Averaged Navier-Stokes (RANS) equations. These models are time averaged models and classified as; zero equation model, one equation model, two equations model and seven equations model. Actually the equation number reflects the number of partial differential equations that are solved while using these models. The well-known models that are derived from one of the above turbulence models are Reynolds stress models, mixing length model, k-ε models and k-ω model. Where the two of the most popular turbulence models are the k-ε model and the k-ω model.

The k-ε turbulence model is the most common model used for computational fluid dynamic problems. The target aim is to simulate the mean flow characteristics when the pervading fluid is under turbulent conditions. The model solves for two variables: the turbulent kinetic energy, k which gives the energy in the turbulence and the turbulent dissipation, ε which determines the rate of dissipation of turbulent kinetic energy.

Wall functions are used in this model, so the flow in the buffer region is not simulated. The k-ε model is very popular for industrial applications due to its good convergence rate and relatively low memory requirements. It does not very accurately compute flow fields that exhibit adverse pressure gradients, strong curvature flow, or jet flow. It does

perform well for external flow problems around complex geometries.

The advantages of k-ε turbulence model is relatively simple to implement and leads to stable calculations while converging easily. On the other hand, the model has poor predictions for certain unconfined flows, swirling and rotating flows and flows with strong separation.

The k-ω is another type of two equation model similar to k-ε, instead however, it solves for omega "ω". Omega is the specific rate of dissipation of turbulent kinetic energy. It also uses wall functions and therefore has memory requirements for computational analyses. Its numerical behavior is similar to that of the k-ε models, but has more difficulty for converging. Hence, the k-ε model is generally solved to generate initial conditions for the problem that will be used by for solving the k-ω model. The k-ω model is useful in many cases such as internal flows like flows through a pipe bend and jets.

In turbulence models, the accurate estimate of the current separation from a flat surface is one of the significant problems. Basic two equation turbulence models regularly cannot guess the onset and the magnitude of flow separation under adverse pressure gradient conditions. Generally, turbulence models which developed from the ε-equation, estimate the onset of separation very late and under predict the amount of separation afterward. Presently, the most advanced two equation models in this field are the k-ω based models by Menter (1994). The k-ω based shear stress transport (SST) model was developed to provide an extremely accurate prediction of the onset and the magnitude of flow separation under adverse pressure gradients by the addition of transport effects into the equation of the eddy viscosity. The accuracy and performance of the SST model have been confirmed in many studies (Huang, Bardina, & Coakley,

18

1997).

The SST model is suggested for simulating high resolution boundary layer, also for free shear flows, this model is preferred than the k-ε model. One of the advantages of the k-ω formulation which makes this model overcome on other turbulence models is, the near wall behavior for low Reynolds number calculations. This model does not include the complex nonlinear equations that is necessary for the k-ε models, therefore more robust and accurate. The base k-ω and SST models will be discussed in next chapter.

2.5 Turbulence Intensity

The root mean square of the turbulent velocity fluctuations at any location within a specified period of time is called the turbulence intensity. The intensity of a quantity gives us an idea of how much that quantity departs from its mean value. Due to the fluctuations associated with eddies, turbulent characteristics of flow can be defined by its random behavior. Therefore, turbulent velocities can be defined using statistical concepts. Considering a quantity of velocity in a turbulent flow field at any particular point it can be written as,

$$u = \overline{u} + u' \tag{2.11}$$

This type of definition of flow velocity is commonly known as Reynolds decomposition. The first term at the right hand side of the Equation (2.11), $\overline{u}$ is the time mean value of the velocity described as,

$$\bar{u} = \frac{1}{T} \int_0^T u(t)dt \qquad (2.12)$$

Here T is the sample time and t is the time. Generally, at turbulent flow conditions the frequencies of turbulent fluctuations are sufficient to help to define time mean of velocity parameters. The necessary time is usually denoted to a second or less. In order to denote a name to this parameter, "mean" or "average" can be used as is used in other research studies. The second term at the right hand side of the Equation (2.11) is the primed velocity. The primed velocity represents the turbulent fluctuations and they are the causes of the horizontal and vertical momentum transfer between layers of turbulent flow. The root mean square is a helpful concept in order to measure the magnitude of the turbulent fluctuations. Therefore, the primed term (turbulent fluctuation) can be defined as,

$$RMS \;\; u' = \sqrt{\overline{u'^2}} = \sqrt{\frac{1}{T} \int_0^T u'(t)^2 \, dt} \qquad (2.13)$$

The root mean square of the velocity fluctuation gives the strength of the turbulence, whereas, large values of root mean square of fluctuations indicate higher levels of turbulence. The ratio between the root mean square of velocity fluctuation and the mean velocity is the definition of turbulence intensity.

$$TI = \frac{u'}{\bar{u}} \qquad (2.14)$$

In which *TI* represents the dimensionless turbulence intensity.

2.6 Turbulent Kinetic Energy (TKE)

The turbulent kinetic energy (TKE) is the product of the three dimensional absolute intensity of velocity fluctuations from the mean velocity and it is defined as,

$$TKE = \frac{1}{2}\rho\left(\overline{u'^2} + \overline{v'^2} + \overline{w'^2}\right) \tag{2.15}$$

where u, v and w represents the velocity fluctuations in X, Y and Z directions respectively. The results of several studies have shown that there is a direct relationship between the turbulent kinetic energy and the bed shear stresses (Galperin, Kantha, Hassid, & Rosati, 1988; Soulsby & Dyer, 1981; Stapleton & Huntley, 1995). The results of these studies have mentioned that this relationship is constant and can be given as,

$$\tau = C_{TKE} \times TKE \tag{2.16}$$

In most of the studies the magnitude of the constant C_{TKE} is found to be around 0.2.

2.7 Secondary Current in Channels

Secondary currents are defined as flow that occur in a plane normal to the axis of primary flow (Prandtl, 1952). There are two different types of secondary flow/current which recognized by researchers. The first one is weak secondary current or stress-induced, initiated by boundary shear stress that distributed non-uniformly, and the second one is strong secondary current or skew-induced, initiated by skewing of cross-stream vorticity into a streamwise direction which is caused by channel bend or bed topography (Perkins, 1970). Mostly, in rivers the secondary current patterns are overcame by skew-induced currents (Bathurst, Hey, & Thorne, 1979), however, the

strength and form of secondary current are totally influenced by platform morphology, channel shape and bed roughness distribution.

One way to characterize the effect of secondary current is the secondary current angle. This parameter can be defined as the divergence angle of velocity from desirable direction usually the streamwise velocity (Masouminia, Türker, & Fasihi, 2014).

2.8 Vegetation Characteristic

One of the parameters that make the effect of vegetation understood by mathematics is the vegetation density. This can be discretized by relation of the momentum that absorb from the project area of single cylinder over canopy volume (Thom, 1971), and it can be written as,

$$\lambda = \frac{Area_f}{Volume} = \frac{D}{S^2} \tag{2.17}$$

where λ is vegetation density with unit of m^{-1}, D is the diameter of the constant cylindrical element which is usually recognized as the stem of a single vegetation element, S is the constant distance between two individual elements in linear and/or staggered position. Also, two other definition that make the vegetation characteristic more understood, the solid volume fraction, φ, and the porosity, η, of vegetation/rods are described as,

$$\varphi \approx \frac{\pi \lambda D}{4} \tag{2.18}$$

$$\eta = 1 - \varphi \tag{2.19}$$

Chapter 3

SIMULATION

3.1 Computer Simulation

In every aspect of science, there is an undeniable influence of computer technology, which helps the scientists and engineers to push the borders of their researches. Computational Fluid Dynamics (CFD) is a computer based software, to simulate the behavior of systems of fluid flow, heat transfer, and other physical processes that related. From the 1970 decade, the algorithms of fluid flow that based on complex mathematics began to be acknowledged, and general goal of CFD solvers were developed. At the beginning of 1980s, these achievements started to appear and very powerful computers needed, as well as a comprehensive knowledge of fluid dynamics, and more time to start simulations. Resultantly, CFD was founded as a tool in research. It works by solving the fluid flow equations in a special form over a region of interest, with known conditions on the region's boundary. In other word, CFD helps the engineers to test their systems by simulating fluid flow in a virtual environment in much less labor intensive, reducing time and, cost. ANSYS, which is known as an engineering simulation software (computer-aided engineering, or CAE) consists of a package of many high performance simulation technology under the subjects of systems and embedded software, electronics, fluid dynamics, structural analysis and multiphasic. The fluid dynamics simulation sub-programs working under the ANSYS software are FLUENT, CFX, ICEM, AQWA, etc. The following paragraphs describe about two of these programs which were used in this study (CFX, 2009).

3.1.1 ANSYS CFX

ANSYS CFX is a general purpose CFD software suite that merges an advanced solver, powerful pre and post processing together. It contains the below features:

- An advanced coupled solver that is both reliable and robust.

- Full integration of problem definition, analysis, and results presentation.

- An intuitive and interactive setup process, using menus and advanced graphics.

One of the best features of ANSYS CFX is the use of a coupled solver, which means it can solve all the hydrodynamic equations as a single system. The advantage of coupled solver is that, it calculates faster than the previous segregated solver and also less iterations are needed to reach a converged flow solution (CFX, 2009).

3.1.2 ANSYS ICEM CFD

ANSYS ICEM CFD prepares a comfortable environment for complicated geometry, mesh generation, and also mesh optimization component to achieve the requirement for integrated mesh generation for today's analyses. Preserving a good relationship with the geometry while generating the meshes, it is used particularly in engineering applications like computational fluid dynamics and also structural analysis (Ansys, 2009).

ANSYS ICEM CFD connects directly geometry and analysis together. Then, the outcome of any kind of meshes, topology, inter domain connectivity and boundary conditions forms into a database where they can be exported to any input files formatted for a special solver (Ansys, 2009).

3.2 The Description of Model

The group of equations which explain the processes of momentum, heat and mass

transfer are known as the Navier-Stokes equations. These partial differential equations were derived in the early nineteenth century and it is not possible to solve these equations analytically. However, it is easy to discretized and solve Navier-Stokes equations numerically. Often, an approximation is used to derive these equations and the turbulence models are particularly important example of the numerical (computational) solution of Navier-Stokes Equations.

There are a number of different solution methods that are used to model turbulent flow conditions in CFD codes. The most common, and the one on which CFX is based, is known as the finite volume technique.

In this technique, the region of interest is divided into small sub-regions, called control volumes. The equations are discretized and solved iteratively for each control volume. As a result, an approximation of the value of each variable at specific points throughout the domain can be obtained. In this way, one derives a full picture of the behavior of the flow (CFX, 2009).

3.2.1 Governing Equations

ANSYS CFX solves sets of equations of the unsteady Navier-Stokes in their own conservation form. The conservation of momentum in fluid dynamic will be represented by the Navier-Stokes equations, meanwhile the continuity equation shows the conservation of mass. These equations are as follow,

The Continuity Equation:

$$\frac{\partial \rho}{\partial t} + \nabla \cdot (\rho U) = 0 \tag{3.1}$$

25

The Momentum Equations (the Navier-Stokes equations):

$$\frac{\partial(\rho U)}{\partial t} + \nabla \cdot (\rho U \times U) = -\nabla p + \nabla \cdot \tau + S_m \qquad (3.2)$$

where U represents the velocities, p is the pressure, S_m is body forces and the viscous stress tensor "τ" is defined as,

$$\tau = \mu \left(\nabla U + (\nabla U)^{Tr} - \frac{2}{3} \delta \nabla \cdot U \right) \qquad (3.3)$$

In Equation (3.2), the left hand side correspond to the inertia forces; on the right hand side, the first term represent pressure forces, the second term defines the viscous forces and the last one shows the body forces. The δ is the kronecker delta and Tr is transpose operation.

Generally, laminar and turbulent flows can be described by the Navier-Stokes equations without any need of additional equations. Yet, turbulent flows at applicable Reynolds numbers cover a large array of turbulent time and length scales, which may make to have length scales considerably smaller than the tiniest finite volume mesh, that can be actually used by a numerical analysis. Most of the turbulent models which will be used are statistical models. Generally, turbulence models try to change the basic unsteady Navier-Stokes equations by defining the averaged and fluctuating quantities to introduce the RANS equations. These formulas only describe the average flow quantities, while modeling the effect of turbulence without solving the turbulent fluc-

tuations. The statistical turbulence models are those which based on the RANS equations. The modified Navier-Stokes equations for RANS models introduced as,

$$\frac{\partial(\rho U_i)}{\partial t} + \frac{\partial}{\partial x_j}\left(\rho U_i U_j\right) = -\frac{\partial p}{\partial x_i} + \frac{\partial}{\partial x_j}\left(\tau_{ij} - \rho \overline{u_i u_j}\right) + S_m \qquad (3.4)$$

Here, x_i or x_j and U_i or U_j are distance and velocity components in X, Y and Z directions, $-\rho \overline{u_i u_j}$ represent the Reynolds stress.

Many CFD research has focused on methods which can predict the turbulence. One of this suggestion is that turbulence contains of small eddies which are always generating and vanishing, and the Reynolds stresses are presumed to be proportional to mean velocity gradients and also referenced as "eddy viscosity model".

The eddy viscosity model undertakes that the Reynolds stresses are related to the mean velocity gradients and eddy viscosity (eddy turbulent) by the gradient diffusion hypothesis, in a way analogous to the link between the stress and strain tensors in laminar condition of Newtonian flow.

$$-\rho \overline{u_i u_j} = \mu_t\left(\frac{\partial U_i}{\partial x_j} + \frac{\partial U_j}{\partial x_i}\right) - \frac{2}{3}\delta_{ij}\left(\rho k + \mu_t \frac{\partial U_k}{\partial x_k}\right) \qquad (3.5)$$

Where μ_t is defined as the turbulent viscosity or the eddy viscosity.

Subject to the eddy viscosity model, the RANS equations become,

$$\frac{\partial(\rho U_i)}{\partial t} + \frac{\partial}{\partial x_j}(\rho U_i U_j) = -\frac{\partial p_m}{\partial x_i} + \frac{\partial}{\partial x_j}\left[\mu_{eff}\left(\frac{\partial U_i}{\partial x_j} + \frac{\partial U_j}{\partial x_i}\right)\right] + S_m \tag{3.6}$$

where p_m is the modified pressure and μ_{eff} represents the effective viscosity and they are given as,

$$\mu_{eff} = \mu + \mu_t \tag{3.7}$$

$$p_m = p + \frac{2}{3}\rho k \tag{3.8}$$

The *k-ω* and shear stress transport (SST) models:

In the *k-ω* based model, the turbulence viscosity is related to the turbulence kinetic energy and turbulent frequency by the Equation (3.9).

$$\mu_t = \rho\frac{k}{\omega} \tag{3.9}$$

The first definition of the current formulation was the *k-ω* model developed by Wilcox (1988). In this method, two transport equations were solved, first one was for the turbulent kinetic energy per unit of density, *k* Equation (3.10), and the second one was for the turbulent frequency, *ω* Equation (3.11). The stress tensor is calculated from the eddy viscosity concept which was defined in Equation (3.5).

$$\frac{\partial(\rho k)}{\partial t} + \frac{\partial}{\partial x_j}(\rho U_j k) = \frac{\partial}{\partial x_j}\left[\left(\mu + \frac{\mu_t}{\sigma_k}\right)\frac{\partial k}{\partial x_j}\right] + P_k - \beta'\rho k\omega \tag{3.10}$$

$$\frac{\partial(\rho\omega)}{\partial t} + \frac{\partial}{\partial x_j}(\rho U_j \omega) = \frac{\partial}{\partial x_j}\left[\left(\mu + \frac{\mu_t}{\sigma_\omega}\right)\frac{\partial\omega}{\partial x_j}\right] + \alpha\frac{\omega}{k}P_k - \beta\rho\omega^2 \qquad (3.11)$$

The $\sigma_k, \beta', \sigma_\omega, \alpha$ and β are constant parameters while for this model, they are taken 2, 0.09, 2, 5/9 and 0.075, respectively.

The turbulence production "P_k" due to viscous forces, which is Equation (3.12).

$$P_k = \mu_t\left(\frac{\partial U_i}{\partial x_j} + \frac{\partial U_j}{\partial x_i}\right)\frac{\partial U_i}{\partial x_j} - \frac{2}{3}\frac{\partial U_k}{\partial x_k}\left(3\mu_t\frac{\partial U_k}{\partial x_k} + \rho k\right) \qquad (3.12)$$

In SST model, a limiter was introduced for the basic k-ω model by Menter (1994) in the eddy viscosity Equation (3.5), making this model to generate appropriate solution for the transport of the turbulent shear stress.

$$\upsilon_t = \frac{\alpha k}{\max(\alpha\omega, S_r F)} \qquad (3.13)$$

$$\upsilon_t = \frac{\mu_t}{\rho} \qquad (3.14)$$

Where F is the blending function and S_r is defined as the invariant measure of the strain rate.

3.2.2 Geometry of the Model

In every study there is a part of collecting the data and equipment which will be used. This study tries to simulate flow characteristics in a semi-trapezoidal channel which

covered by vegetation on the bank. The flume that was used here has the same dimensions of the flume at the University of Glasgow Water Engineering Laboratory. It has a 14 meters long and 1.8 meters wide with a side slope of 17° on the bank. Instead of vegetation, the study used non-flexible (rigid) rods with 6 mm diameter that fixed in panel from the top of the flume. These details were used for drawing the flume in AUTOCAD software, after, it will be used in ANSYS geometry component. The same procedure was used to draw all other configurations that covered flume by vegetation. All the details are shown in Figure 3.1,
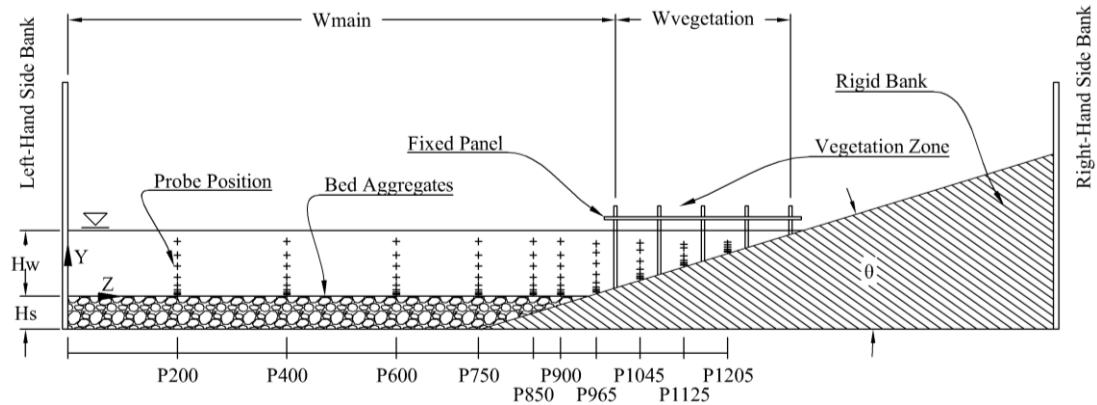
Figure 3.1: Cross-sectional view of the flume under study covered by vegetation

where $H_w = 0.12$ m, $H_s = 0.06$ m, $W_{main} = 1.0$ m, $W_{vegetation} = 0.32$ m and $\theta = 17°$ indicating the water depth, thickness of the bed aggregates, the width of the main channel, the width of the vegetated area and the channel bank side slope, respectively. The vegetation are placed in longitudinal direction, along 3 meters of channel. As shown in Figure 3.1, the effect of inclination of the right bank starts when $z \cong 950$ mm. The simulation initially conducted for ambient channel. Later, the rigid vegetation was placed, named as configuration 1 (Figure 3.2). Next step was to keep the configuration 1 as it is, and by adding more elements, try to increase the vegetation density. This was

achieved by obtaining configuration 2. This procedure continued until the configuration 5 was obtained and the flow simulation was applied for each step.

Table 3.1: Locations of the data collection at 12 cm before last vegetation

Location of data collection	Distance from left bank, Z (mm)									
	Main Channel						Vegetated Bank			
	200	400	600	750	850	900	965	1045	1125	1205
Height from bottom of channel h (mm)	100	100	100	100	100	100	91	68	51	21
	75	75	75	75	75	75	75	55	35	16
	55	55	55	55	55	55	55	35	20	12
	35	35	35	35	35	35	35	20	12	8
	20	20	20	20	20	20	20	12	8	5
	12	12	12	12	12	12	12	8	5	3
	8	8	8	8	8	8	8	5	3	
	5	5	5	5	5	5	5	3		
	3	3	3	3	3	3	3			

The position of rods in a unit panel and along the channel were shown in Figure 3.2. The vegetation characteristics were described in the Chapter 2. Here to characterize this panel, those parameters were calculated and placed in Table 3.2. The bed roughness in the channel was 1.4 mm height and the streamwise mean velocity in the channel was 0.047 m/s. Accordingly, the constant discharge through the experiments was 6.5 lit/s. Under these geometric and flow characteristics the Froude Number during the simulations was inducting subcritical properties with a magnitude around 0.046.
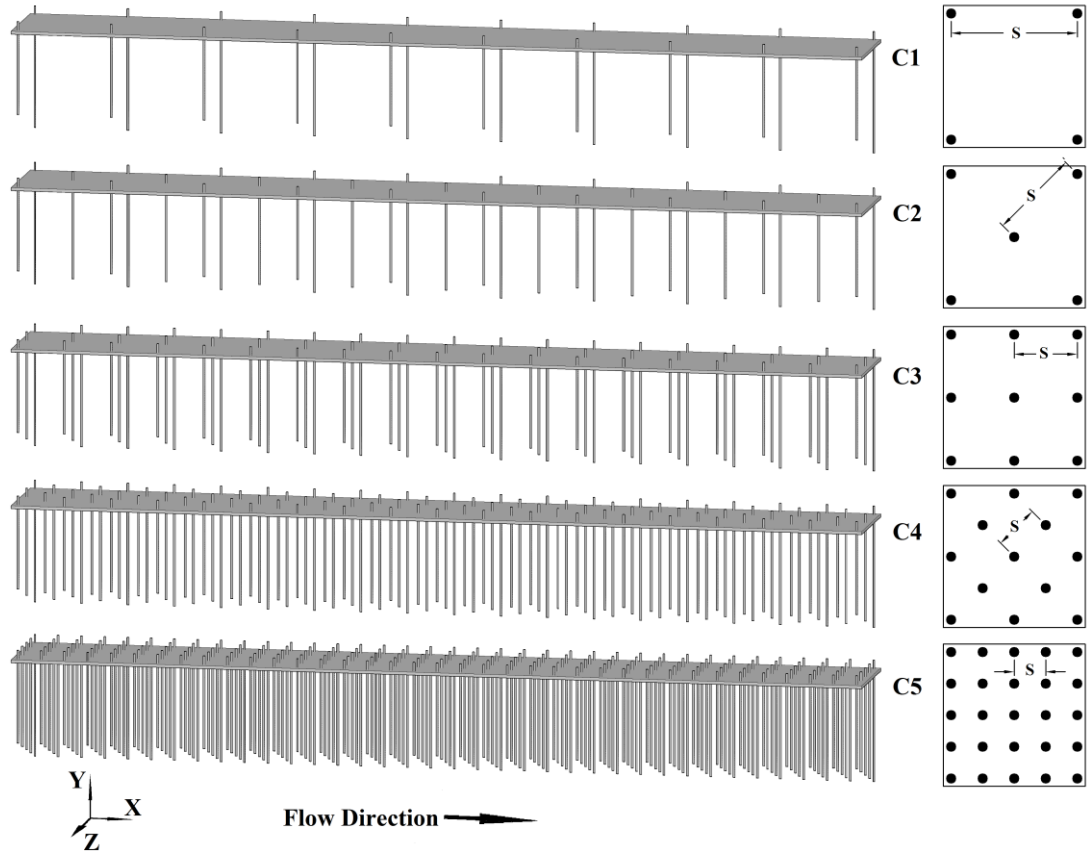
Figure 3.2: Vegetation Configurations

All the above dimensions were used for drawing the model's geometries in AUTO-CAD software except the H_s which was neglected in order to simplify the model. Figure 3.3 shows the geometry of configurations C2 as a sample:

Table 3.2: Vegetation Characteristics

Configuration	Condition	S(m)	$\lambda(m^{-1})$	φ	η
C1	Linear	0.32	0.05859	0.00028	0.99972
C2	Stagger	$0.16\sqrt{2}$	0.11719	0.00055	0.99945
C3	Linear	0.16	0.23438	0.00110	0.99890
C4	Stagger	$0.08\sqrt{2}$	0.46875	0.00221	0.99779
C5	Linear	0.08	0.93750	0.00442	0.99558
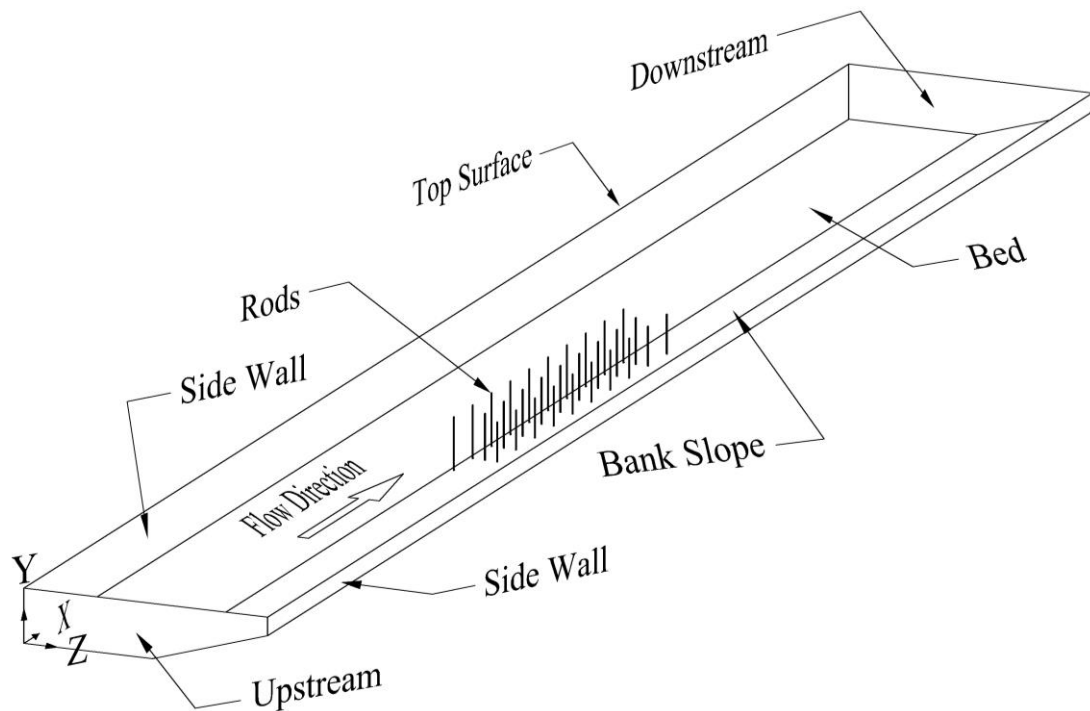
Figure 3.3: Geometry of model C2

3.2.3 Meshing Procedure

ANSYS package has many meshing components; the one that carried out in this simulation was ICEM CDF. The advantage of the ICEM CFD component was described before in this chapter. In this component, a structured quadrilateral mesh was chosen to make the finite volume cells. The first node distance from the entire solid surface equal to 1.5 mm was kept constant for all geometries. Due to avoiding the high number of nodes in meshing process the aspect ratio, the ratio of the length of the longest edge of the cell to the shortest one, was kept less than 1.25. This helped to have more dense meshes near the areas that require more number of nodes and less number of nodes on other areas. The number of nodes at the edges that presented the main channel, vegetated area, water depth and the height above the water surface were 75, 40, 33 and 11, respectively. The maximum cross-sectional distance for mesh sittings were 25 cm. As an example for all the models, the surface meshes of model C2 were presented in Figure 3.4-3.7:
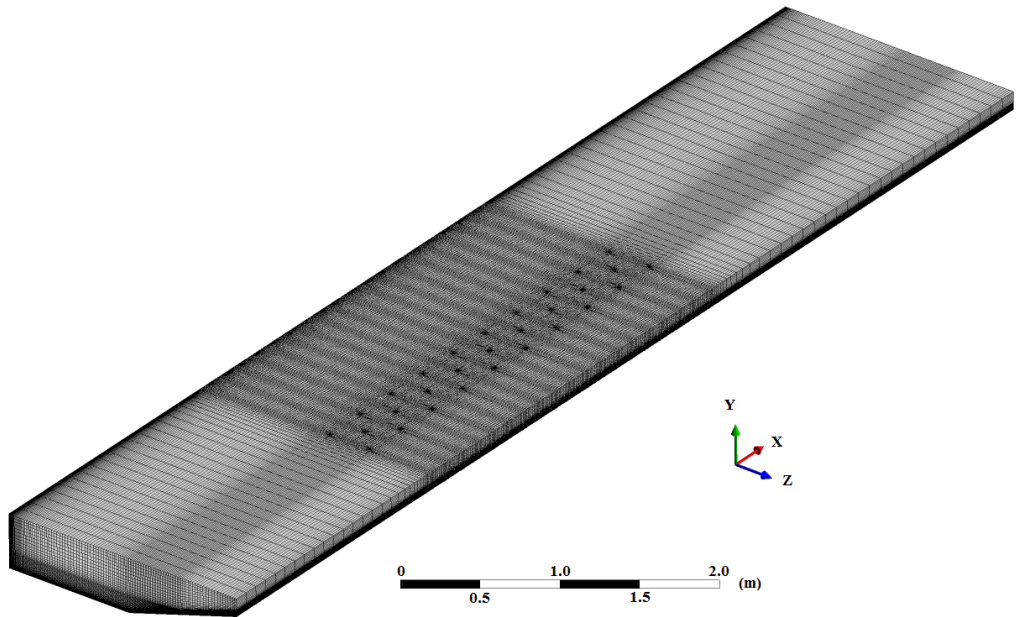
Figure 3.4: Isometric view of C2 surface mesh
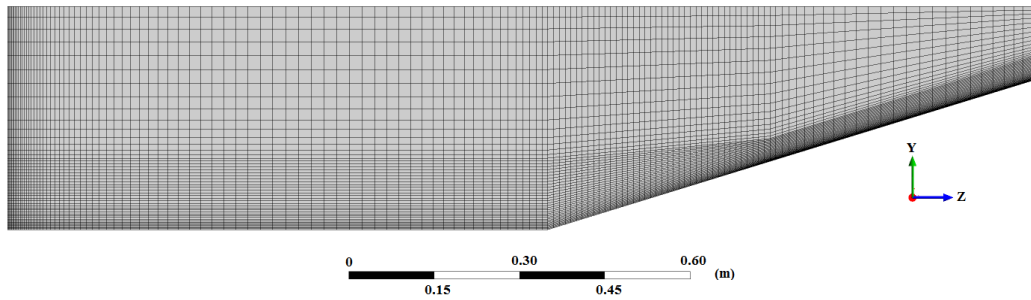
Figure 3.5: Cross-sectional view of C2 surface mesh
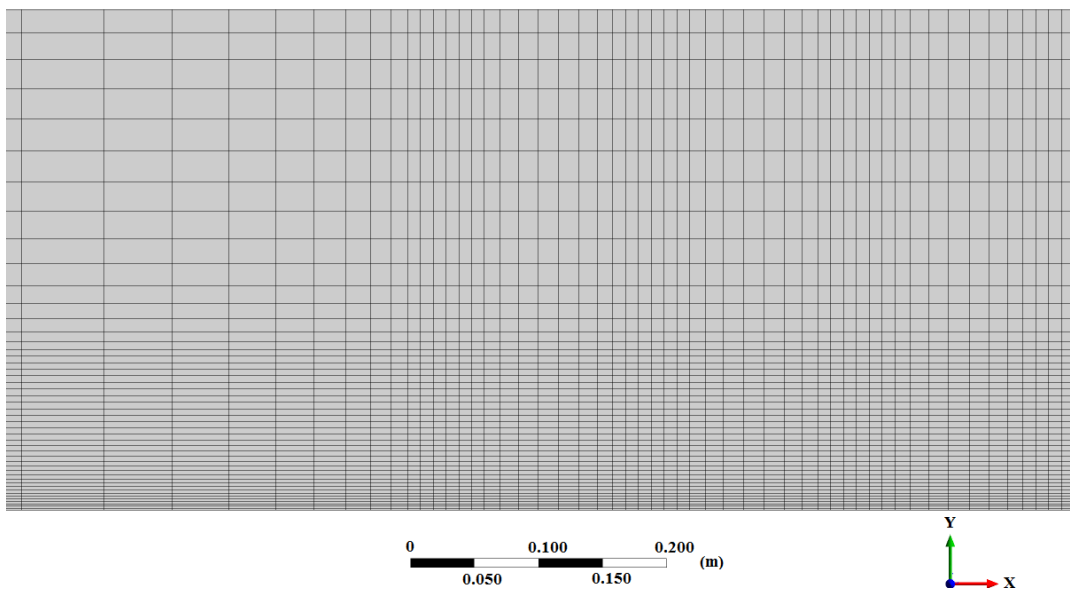
Figure 3.6: Side view of C2 surface mesh

34
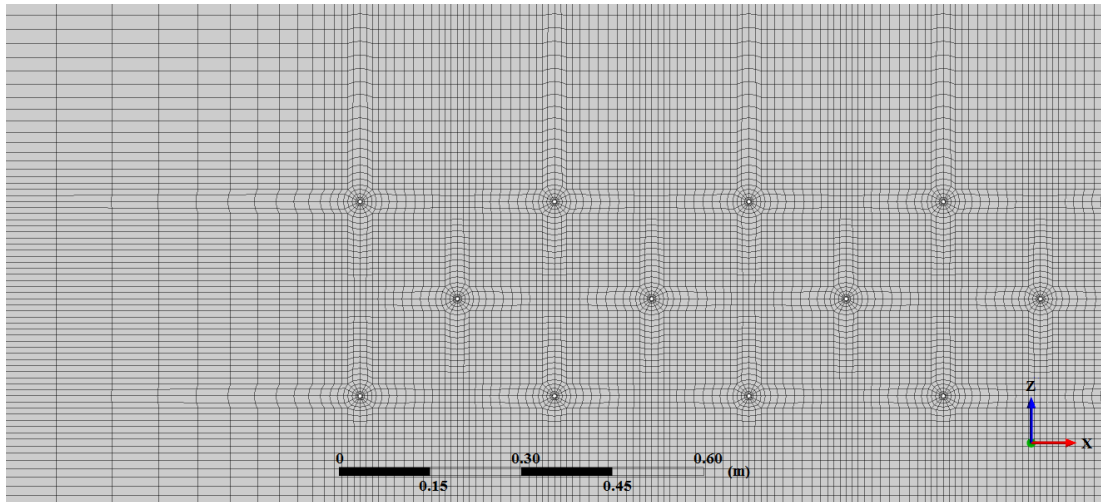
Figure 3.7: Top view of C2 surface mesh

3.2.4 Quality of Meshes

The meshing quality is necessary to confirm an accurate analysis of the simulation. For more information on the quality of meshing, it can be said that a fine mesh will generate more accurate outcomes than a coarse mesh while the quality of mesh cells are of the equal or better. The maximum aspect ratio, the minimum determinant, and orthogonally angle, and the maximum expansion factor are the parameters which can qualify how good the meshing process is.

The aspect ratio of a cell, as described before, shows the ratio of the length of the longest edge to the shortest one. It can also be used to decide how close to ideal a face or cell is, as an example, an equilateral cell (e.g., an equilateral square or a triangle, etc.), has the aspect ratio equal to 1.

The determinant is the calculation of the deformation of the cells in the mesh by first computing of the Jacobian of all hexahedron and then normalizing the determinant of the matrix. An acceptable hexahedral cube will be presented by a value equal to 1, while a value of 0 is a completely inverted cube. In general, the value of determinant

35

more than 0.3 will be accepted by most of the solver programs.

The minimum orthogonally angle is defined as the lowest angle of all the internal angles for each cell. The default value is between 0 to 90 degrees, where 0 describes poor and 90 describes perfect orthogonally.

The maximum expansion factor can be explained as follow. At first, the node centered volume is computed for every node in the entire mesh. After, to find the expansion factor, the node centered volume will be compared to the other volumes which are around the nearby nodes to calculate the largest factor. For each cell, the corresponding nodes will be tested and the highest value of them will be used. If this factor has a magnitude of 1, it will show the best quality of mesh. However, the higher value of expansion factor is acceptable for CFD software like ANSYS CFX.

One of the advantages of ICEM CFD that helped this study was its ability to show all the above parameters before the simulation goes on. With this benefit all the 6 models were meshed in optimum condition that can reach by available computer configuration. The meshing details of all geometries are shown in the following Figure 3.8-3.11 and Table 3.3:
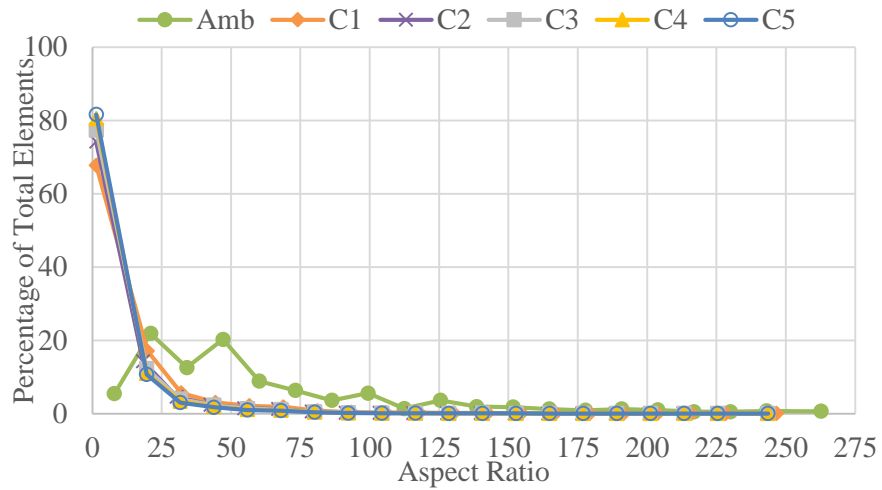
Figure 3.8: Aspect ratio chart of all configurations
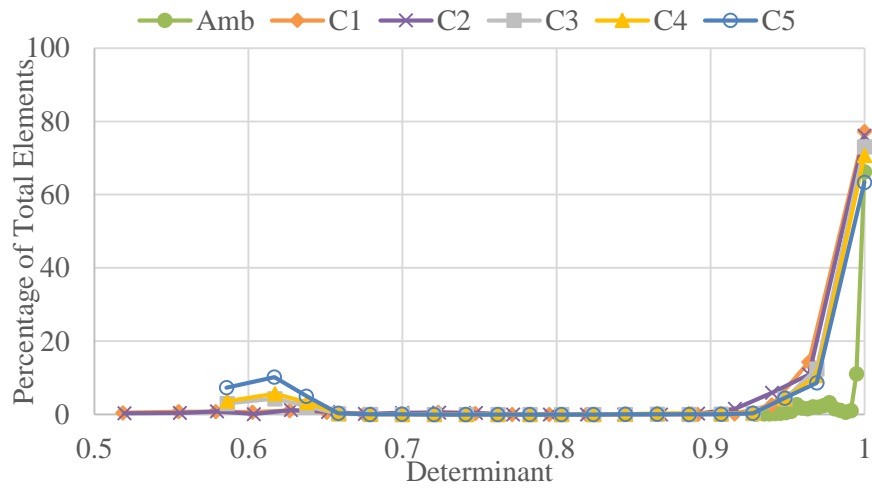
Figure 3.9: Determinant chart of all configurations
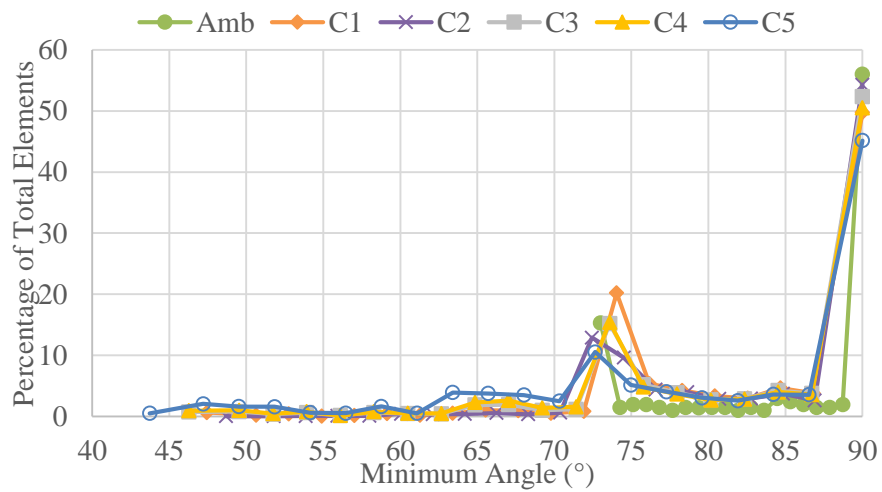
Figure 3.10: Minimum angles chart of all configurations
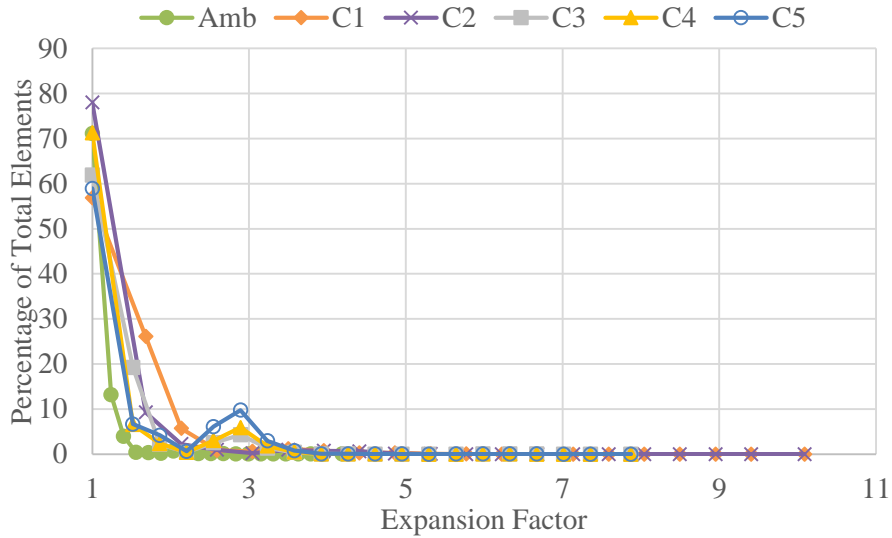
Figure 3.11: Expansion factor chart of all configurations

Table 3.3: Meshing parameters

Geometry Name	Total Number of Elements	Max Aspect Ratio	Min Determinant	Min Orthogonally Angle (°)	Max Expansion Factor
Amb	347424	263	0.929	73	4.19
C1	1341888	238	0.518	55	8
C2	2076288	238	0.519	67	8
C3	2162304	238	0.586	56	6
C4	2630592	238	0.586	56	6
C5	2913216	238	0.585	55	6

By viewing the pervious Figures, it can be said that all the model's mesh have reliable quality and also, the data of the Table 3 are in acceptable range which is required for ANSYS CFX solver.

3.3 Implementing the Model Solver

Previously, segregated solvers were generating a solution plan for computational dynamics such that the momentum equations were solved at the beginning of the simulation by using an estimated pressure and then an equation for a pressure correction were achieved. On the other hand, ANSYS CFX takes an advantage of a coupled solver, which all the hydrodynamic equations for u, v, w, and p are solved by a single system. This solution method uses a fully implicit discretization of the equations at

38

any specified time step. The time step in steady state problems, acts as an acceleration parameter, to lead the estimated solutions to a steady state solution. This can reduce the maximum number of iterations which is required for convergence to a steady state, or to compute the answer for each time step in a time dependent system.

At primary iterations of the simulation, the scheme for the advection term was set to upwind, also the first order scheme was selected for turbulence and a steady state condition with auto time scale mode. These settings help the simulation to reach an acceptable initial value for the entire model. After this part, the transient condition was chosen to make the numerical model converge to its criteria. The maximum residuals for convergence set to 10^{-3} also the time step in transient condition ($\Delta t \approx L/U$, where L is length scale) was 0.04 second during 6 seconds of time duration. Reaching the maximum residuals below the target is not the only parameter which should be noticed, also the imbalance of parameters less than 1% should be checked. Due to multiphase condition (water and air phases) of the model, the volume fraction coupling set to coupled, also the density difference option was selected for modeling the fluid buoyancy.

3.4 Boundary conditions

In the setting of the boundary conditions for the models, it is necessary that they best be similar to the actual situation that will occur in reality. If the boundary conditions vary from the actual conditions, then the study would not be valid.

Totally, in this study, seven different boundaries exist to define the model. These boundaries are top surface, channel bed, side walls, upstream and downstream cross sections, bank slope, and the surface of the rods. The boundary conditions which selected for these surfaces are shown in Figure 3.12. The top surface defined as opening

boundary with zero gradient condition, also this boundary was chosen for the down-stream cross section. The upstream cross section was set to inlet boundary with the magnitude of mean velocity in longitudinal direction equal to 0.047 m/s.

The wall boundary condition was selected for all the other surfaces like bank slope, rods and side walls with the roughness height of 0.1, 0 and 0.1 mm, respectively. As was mentioned before on geometry topic, the sand covered bed height was neglected, but the effect of sand roughness on channel's bed is embedded as a wall boundary with a roughness height of 1.4 mm.
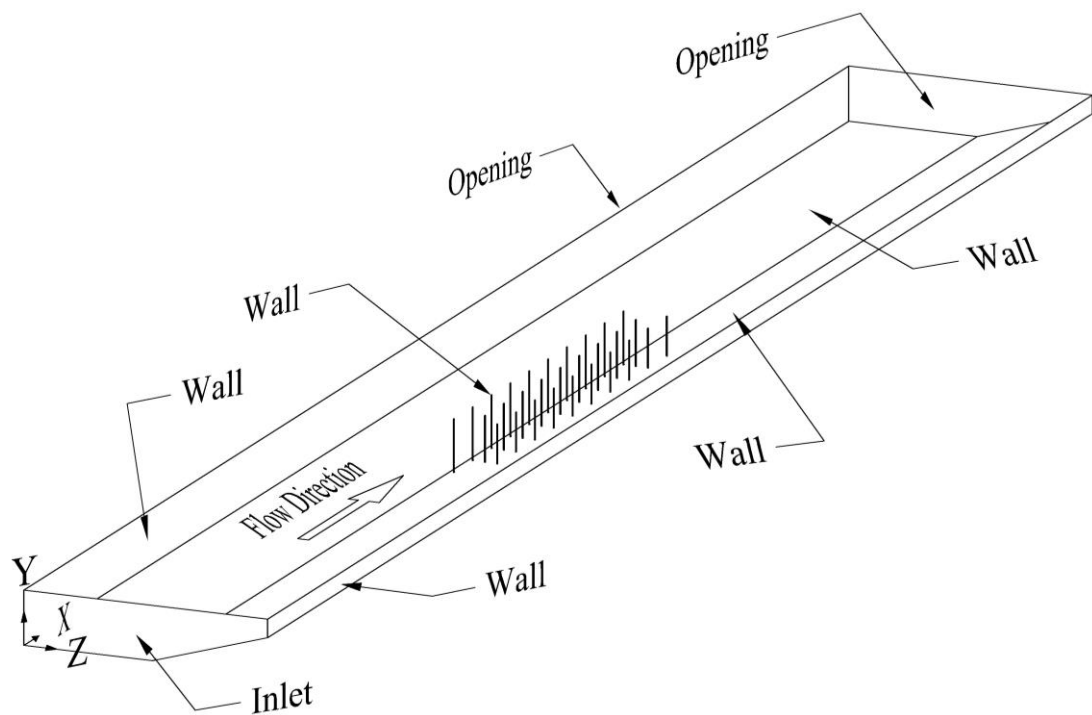
Figure 3.12: Boundary condition of channels

3.5 Assumptions

Through the simulation of ambient flow, it was observed that the dimension of the flume is large enough to let the flow become fully developed after 3 meters of the beginning of the channel. Therefore, for simulating other configurations to make

40

model smaller, which makes the reduction in mesh elements and time, the length of the flume for model reduced to 8 meters. In this situation the velocity of flow through inlet selected as a fully developed flow instead of uniform. To let this happen, the results of ambient simulation of cross-section at the 3 meters length from the beginning of ambient channel were chosen as the inlet inputs. After 2 meters of new length, the vegetation placed for 3 meters long. All the results obtained at the cross section that placed 12 centimeters before the last cylinder row.

Chapter 4

RESULTS AND DISCUSSIONS

4.1 Validation of Models

4.1.1 Distribution of Streamwise Velocity in Ambient Flow Conditions

In order to validate the results of computational analyzes of the effect of bank vegetation on main channel flow velocities, the results obtained from Valyrakis et al. (2015) are used. Following figures (Figure 4.1-4.10), shows the results of Valyrakis et al. (2015) as a dot plot for reporting the point velocity of flow at laboratory conditions measured by Acoustic Doppler Velocity meter (ADV) and the profile given as line is the results obtained in this study by computational analyses. The measurements are done at 200, 400, 600, 750, 850, 900, 965, 1045, 1125 and 1205 mm away from the vertical bank of the open channel.

The experimental results and the computationally obtained data were in good agrees. The logarithmic velocity profiles are also following the same path with the experimental results, except some deviations. In order to estimate the magnitude of these differences, root mean square error analyses were applied.

$$RMS_E = \sqrt{\frac{\sum_{i=0}^{m}\left(u_{i\,predicted} - u_{i\,actual}\right)^2}{m}} \tag{4.1}$$

Where m is the total number of data point.

Since the laboratory results received from experiments has high probability error close to the bed of the channel, RMS_E analysis were proceeded for those data obtained above 8 mm from bed of the channel. Also, the data measured above the inclined bank were omitted since, the depth of the flow was not high enough to capture good results for RMS_E calculations.

RMS_E is useful whenever it is required to calculate the difference between the predicted values from numerical or computational analyses and the observed values. By this way, the magnitude of fitted quality of the two data can be compared.

The results of root mean square errors for all the data are shown in Figure 4.11. The results show that the simulation results are in acceptable range when compared to experimental data.
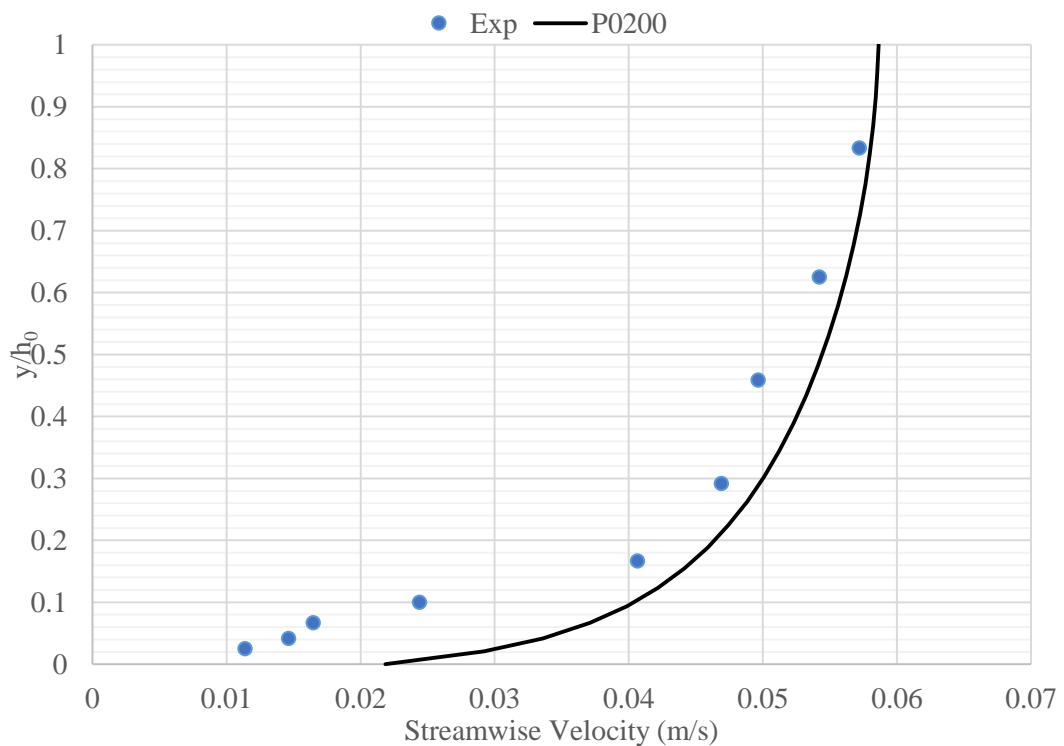
Figure 4.1: Comparisons between experimental data and simulation results at 200 mm from vertical channel wall
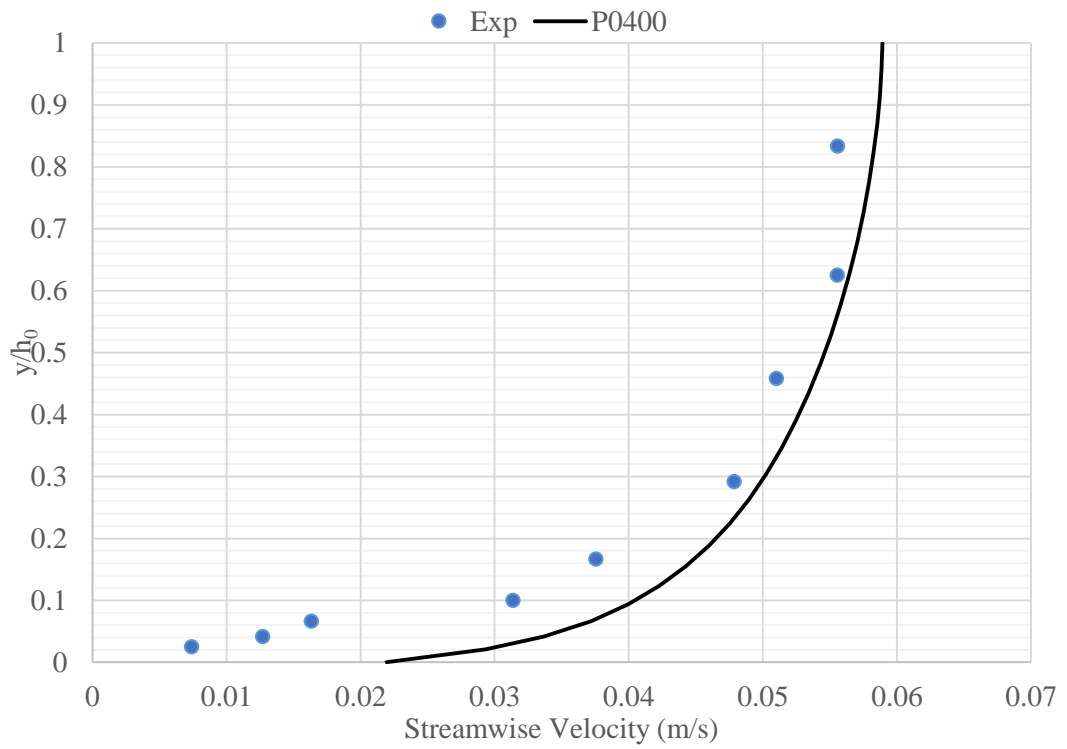
Figure 4.2: Comparisons between experimental data and simulation results at 400 mm from vertical channel wall
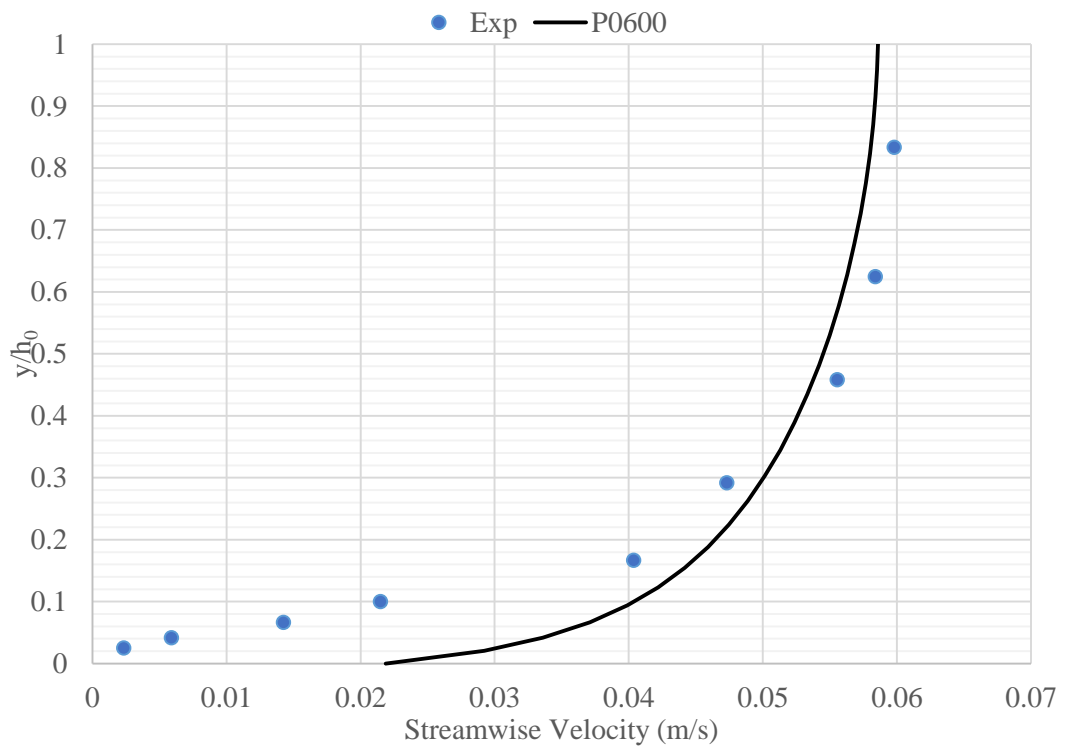
Figure 4.3: Comparisons between experimental data and simulation results at 600 mm from vertical channel wall
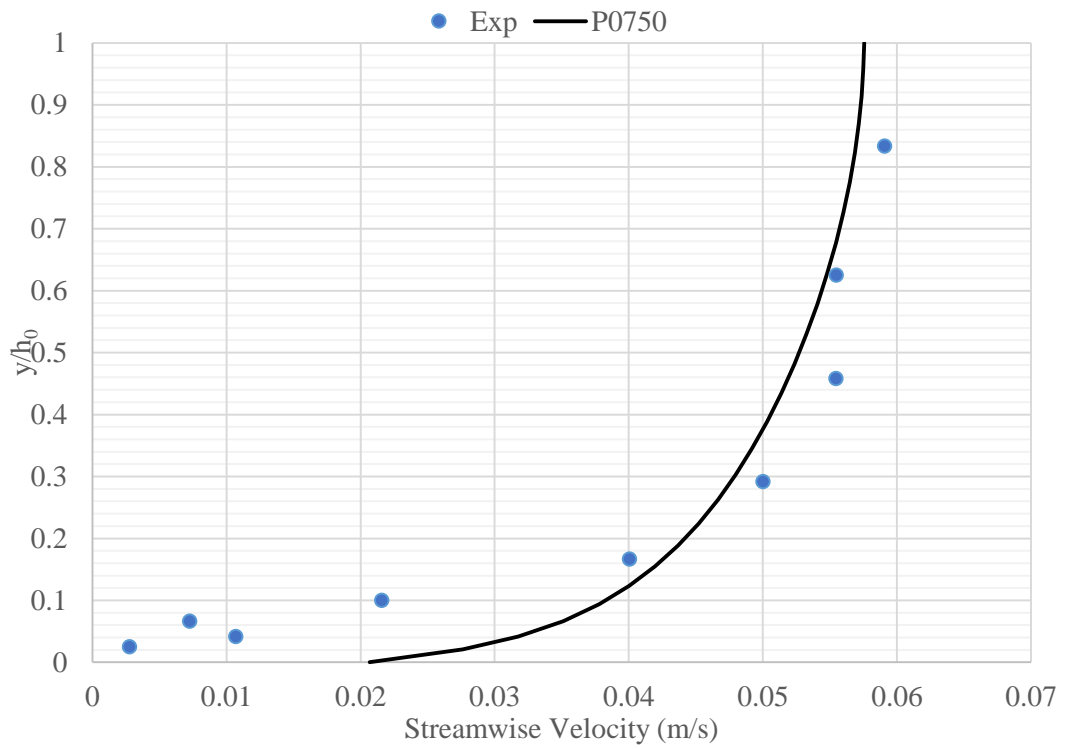
Figure 4.4: Comparisons between experimental data and simulation results at 750 mm from vertical channel wall
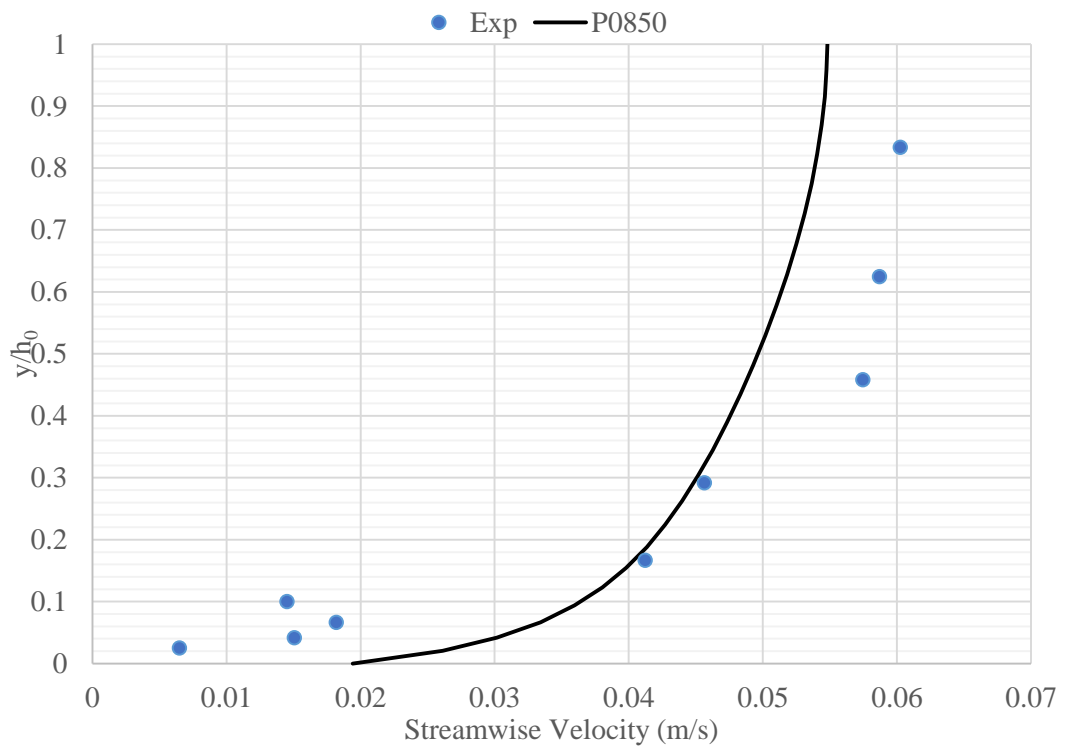
Figure 4.5: Comparisons between experimental data and simulation results at 850 mm from vertical channel wall
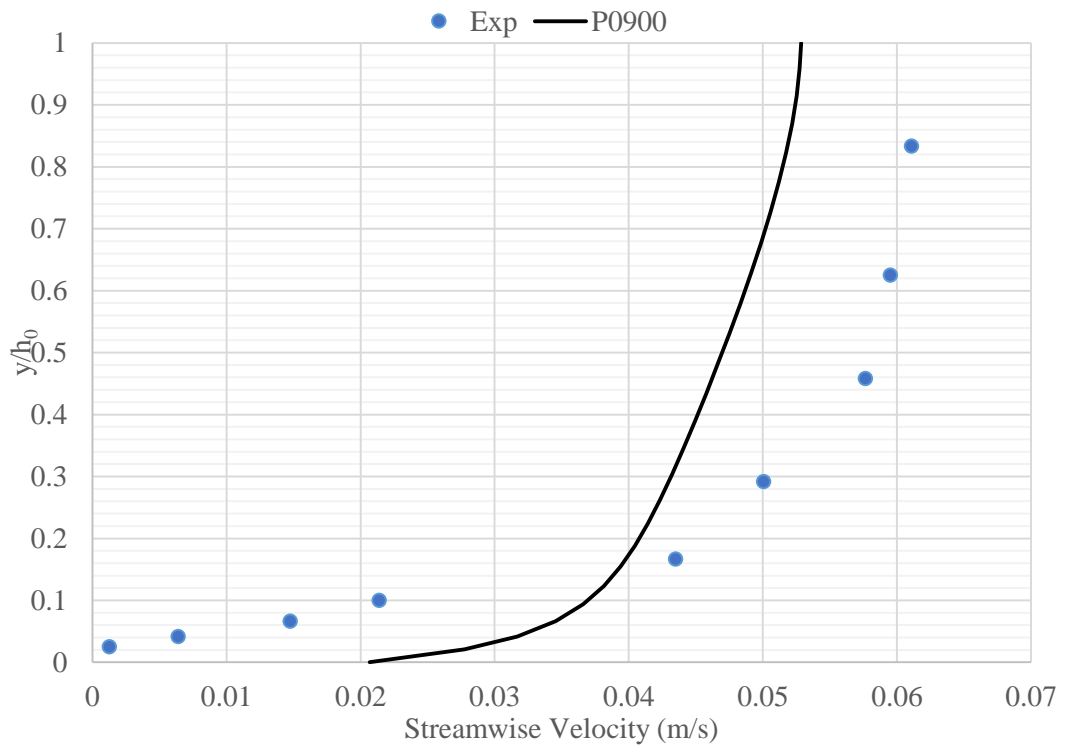
Figure 4.6: Comparisons between experimental data and simulation results at 900 mm from vertical channel wall
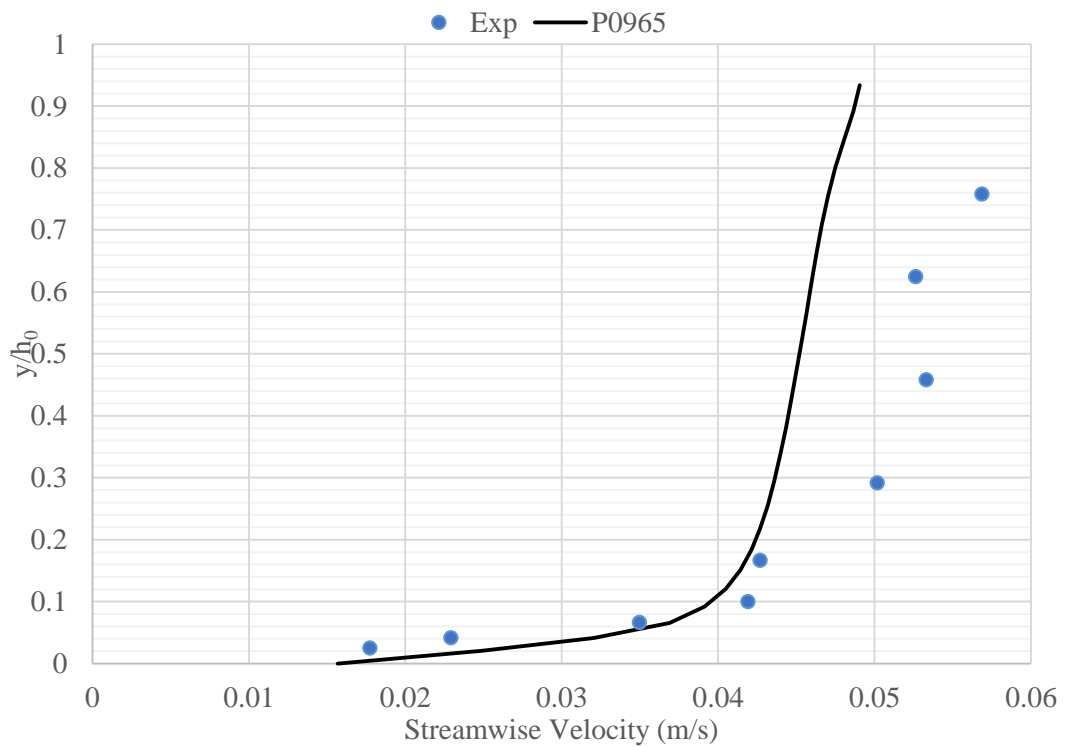
Figure 4.7: Comparisons between experimental data and simulation results at 965 mm from vertical channel wall
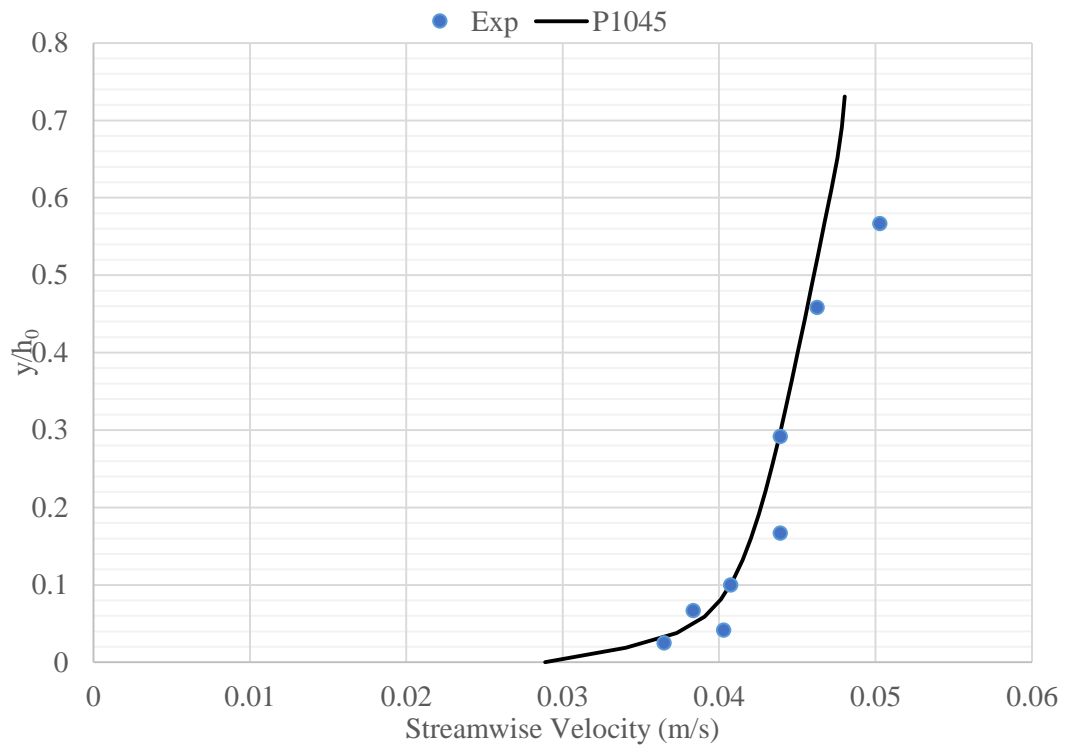
Figure 4.8: Comparisons between experimental data and simulation results at 1045 mm from vertical channel wall
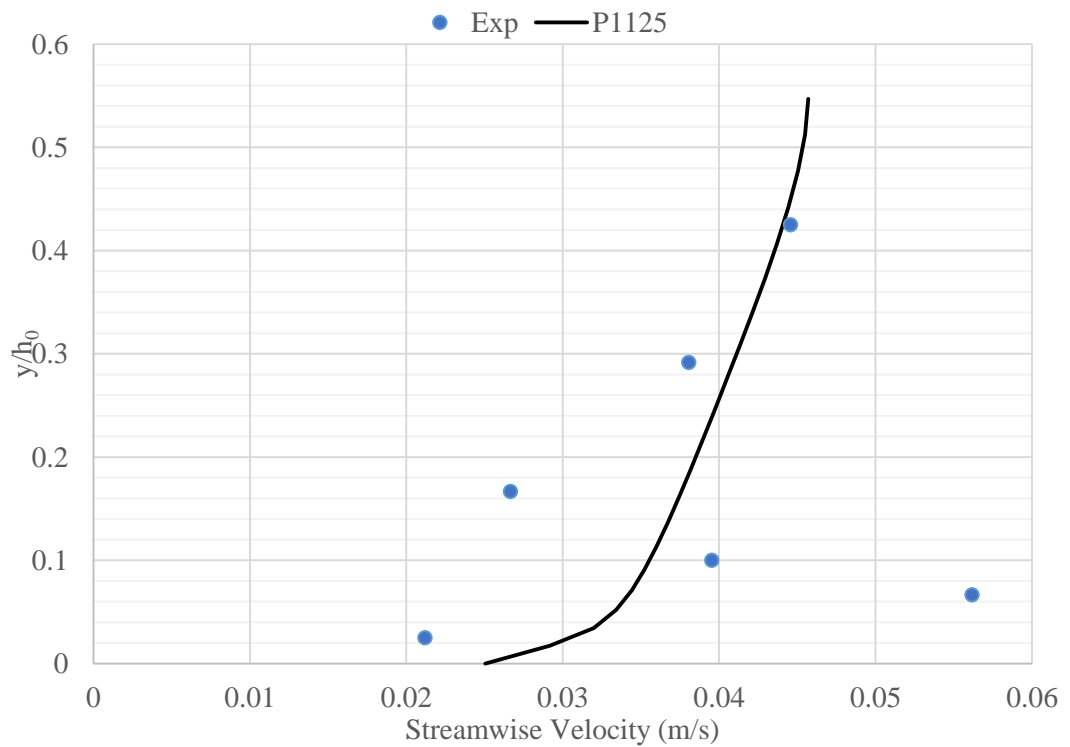
Figure 4.9: Comparisons between experimental data and simulation results at 1125 mm from vertical channel wall
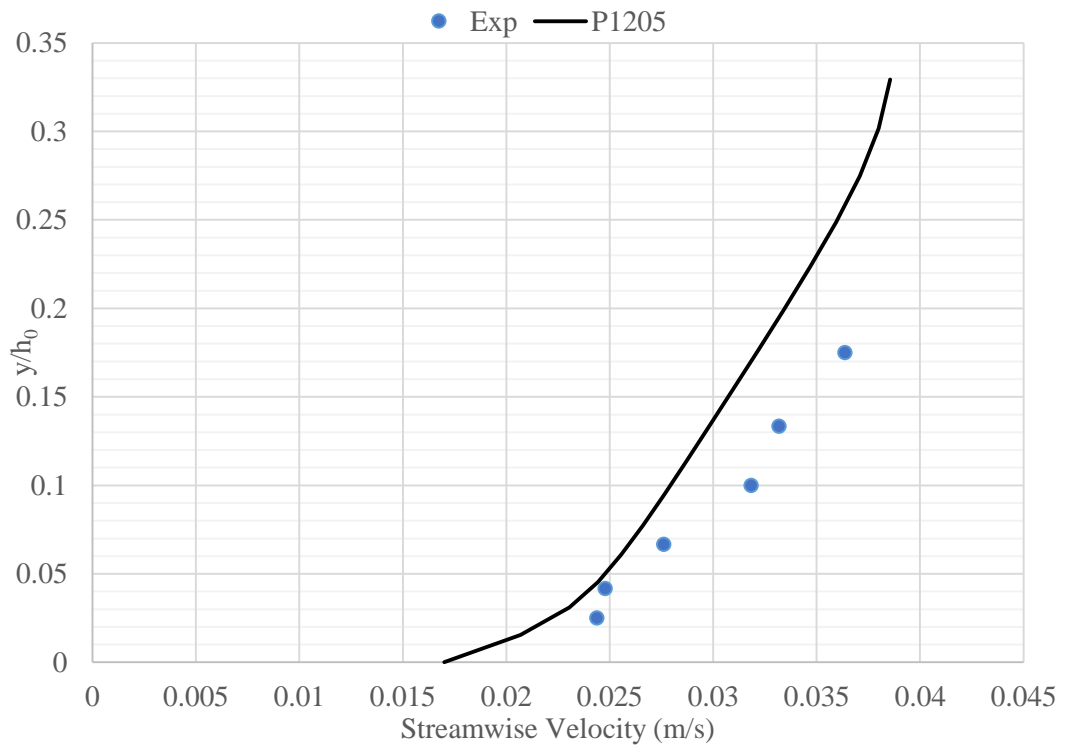
Figure 4.10: Comparisons between experimental data and simulation results at 1205 mm from vertical channel wall
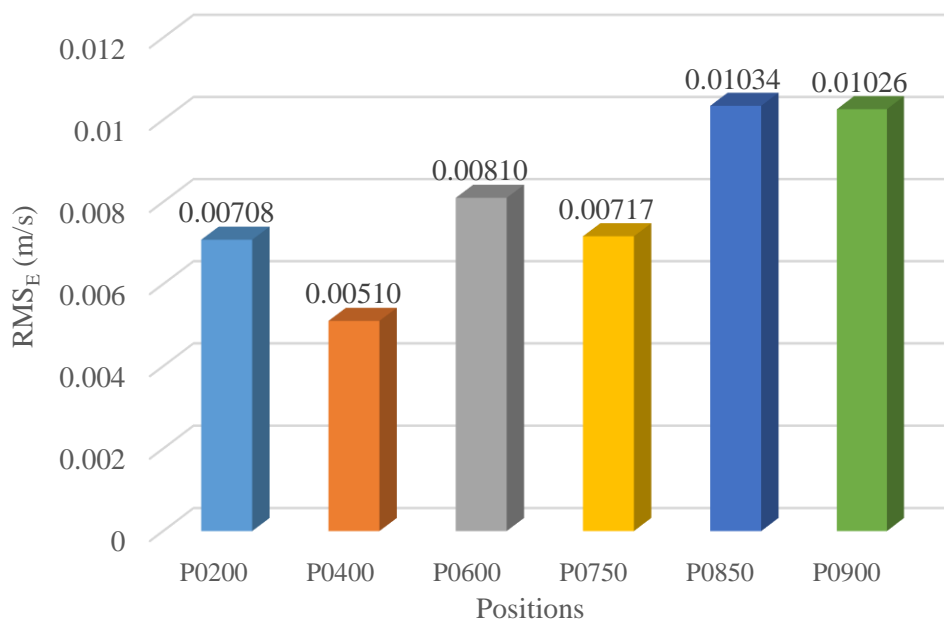
Figure 4.11: Results of RMS_E between the experiment and the simulation data for different positions

The maximum RMS_E, occurs at a section 850 mm away from vertical channel's wall.

As it can be seen from Figure 4.11, by approaching to the vertical bank this magnitude decreases. The amount of error in between the laboratory results and the simulation changes in between 10 to 20%. These results show that the errors are in acceptable range.

4.2 Results and Discussion

4.2.1 Results and Discussion on Time Average Velocity Based Distribution

One of the aims of this study was to observe, how the rigid bank vegetation affects the flow velocity in the main channel. Wide channel (width 1.8 m) is also providing a chance to delineate the necessary width, where the effect of rigid bank vegetation minimum.

Figure 4.12-4.21 show the results of computational analyses of longitudinal velocity profiles at a distance of 200, 400, 600, 750, 850, 900, 965, 1045, 1125 and 1205 mm away from the vertical bank of the open channel. Each Figure show the velocity profile at a fixed distance from the vertical bank for different densities of bank vegetation (Amb, C1, C2, C3, C4, C5).
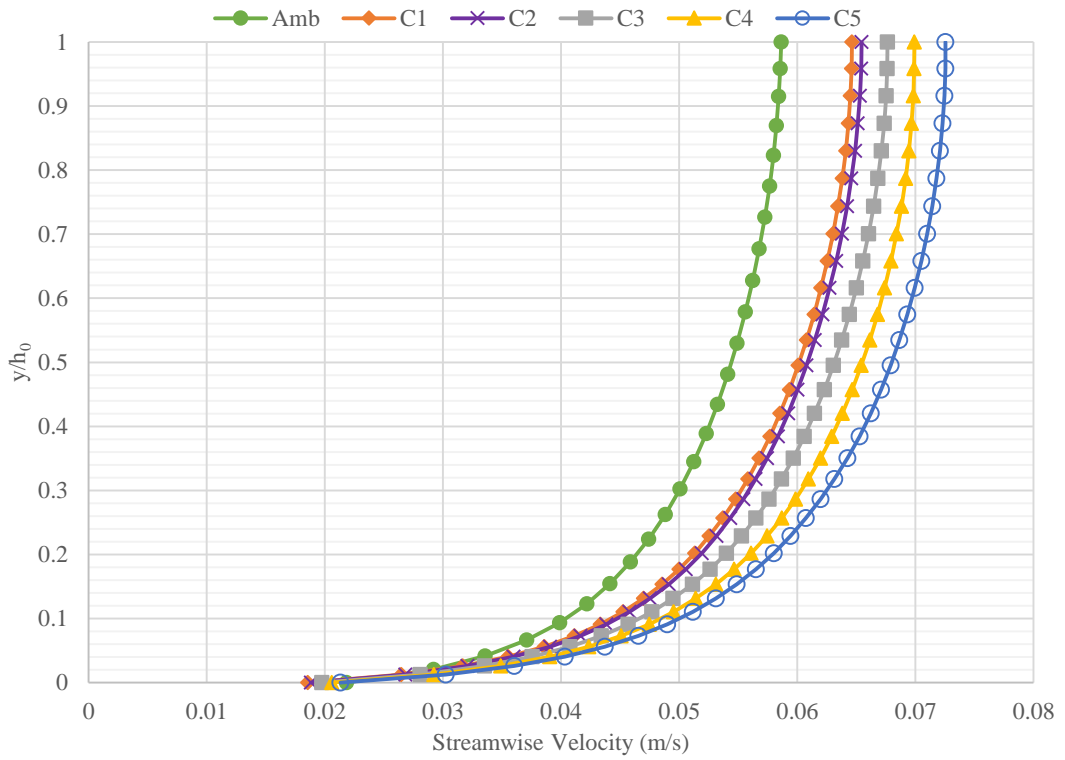
Figure 4.12: Comparisons of velocity profiles at z = 200 mm for different configurations
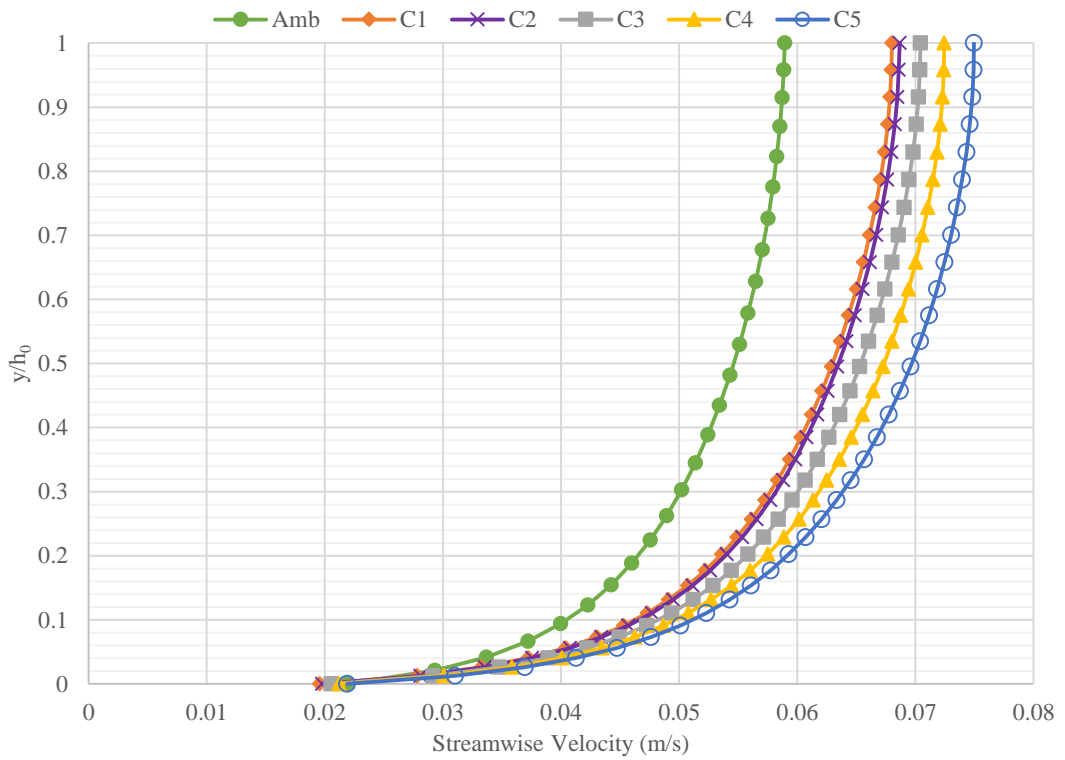
Figure 4.13: Comparisons of velocity profiles at z = 400 mm for different configurations
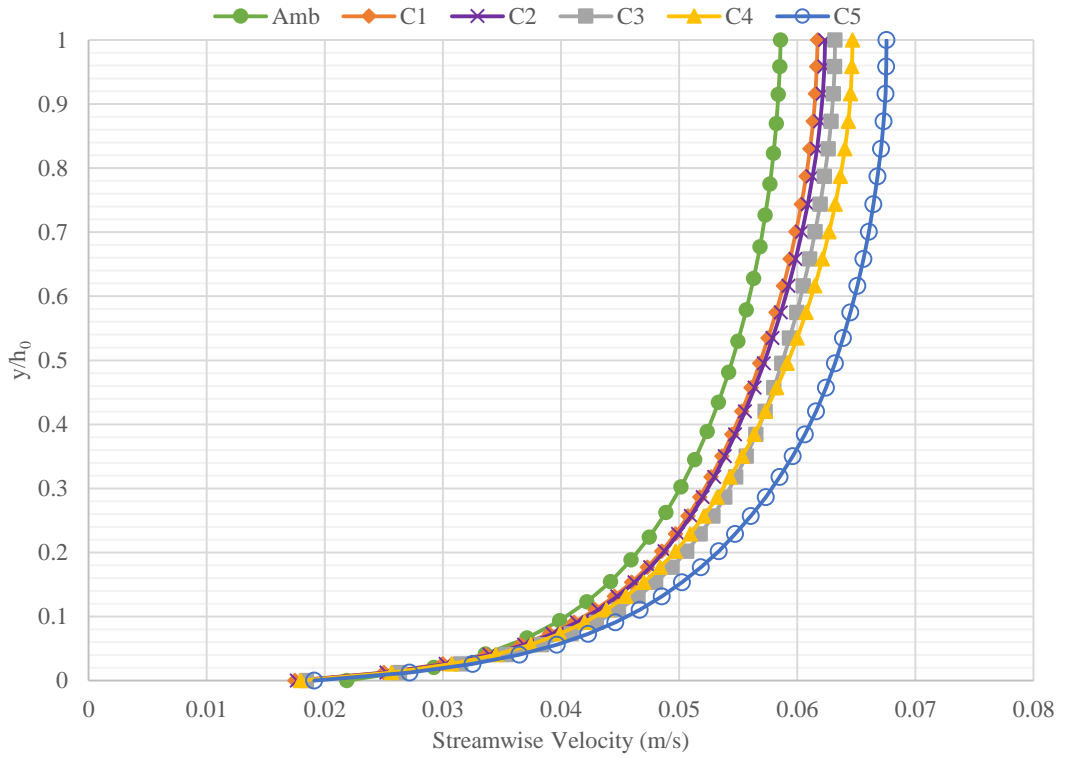
Figure 4.14: Comparisons of velocity profiles at z = 600 mm for different configurations
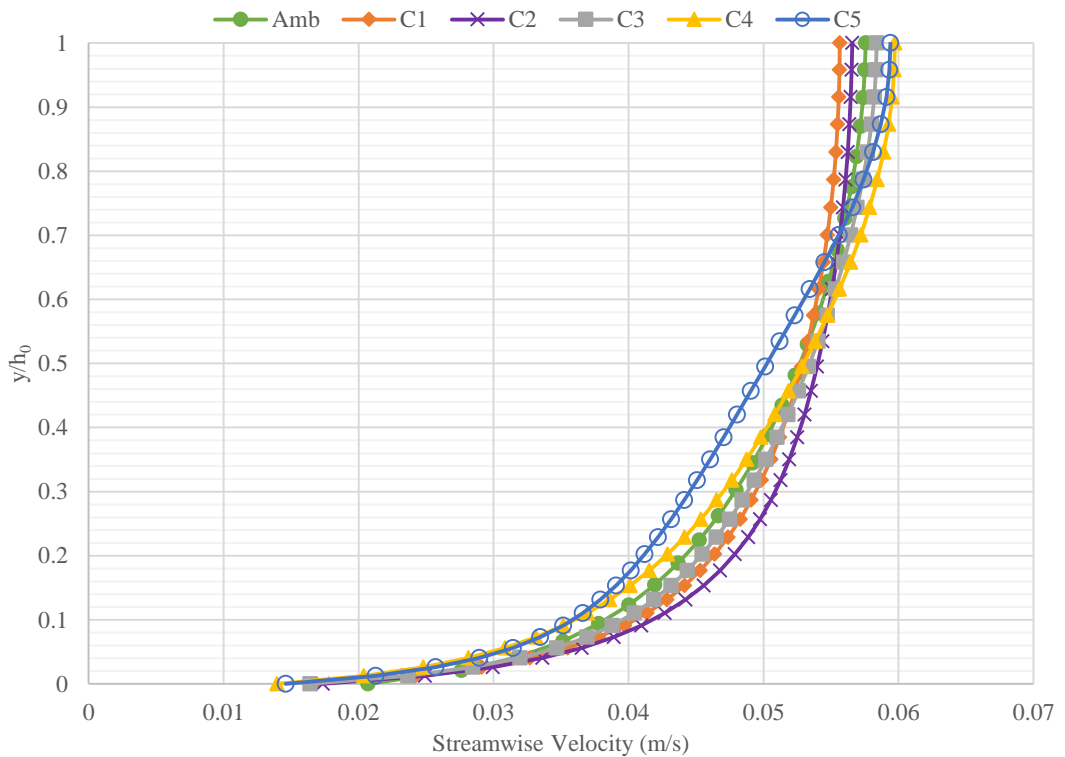
Figure 4.15: Comparisons of velocity profiles at z = 750 mm for different configurations
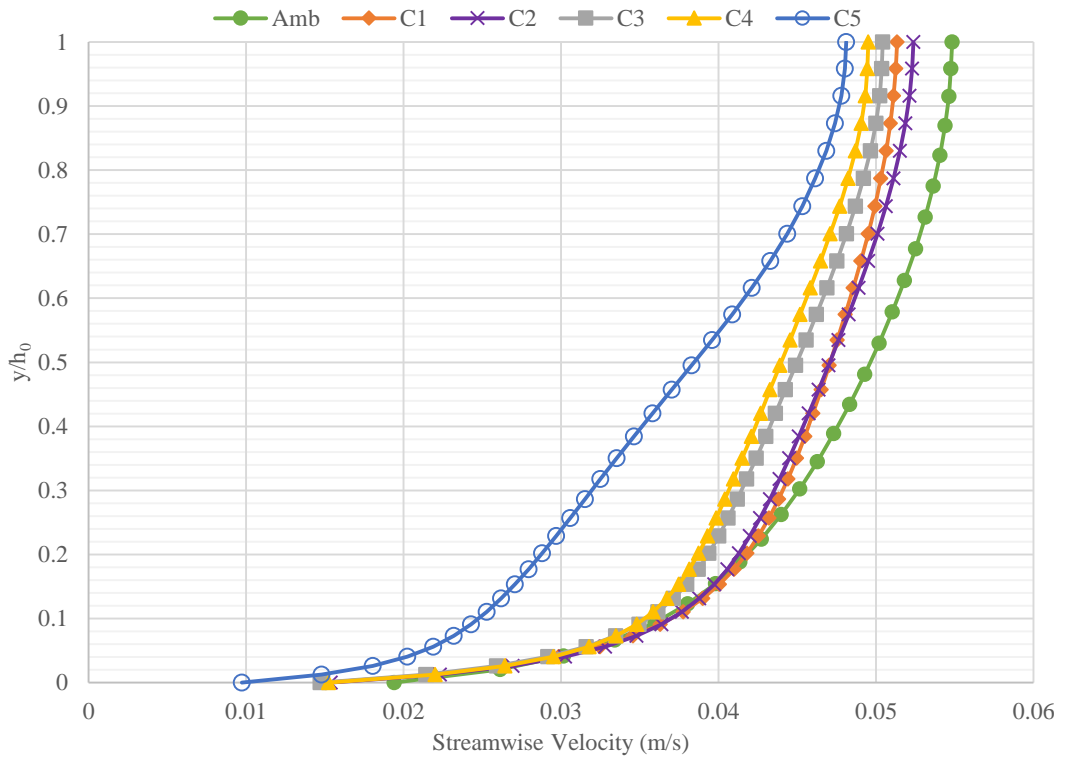
Figure 4.16: Comparisons of velocity profiles at z = 850 mm for different configurations
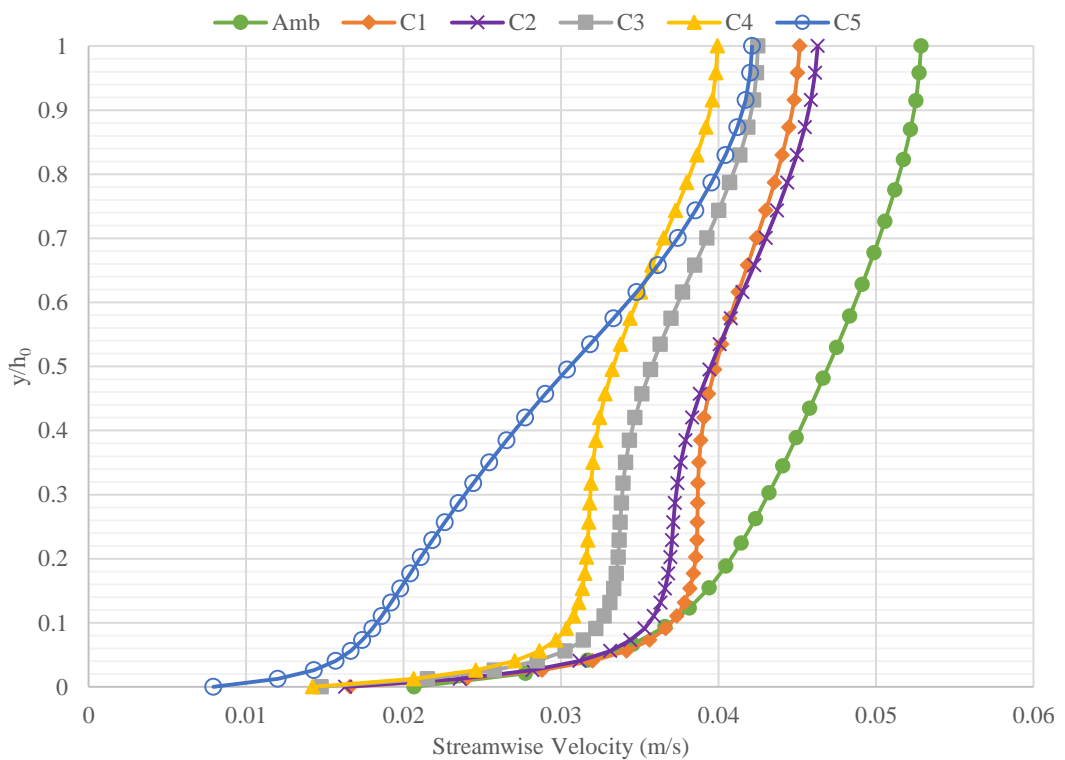
Figure 4.17: Comparisons of velocity profiles at z = 900 mm for different configurations
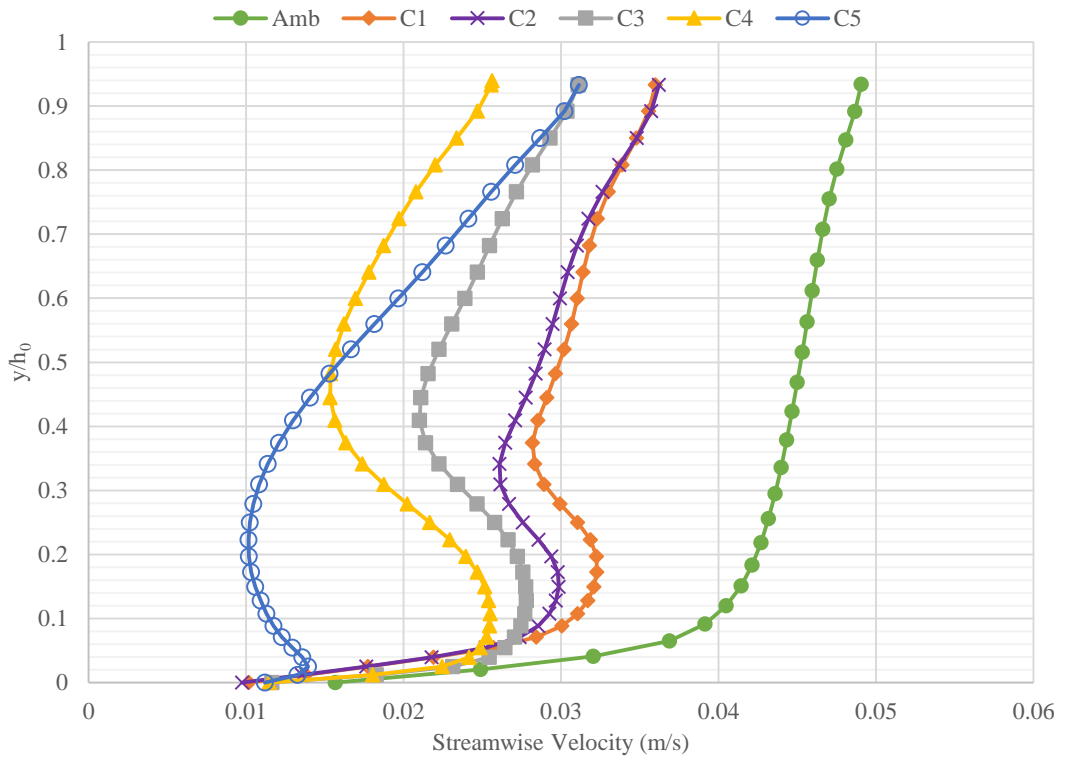
Figure 4.18: Comparisons of velocity profiles at z = 965 mm for different configurations
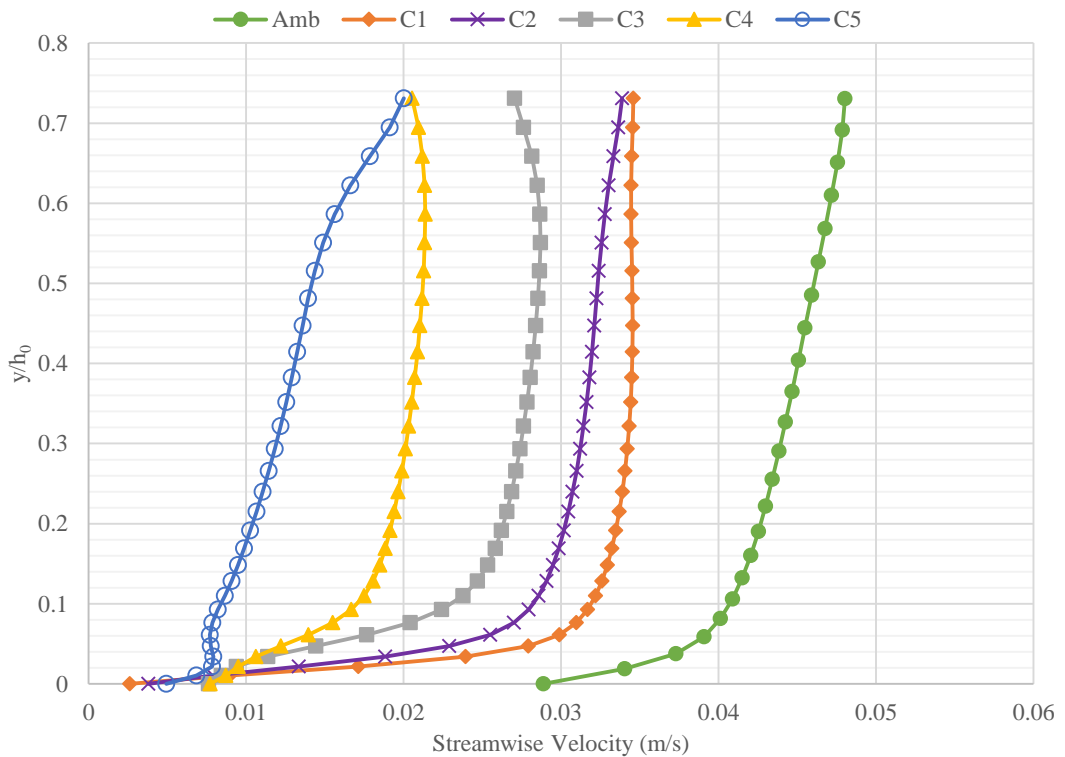
Figure 4.19: Comparisons of velocity profiles at z = 1045 mm for different configurations
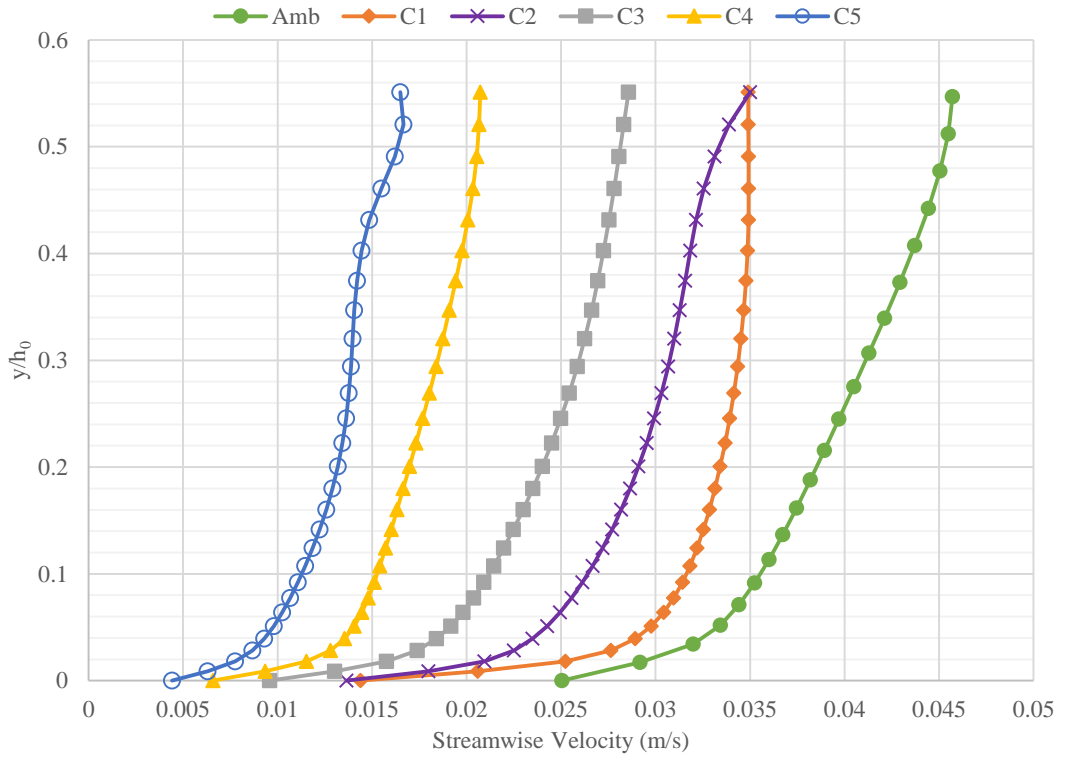
Figure 4.20: Comparisons of velocity profiles at z = 1125 mm for different configurations
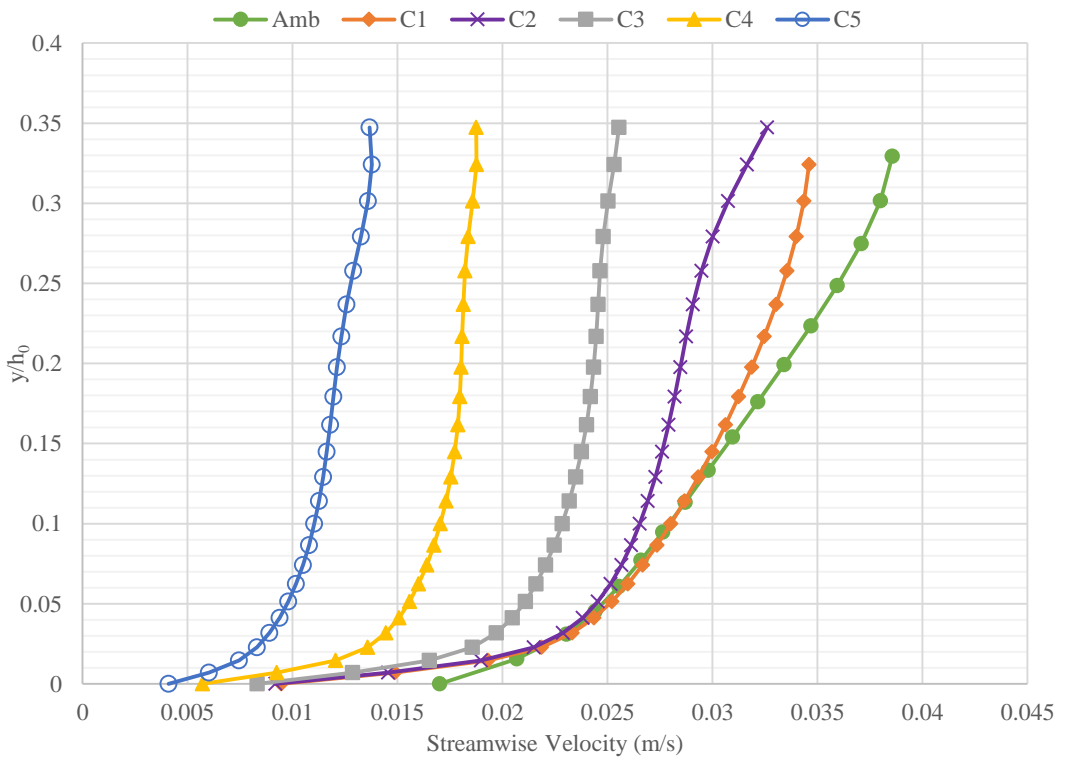
Figure 4.21: Comparisons of velocity profiles at z = 1205 mm for different configurations

Once the bank of the channel is covered with rigid vegetation, the velocity profiles in Figure 4.12-4.21 show variances as long as one goes away from the inclined vegetated bank. Actually, the results can be divided into two sections; one as flow characteristics at the main channel and the other flow characteristics within the inclined bank.
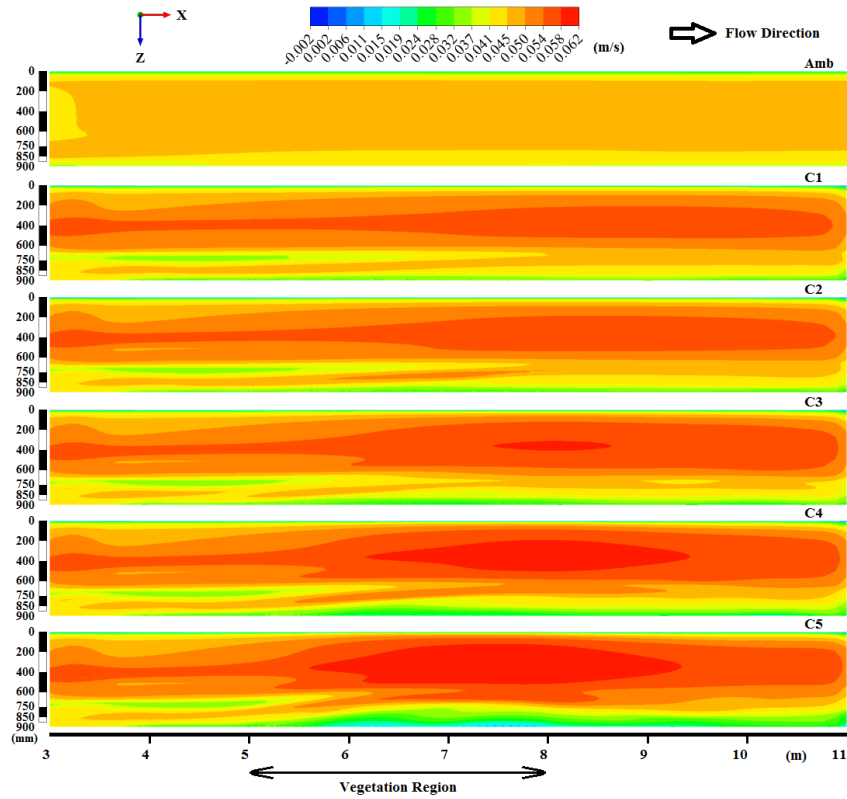
Figure 4.22: Plan view of streamwise velocity at $y/h_0 = 0.25$ due to effect of vegetation region
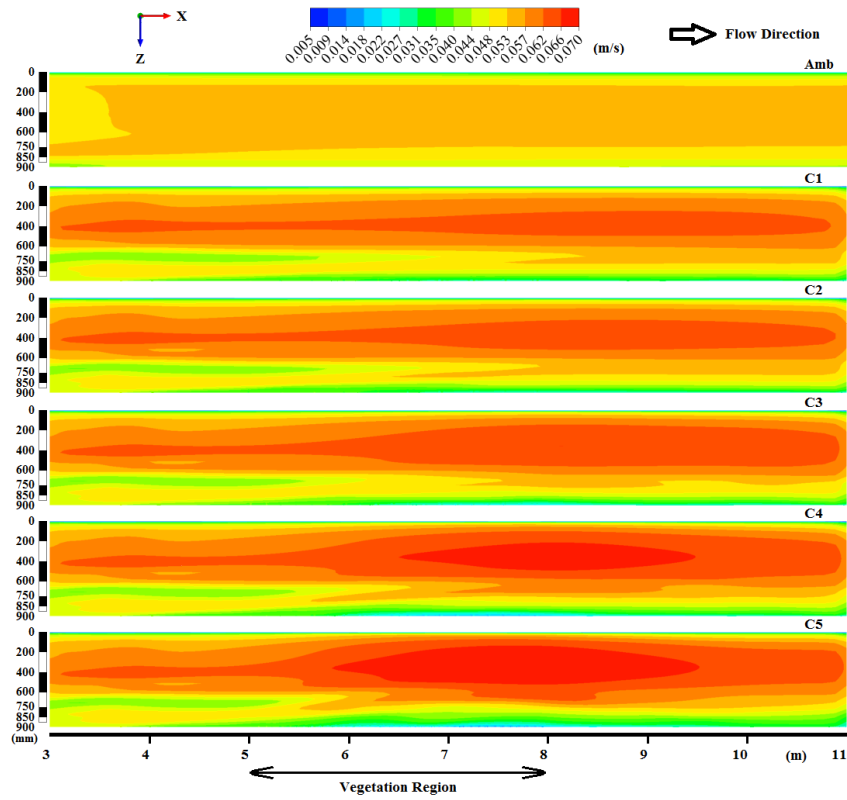
Figure 4.23: Plan view of streamwise velocity at $y/h_0 = 0.5$ due to effect of vegetation region
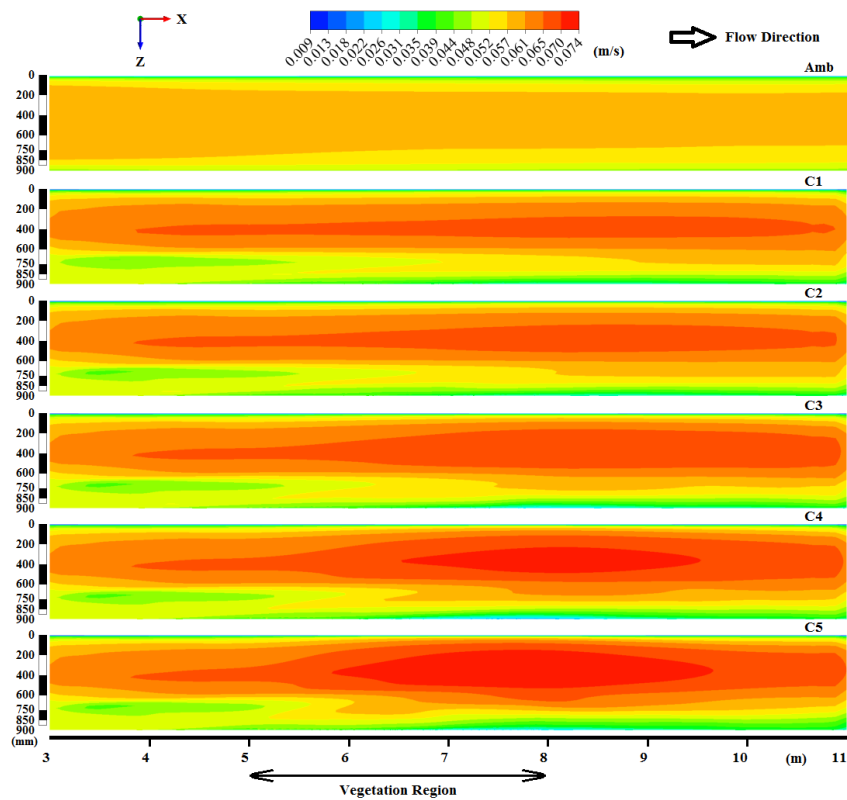
Figure 4.24: Plan view of streamwise velocity at $y/h_0 = 0.75$ due to effect of vegetation region

56
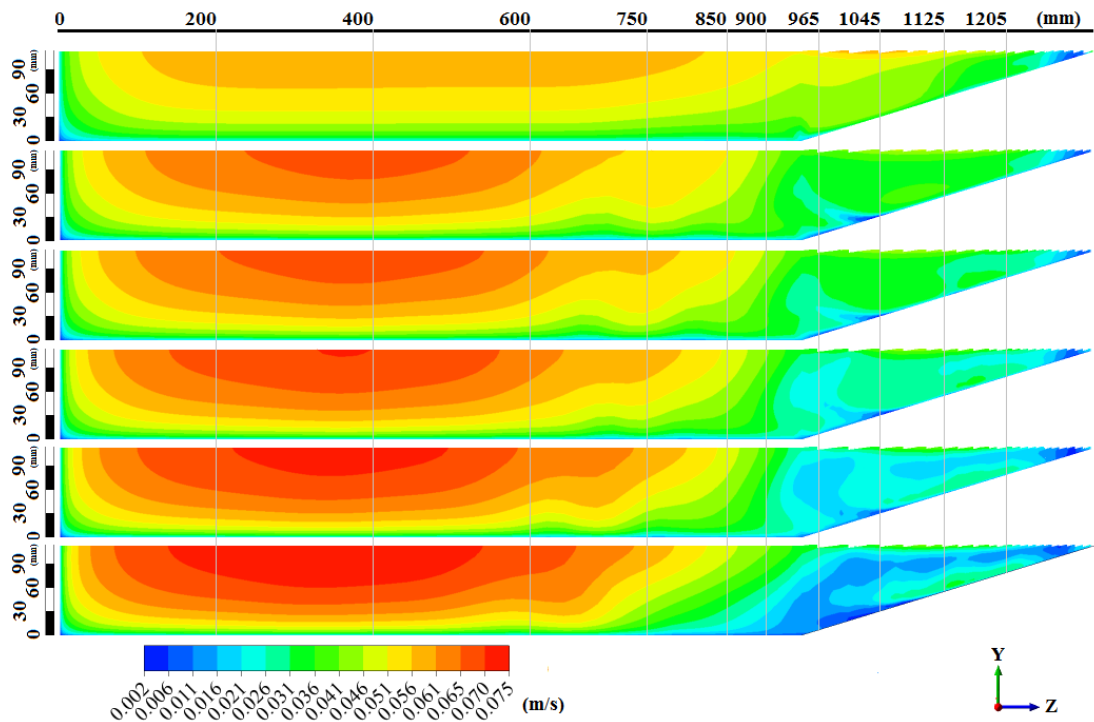
Figure 4.25: Velocity contours at cross-section placed 12 cm before last vegetation

4.2.1.1 Velocity Profile at the Main Channel

It is clear that the velocity profile at and after 850 mm away from vertical bank (just main channel side of main channel/bank interface and after) shows that, the mean flow velocity at ambient flow conditions is bigger than the mean velocity with bank vegetation (Figure 4.16-4.21). As the density of vegetation increases the mean velocity in the channel decreases (Figure 4.16). However, vice-versa occurs as one moves away from the inclined bank. At 200 mm away from interface, all the velocity profiles get close to each other and follows similar logarithmic profiles as ambient flow (Figure 4.15).

When the velocity profiles at sections before 750 mm away from the vertical bank, are under consideration, it is clear that as it was expected the mean velocity of vegetated configurations are higher than the ambient flow conditions (Figure 4.12-4.14). The

mean velocity of vegetated configurations are increasing as the density of bank vegetation increases.

Another observation from the results depicted that, the magnitude of maximum velocity in the main channel is shifting away from the vegetated bank as the density of vegetation increases. This phenomena can be seen clearly in Figure 4.22-4.24 at different elevation from the channel's bed and also, in Figure 4.25. These Figures also show that, the area with maximum velocities increases as the vegetation becomes denser. The output of Figure 4.25 shows two important results that describes the behavior of main channel with inclined bank vegetation. The cross-sectional view depicts to different maximum velocities in the total flow area. While one of them occurs at the main channel, the second one occurs on the bank. This is the indication of compound channel behavior. Therefore, even though the channel looks like a single channel due to the vegetation at the bank the channel serves as a compound channel. Off course, the vegetation on the bank brings about different roughness surfaces on the channel. This ends up with different roughness on different surfaces that turns the channel into a composite one. As a result the study covers the effect of bank vegetation on the main channel in which the channel is a semi-trapezoidal compound and composite channel. Second, the two maximums in the flow direction, one at the bank other at the main channel, is a proof of interface occurring in between the main channel and the inclined bank.

4.2.1.2 Velocity Profile at the Bank

Even though the velocity profile and changes in profile are not the main objective of this study, flow velocities also discussed since the drag effect of the rigid vegetation is clearly observable. Although, at lower depths of flow, the flow velocity of ambient flow is greater than the others also, the magnitude of velocity decreases as the density

of vegetation increases (Figure 4.19-4.21). On the other hand, the velocity profiles as the bank show more uniform shape than a logarithmic profile. Even S-shape profile is observed when the flow occurs close to the interface of the channel (Figure 4.18). The reason of this S-shape is the secondary currents occurring at the interface of the channel.

4.2.2 Results and Discussions on Reynolds Shear Stress

The turbulent fluctuations in the channel that generates momentum exchange in the flow structure gives birth to Reynolds shear stresses, $-\rho\overline{v'u'}$ (the bar is representing the time average and the prime denoting the fluctuating quantity). Figure 4.26 shows the variations of the magnitude of the Reynolds shear stresses which is calculated by Equation (3.5), along the YZ plane just 12 cm before the end of the vegetation cover. As it was discussed in the previous chapter, the mean velocity in the main channel is higher than velocities in the vegetated inclined bank a huge momentum exchange occurs at the interaction region between the main channel and the vegetated bank of the channel. It is clear in the Figure 4.26 that during the ambient flow conditions the momentum transfer is dominant at the inclined bank since the shear stresses are more due to the inclined surface. Over the bank (inclined surface) the flow velocity becomes less than the velocity over the main channel that initiates a momentum transfer from high velocity to lower velocity regions. Due to this momentum transfer over the inclined surface the shear stresses over the bank increases. During the ambient flow conditions on the other hand, the Reynolds shear stresses becomes comparably small since the flow velocity is not changing in the streamwise direction.

As the density of vegetation increases over the bank of the flow the Reynolds stress attains peak values in the vicinity of the interaction region of the main channel and the

bank. The value of Reynolds stresses are therefore found to be depending on the density of the vegetation and the configuration of the vegetation, the uniform and staggered distribution.
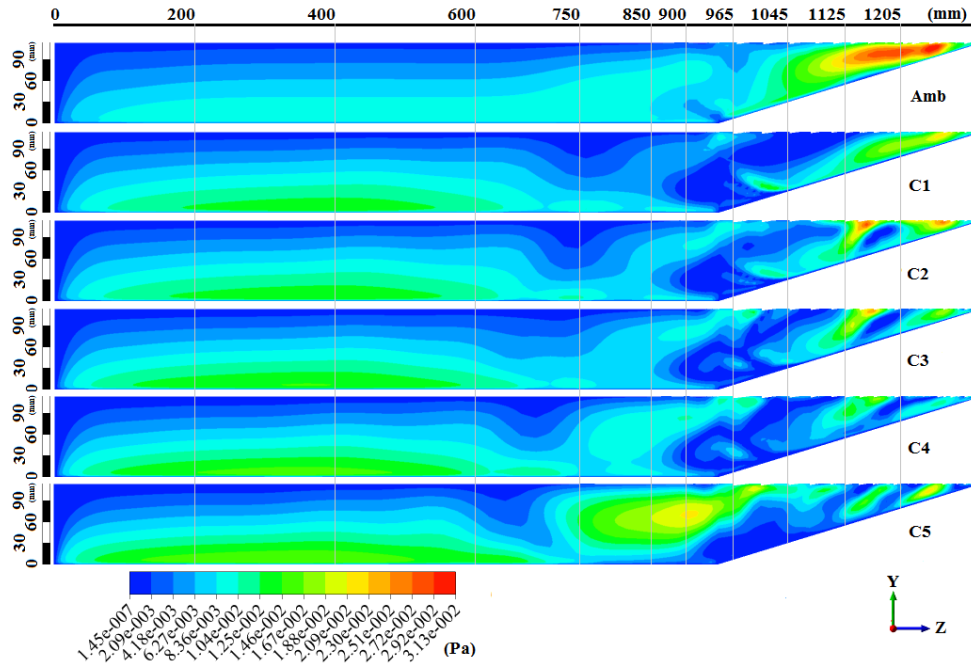

Figure 4.26: Magnitude of Reynolds shear stress at cross section placed 12 cm before end of vegetation

The Reynolds stress profiles that measured perpendicular to the inclined bank for each location at 200 mm, 400 mm, 600 mm, 750 mm, 850 mm, 900 mm, 965 mm, 1045 mm, 1125 mm, and 1205 mm away from the vertical bank are given in Figure 4.27-4.36. Whenever the uniform flow conditions are dominant in open channel flows, the Reynolds shear stress follows linear profile, possessing maximum values at the bed of the channel and the minimum value at the surface of the flow. On the other hand, due to the rigid bank vegetation, the uniform flow is no more pervading due to the turbulent fluctuations and the occurrence of secondary currents. As a result, Reynolds shear stresses distribution follows non-linear structure and shows parabolic shape.
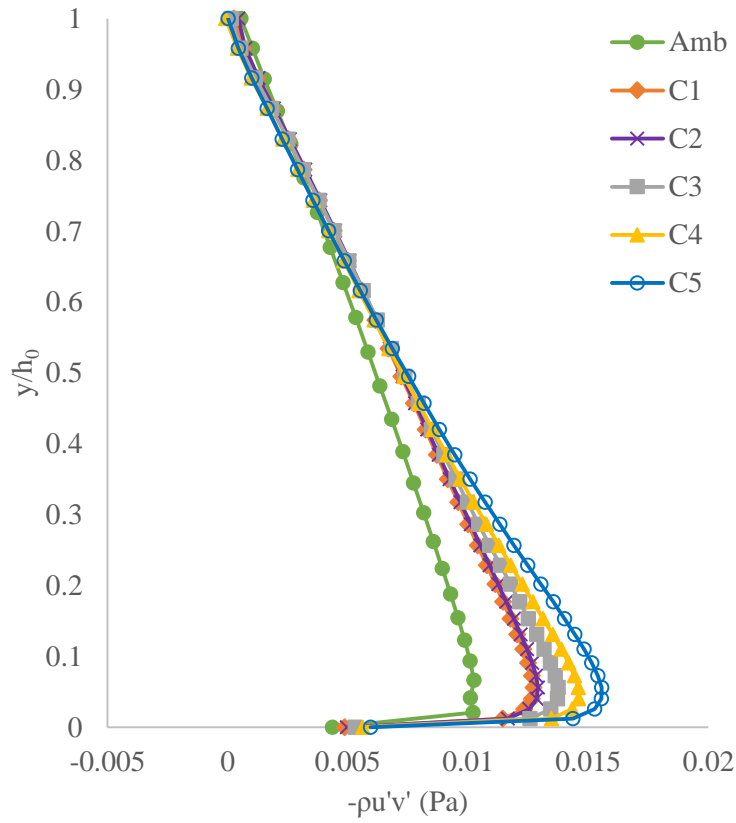
Figure 4.27: The value of Reynolds shear stress at z = 200 mm
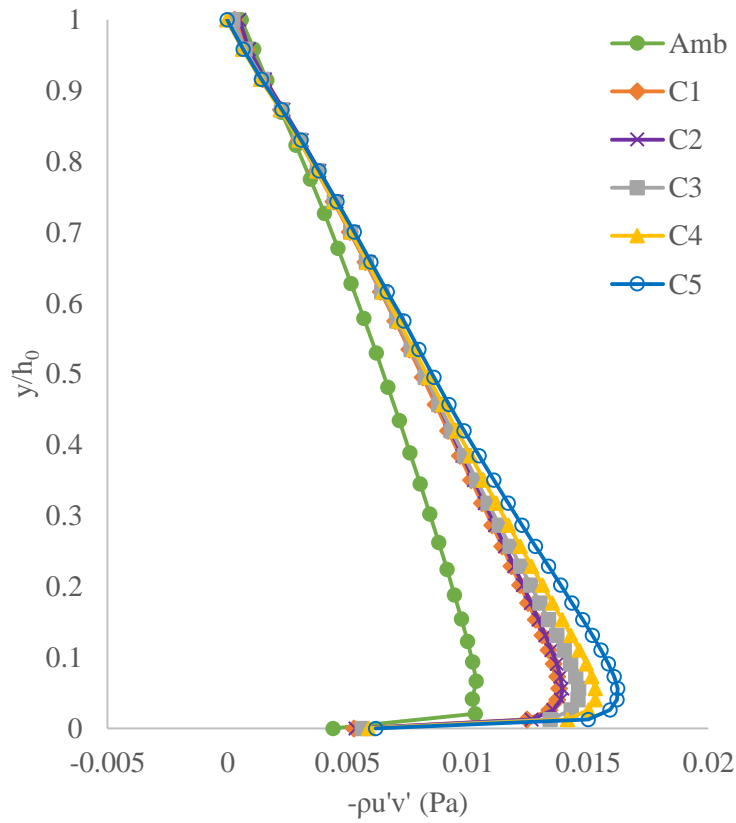
Figure 4.28: The value of Reynolds shear stress at z = 400 mm
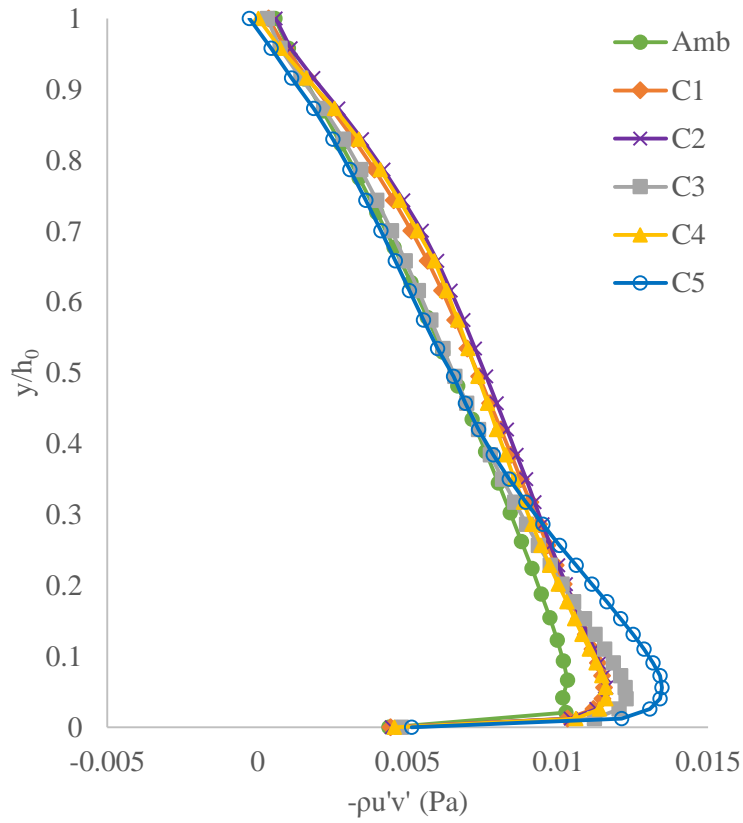
Figure 4.29: The value of Reynolds shear stress at z = 600 mm
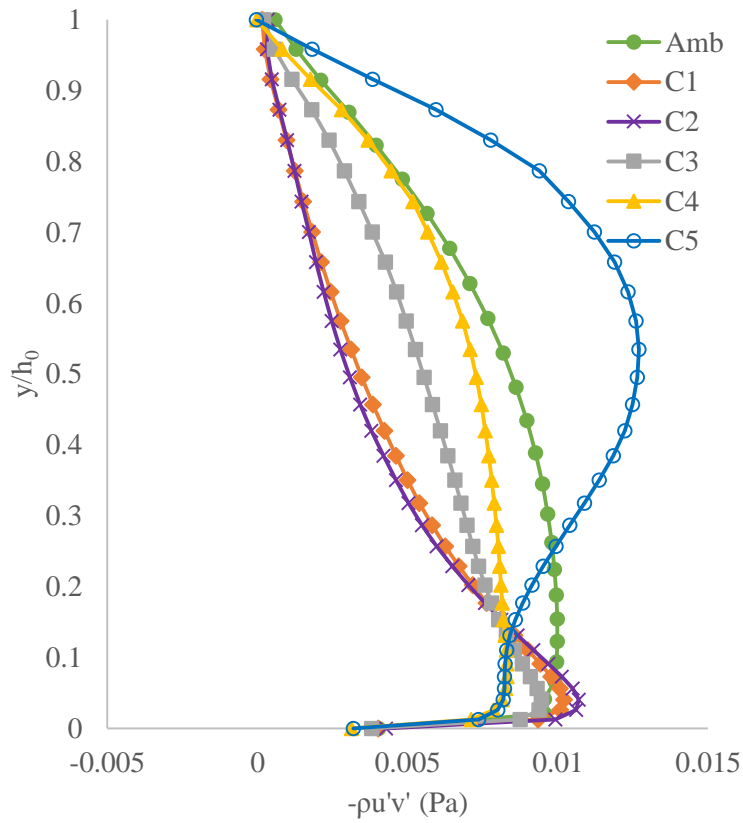
Figure 4.30: The value of Reynolds shear stress at z = 750 mm
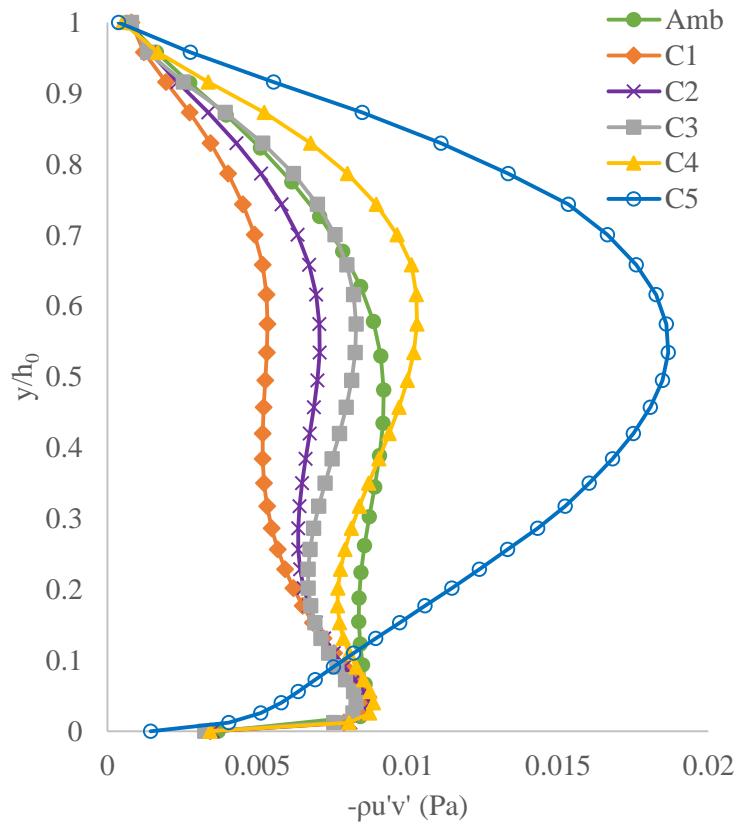
Figure 4.31: The value of Reynolds shear stress at z = 850 mm
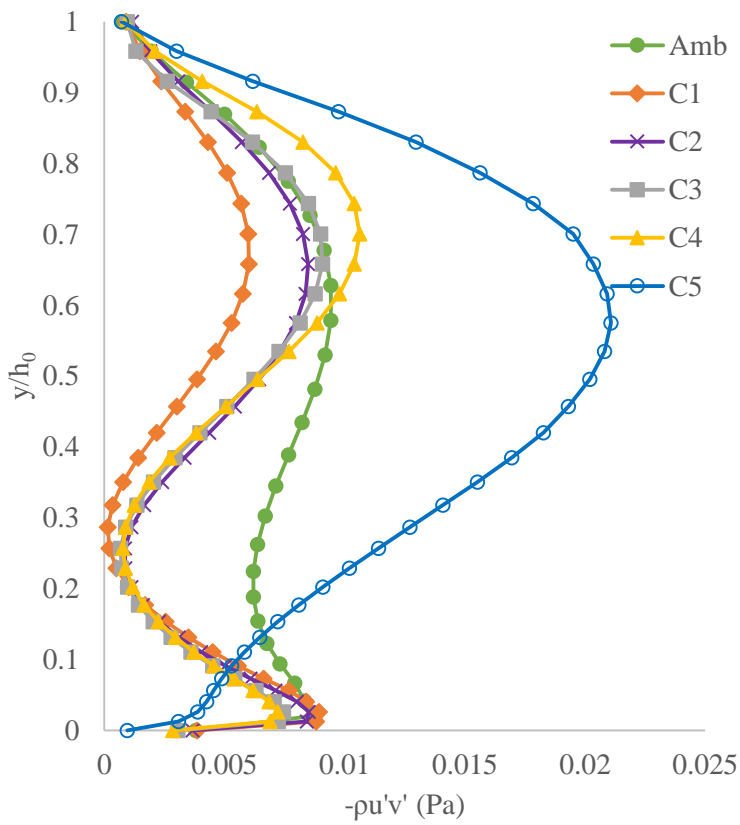
Figure 4.32: The value of Reynolds shear stress at z = 900 mm
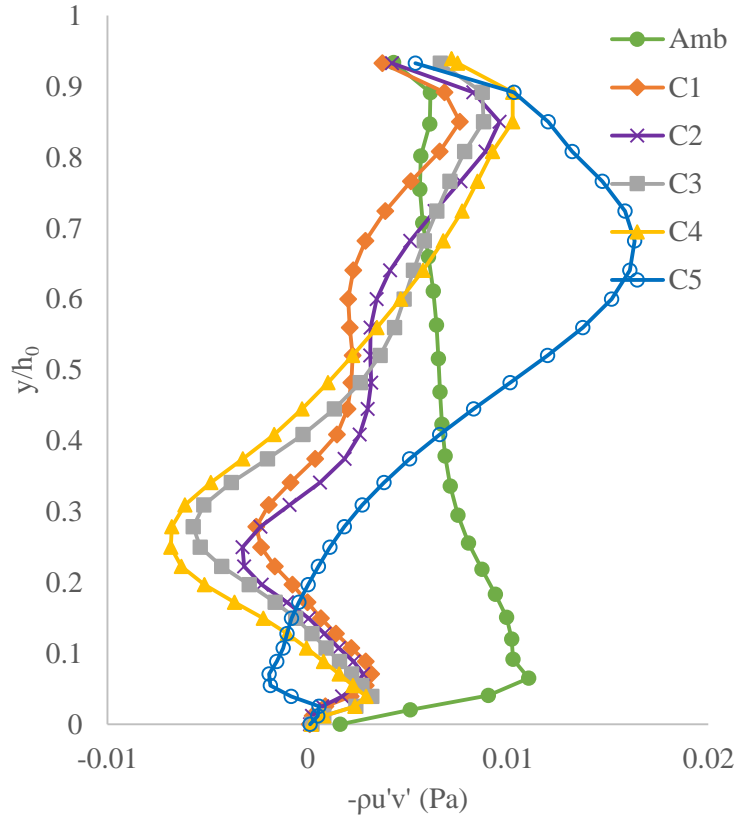
Figure 4.33: The value of Reynolds shear stress at z = 965 mm
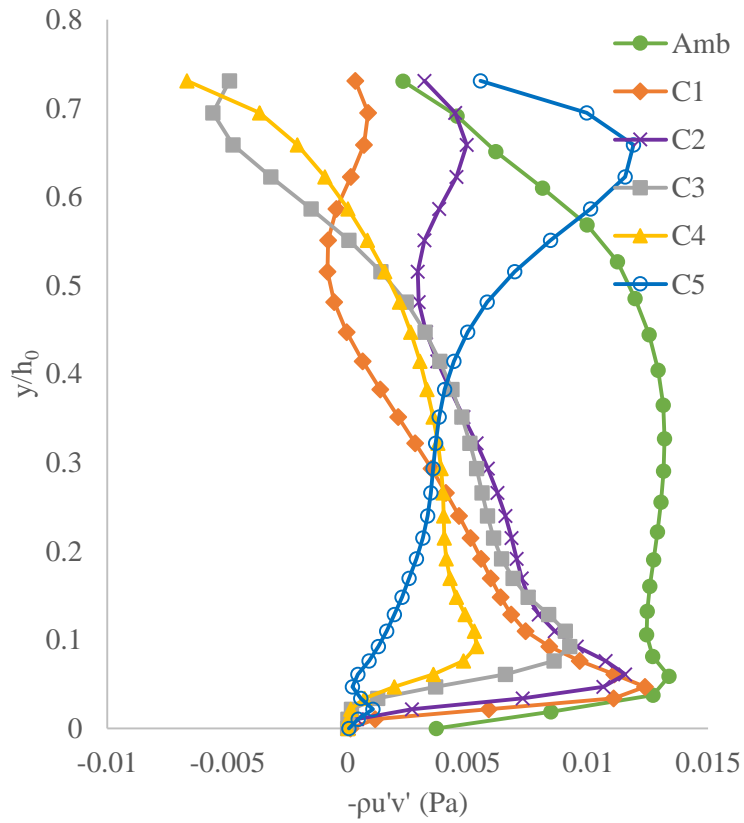
Figure 4.34: The value of Reynolds shear stress at z = 1045 mm
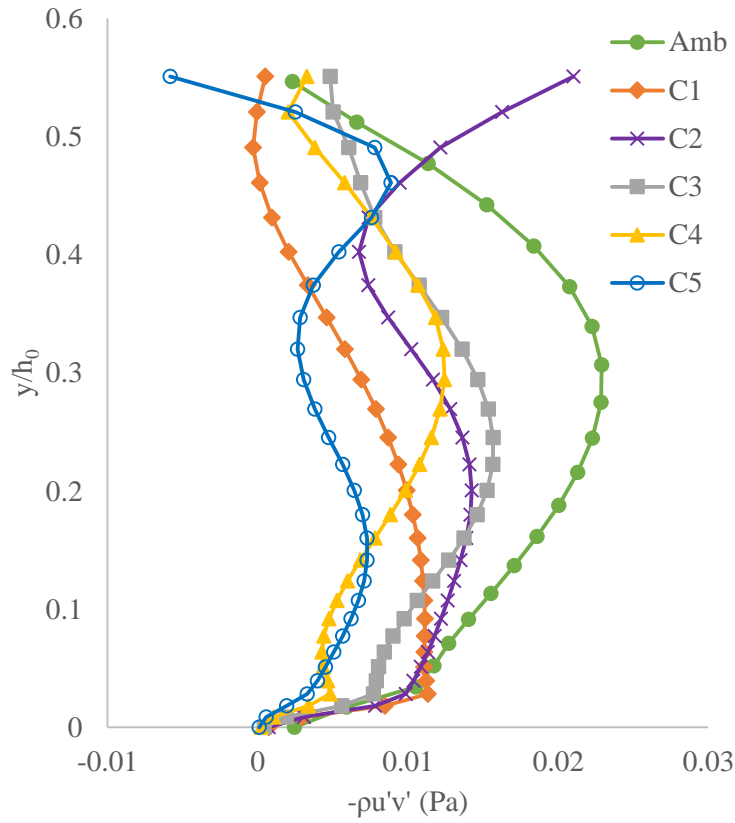
Figure 4.35: The value of Reynolds shear stress at z = 1125 mm
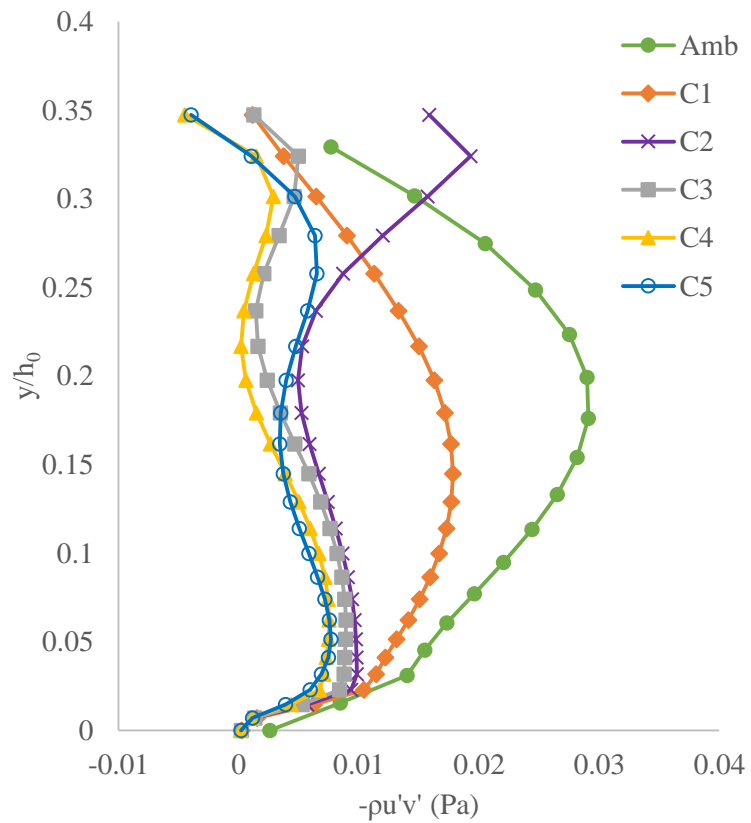
Figure 4.36: The value of Reynolds shear stress at z = 1205 mm

The Reynolds shear stresses represent parabolic distribution between the vertical bank and 600 mm away from it. The maximum Reynolds shear stresses occurs in the vicinity of bed at around $y/h_0 = 0.05$. Comparing the five different configurations of vegetation and the ambient flow for each specific location shows that the maximum Reynolds stresses occurs at high density and minimum Reynolds stresses occurs at ambient flows. The result is supporting the proposed assumptions that mean velocity in the main channel increases as the vegetation density in the channel increases. Mixing of fast main channel flow and the vegetated inclined bank flow induced a momentum exchange that can be easily observable when the section 750 mm away from the vertical bank and other sections are under consideration. The sharp increase in the Reynolds shear stress (0.02 Pa at 900 mm), at configuration 5, experiences reduction while the profile approaches to the interface. Further decrease through the vegetation on the inclined bank finally drops to less than 0.01 Pa at z=1205 mm. Low velocity between the rigid vegetation covers over the inclined bank causes the Reynolds shear stresses to approach to zero. This is because in these regions (over the bank) flow velocity is very small sometimes approaching to almost zero. In addition, negative values of the Reynolds stress are observed in the region due to the velocity retardation effects (due to the drag forces) of the vegetation cover. This is also supporting the results obtained by Afzalimehr and Subhasish (2009).

4.2.3 Results and Discussions on Turbulence Intensity

Turbulent intensities help to calculate how the velocity differs or varies from the mean. In other term, the turbulent intensity gives the strength of the turbulence, in which, large values indicate higher levels of turbulence. Figure 4.37-4.46 show the vertical variation of calculated turbulence intensity for streamwise directions at different locations. As it was before, the computational analyses were performed at 200 mm, 400

mm, 600 mm, 750 mm, 850 mm, 900 mm, 965 mm, 1045 mm, 1125 mm, and 1205

mm away from the vertical bank of the channel. The turbulence intensity in each pro-

file is calculated by using the Equation (2.14) where $u' \equiv \sqrt{2k/3}$ and the result is mul-

tiplied by 100 in order to describe the result in percentages.
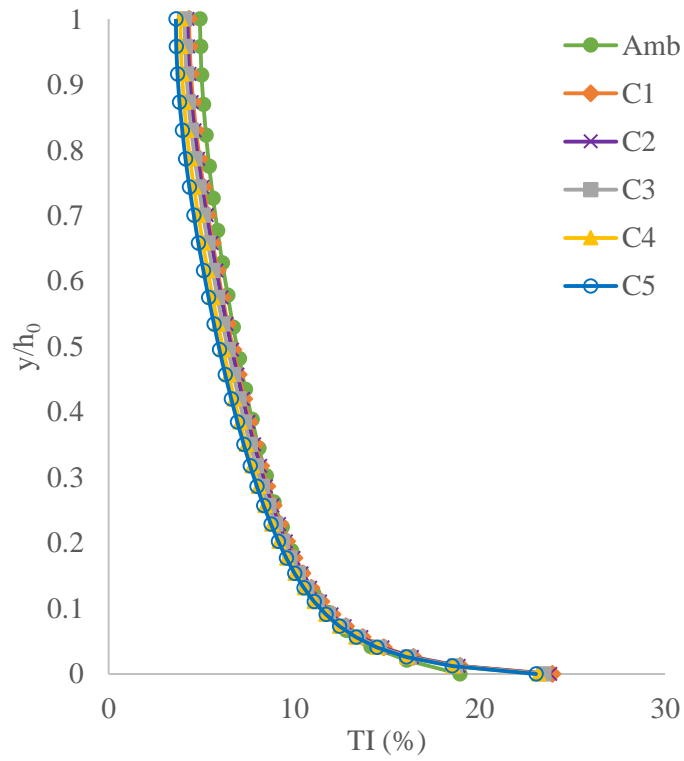
Figure 4.37: Comparison of Turbulence Intensity and vegetation density at z = 200
mm
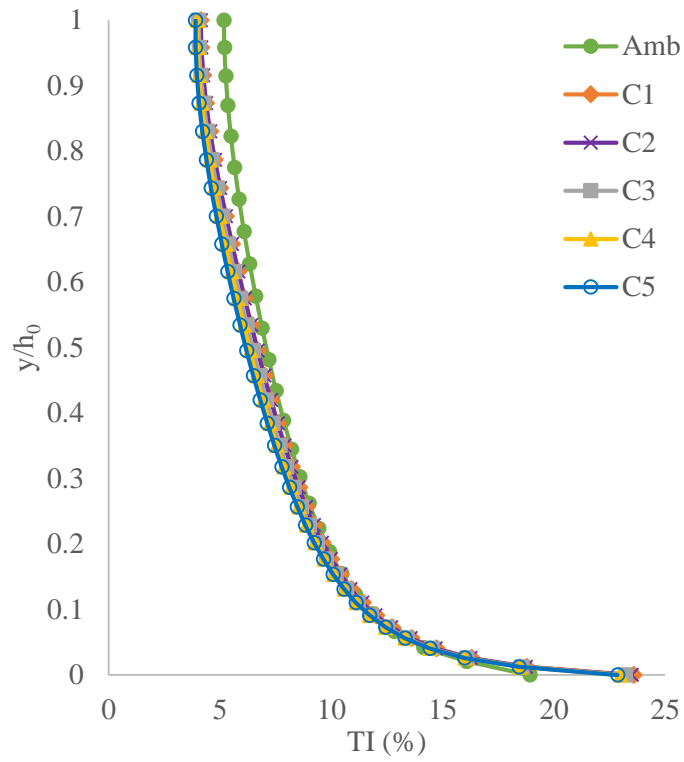
Figure 4.38: Comparison of Turbulence Intensity and vegetation density at z = 400 mm
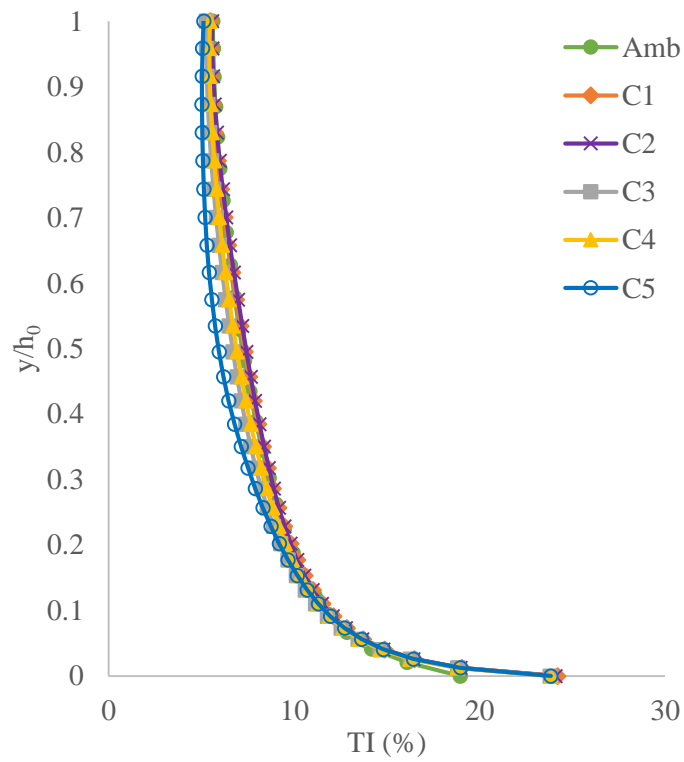
Figure 4.39: Comparison of Turbulence Intensity and vegetation density at z = 600 mm
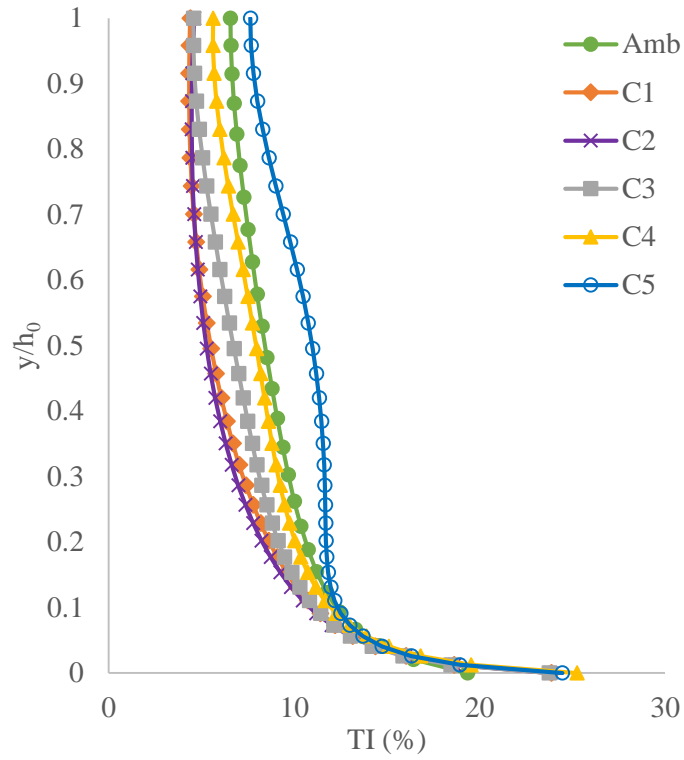
Figure 4.40: Comparison of Turbulence Intensity and vegetation density at z = 750 mm
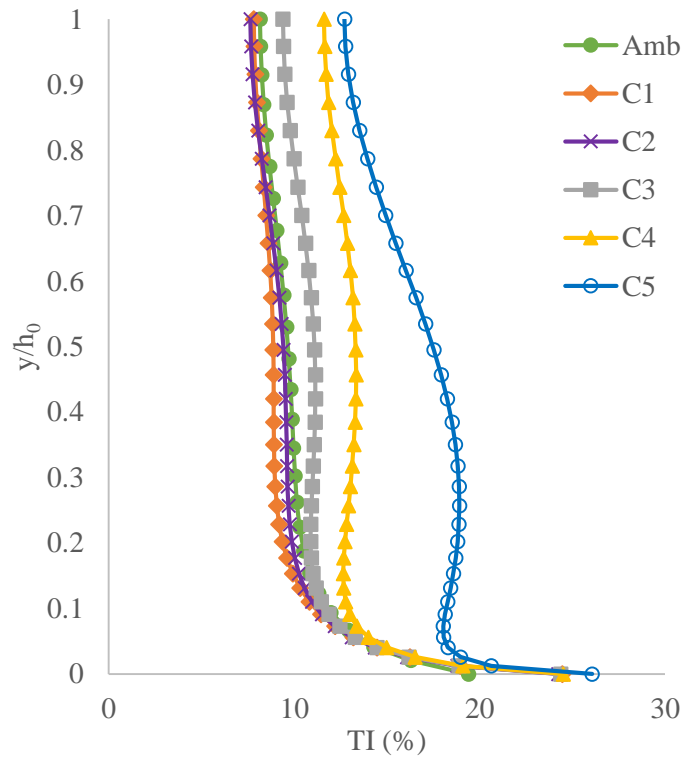
Figure 4.41: Comparison of Turbulence Intensity and vegetation density at z = 850 mm
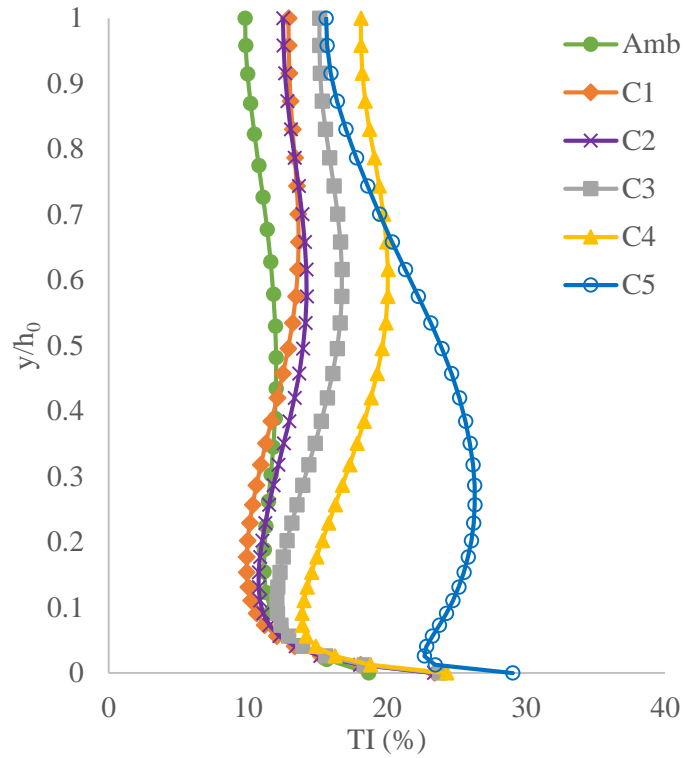
Figure 4.42: Comparison of Turbulence Intensity and vegetation density at z = 900 mm
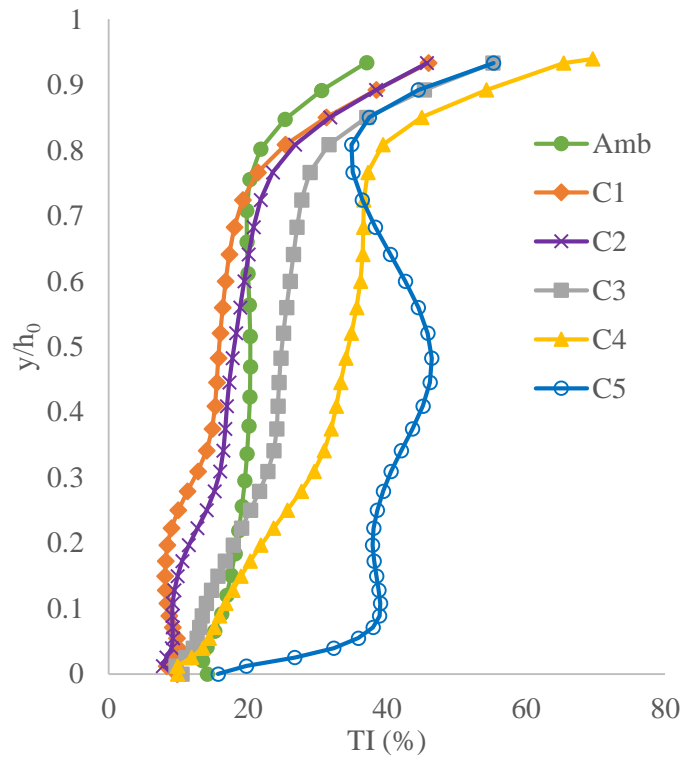
Figure 4.43: Comparison of Turbulence Intensity and vegetation density at z = 965 mm
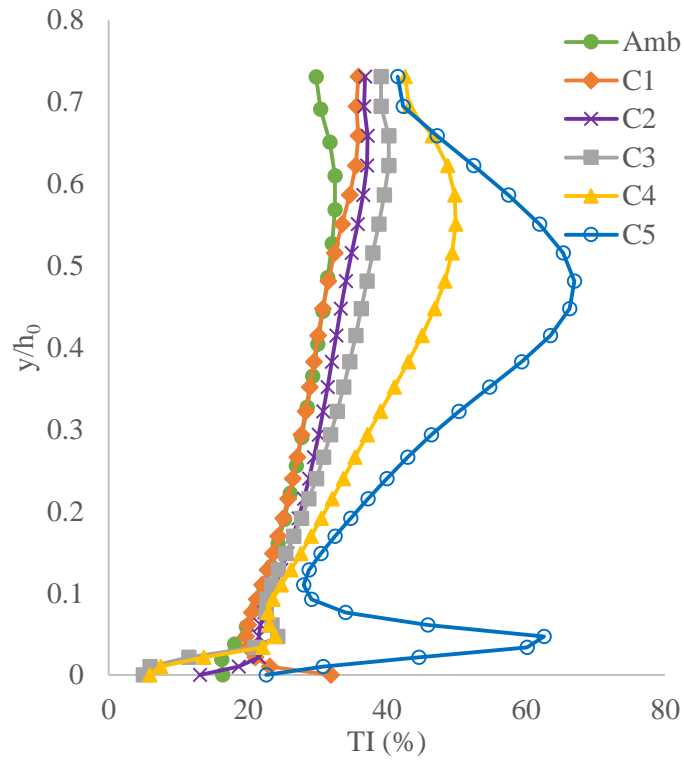
Figure 4.44: Comparison of Turbulence Intensity and vegetation density at z = 1045 mm
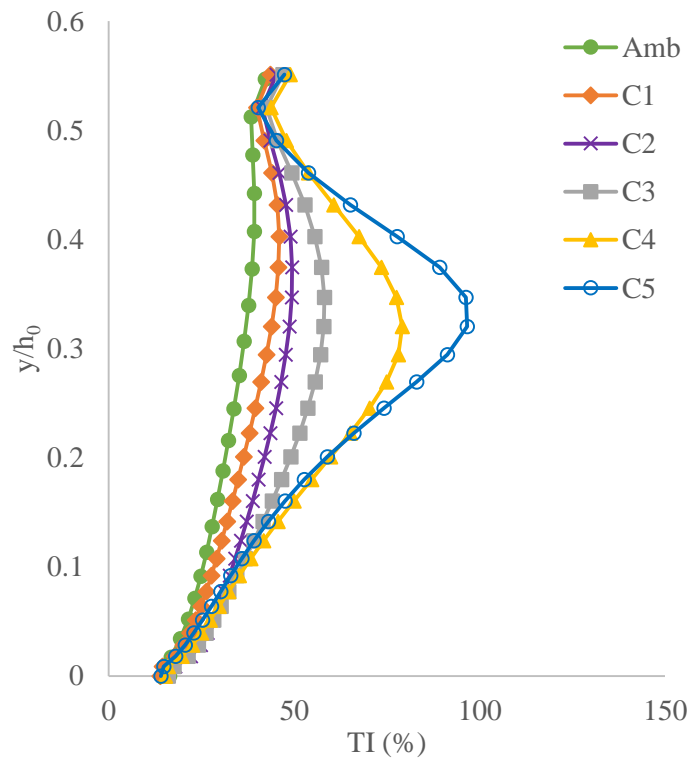

Figure 4.45: Comparison of Turbulence Intensity and vegetation density at z = 1125 mm
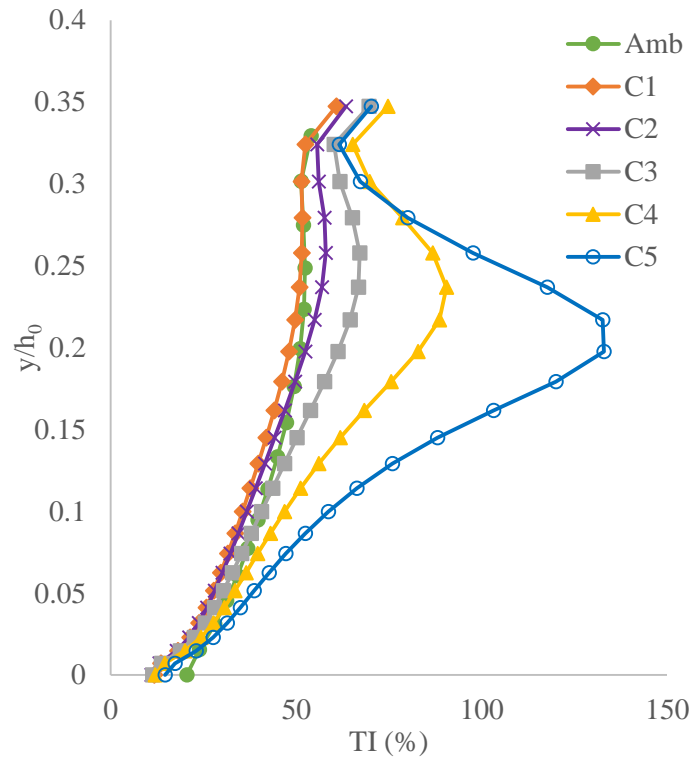
Figure 4.46: Comparison of Turbulence Intensity and vegetation density at z = 1205 mm

Depending on the distribution of velocity profiles (logarithmic, linear or random (S-shaped)) the vertical turbulence intensity profiles were following similar and matching profiles for all the configurations between the vertical bank and 600 mm away from it (z = 600 mm). This probably occurs since the main channel behaves more like a single channel as the distance from inclined bank increases. In these regions, the magnitude of turbulent intensity is varying between 5 and 25. As the sections move towards the inclined vegetated bank the profiles (Figure 4.41) show individual behavior while configuration 5 had the highest magnitude compared to the other turbulent intensity magnitudes. The vertical turbulence intensity profile for all locations at configuration 5 was greater in magnitude than all the other configurations. The streamwise vertical turbulence intensity profiles for the main channel remained almost uniform at all locations. These uniform profiles shift to S-shaped distribution in the vicinity and above

the inclined bank surface. In the main channel the maximum turbulence intensity were occurring at almost all the depths while the maximum occurs almost at the mid depth of flow in the vicinity and above the inclined bank surface. From Figures it can also be observed that the Turbulence intensity will increase while approaching from main channel to inclined bank. It also increases through increasing the vegetation density.

**4.2.4 Results and Discussions on Turbulent Kinetic Energy (TKE)**

Nepf (1999) cited in Hopkinson and Wynn (2009):412 mentioned that "the cross-sectional distribution of TKE represents the competition between the reduced velocity and increased turbulence generated by the addition of stream bank vegetation."

TKE is related to velocity in three directions in a typical 3-dimensional turbulent flow. So the vegetation on the riverbank would definitely affect the TKE on both the inclined bank area and on the main channel, because it obstructs momentum change, particularly in z-direction. Vegetation at riverbank increases the motion resistance, which is the reason why it could cause energy loss and associated velocity reduction at the vegetated zone. TKE would be expected as decreasing because of the higher roughness of the bank zone. However, this is not the case since vegetation on riverbank cannot be simply treated as increasing the bed roughness, because bed roughness is normally corresponding with boundary and the effects should start from boundaries. The magnitude of drag forces are also important at the flow direction, increasing the magnitude of u'. The magnitudes of v' and w' are much smaller than u', which means the streamwise velocity fluctuation play a leading role in TKE. The computational analyses were performed at 200, 400, 600, 750, 850, 900, 965, 1045, 1125, and 1205 mm away from the vertical bank of the channel. The following Figures are shown the values of k obtained from SST model simulation, Equation (3.10). Further, the values of k multiplied by water density will be gave the magnitude of TKE.
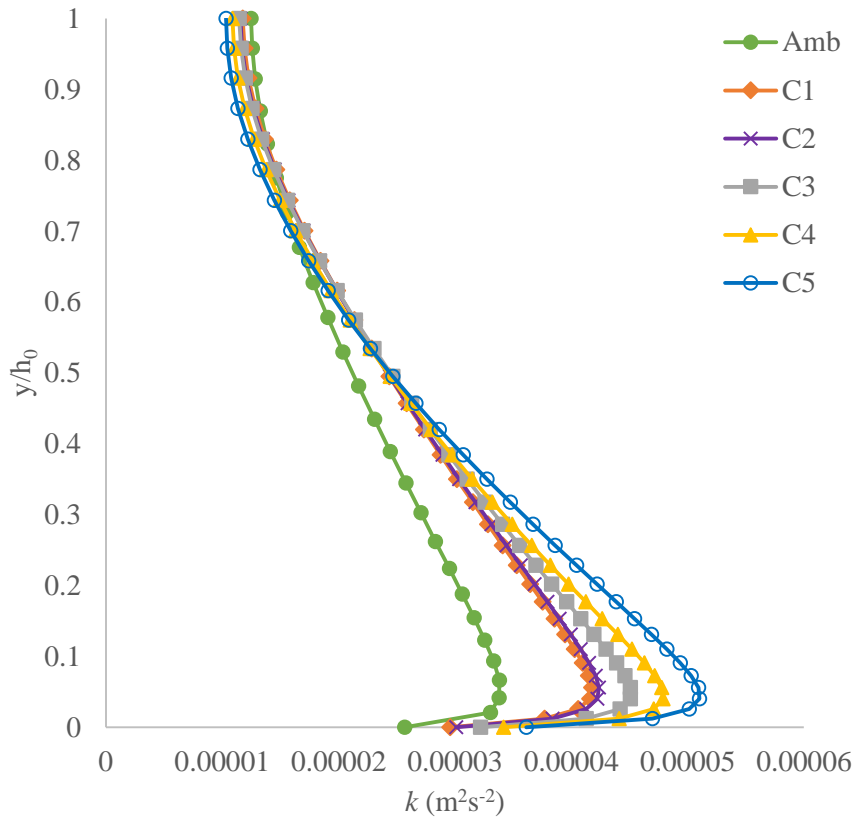
Figure 4.47: k values at z = 200 mm
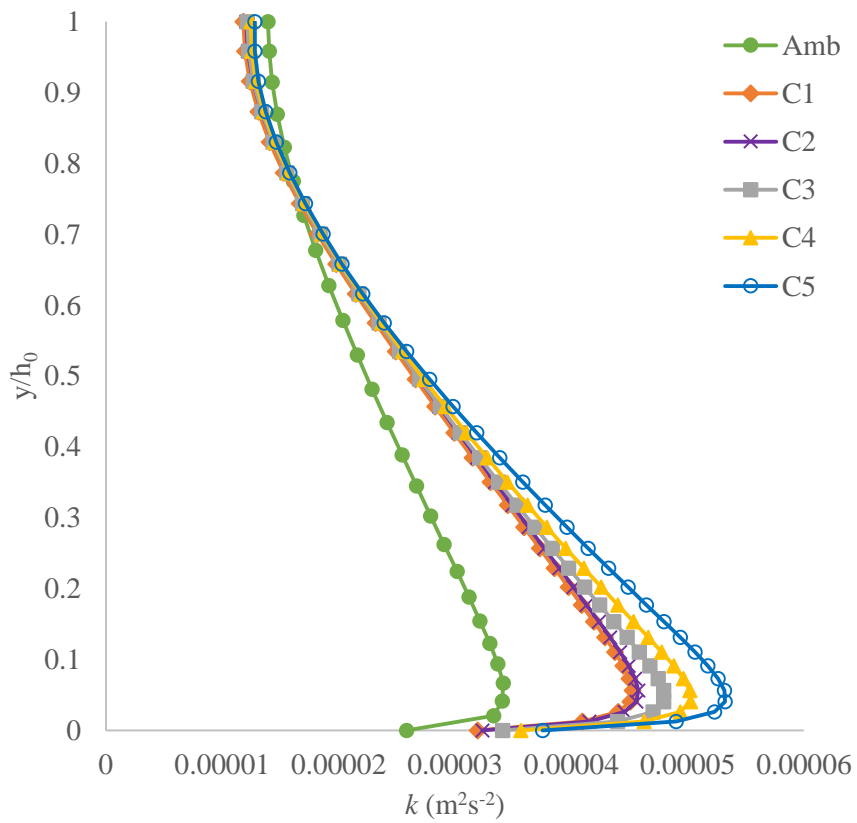
Figure 4.48: k values at z = 400 mm
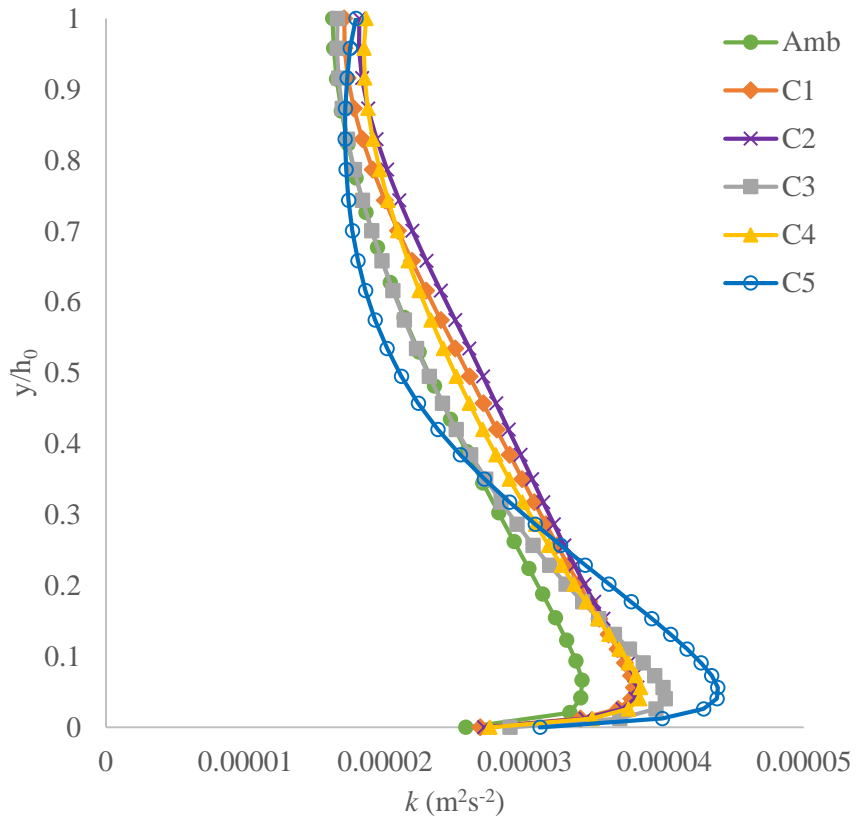
Figure 4.49: k values at z = 600 mm
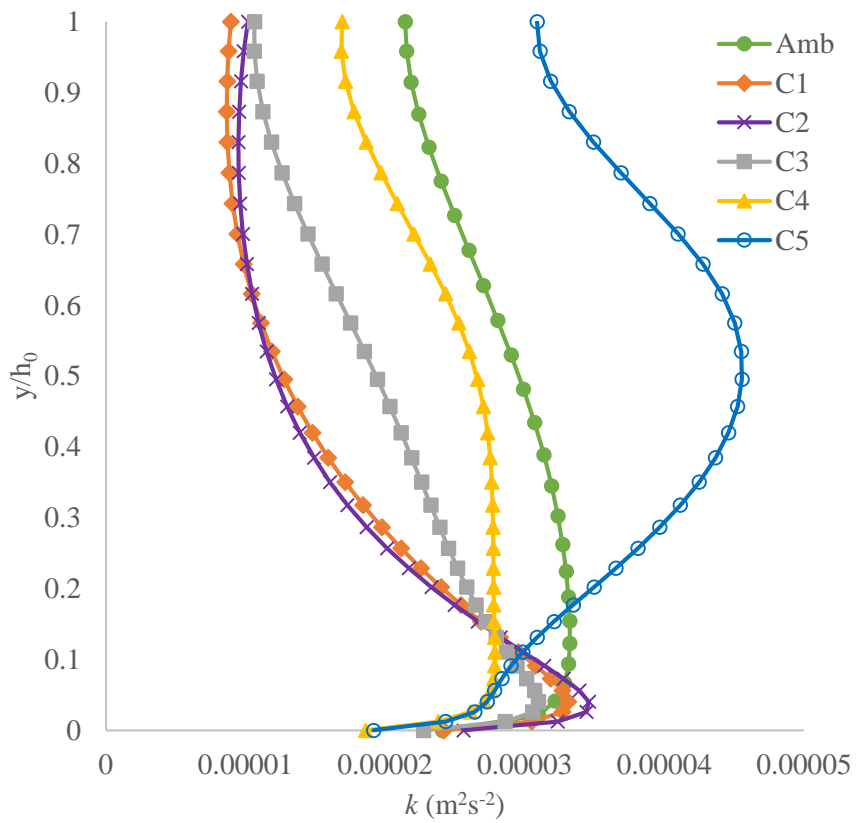
Figure 4.50: k values at z = 750 mm
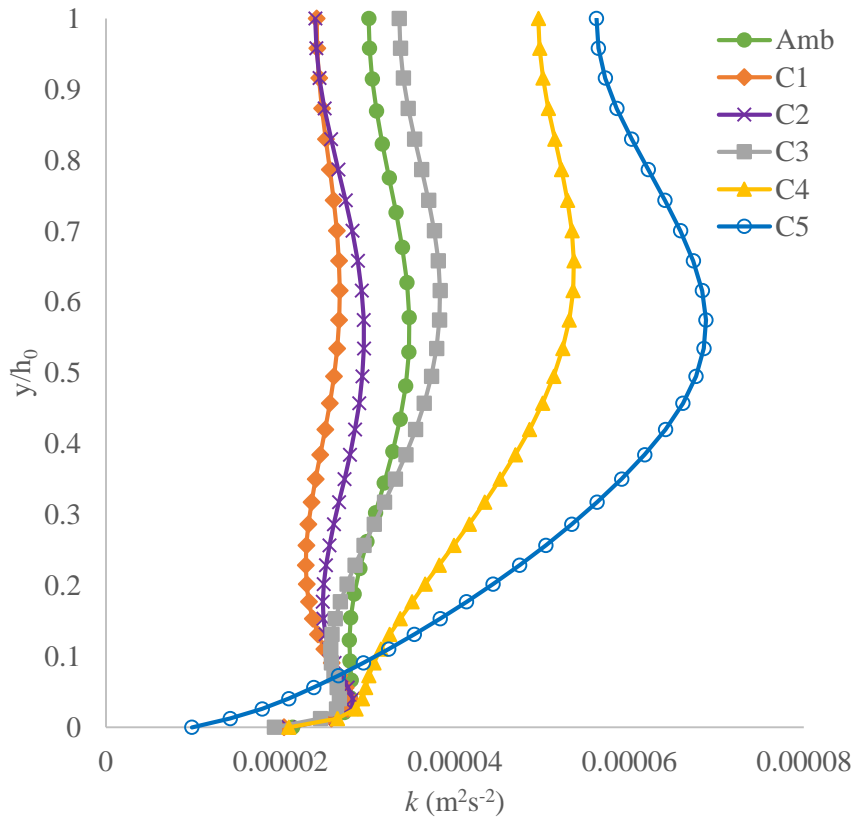
Figure 4.51: k values at z = 850 mm
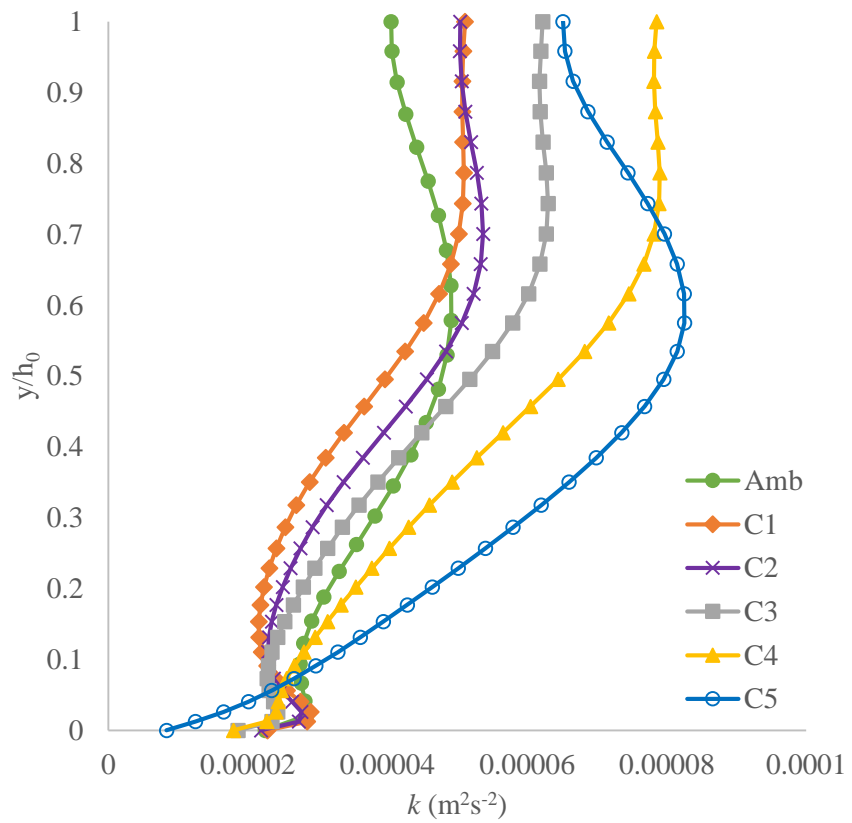
Figure 4.52: k values at z = 900 mm
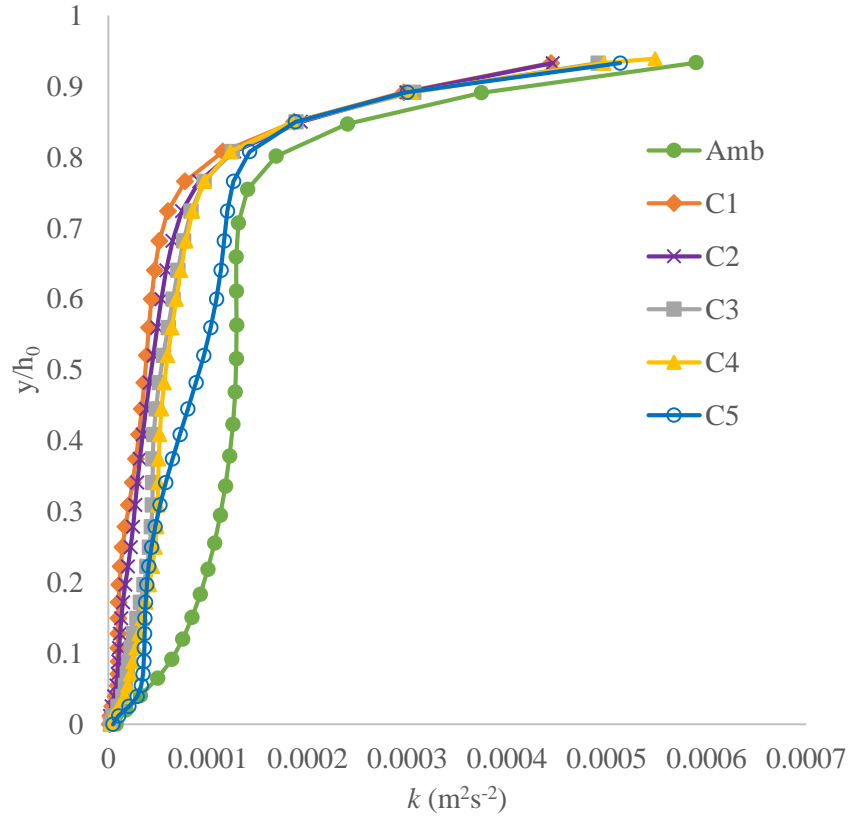
Figure 4.53: k values at z = 965 mm
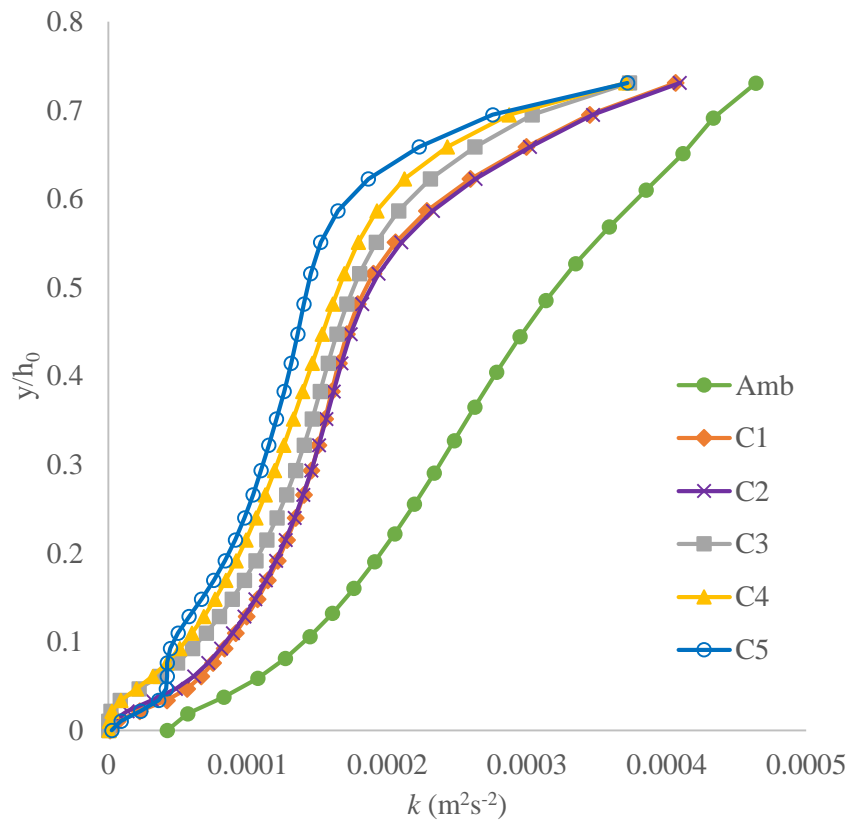

Figure 4.54: k values at z = 1045 mm
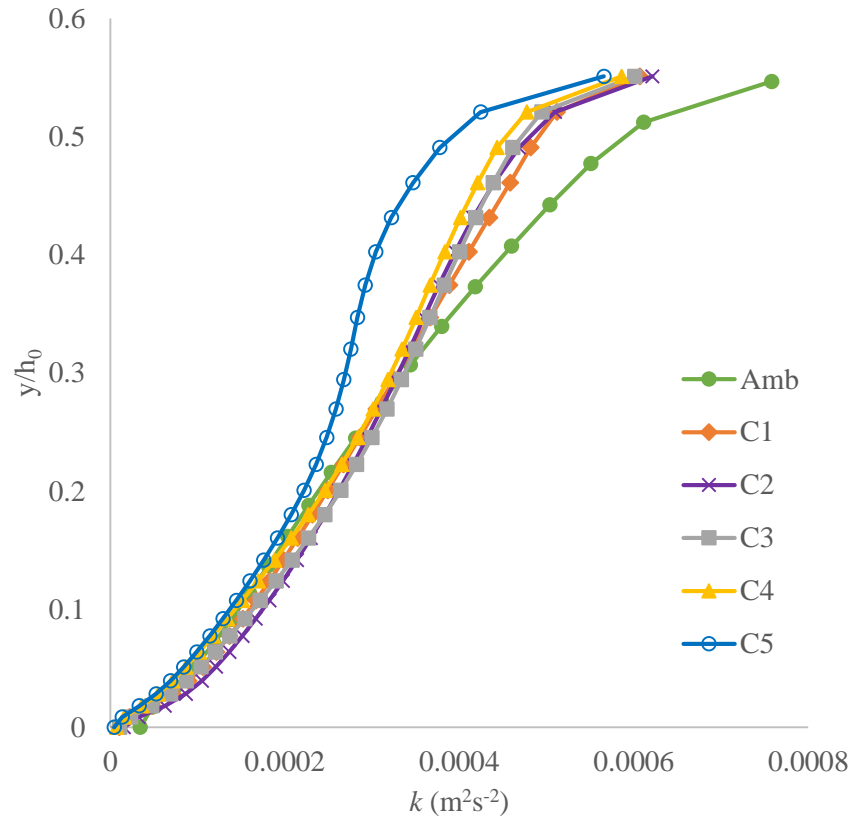
Figure 4.55: k values at z = 1125 mm
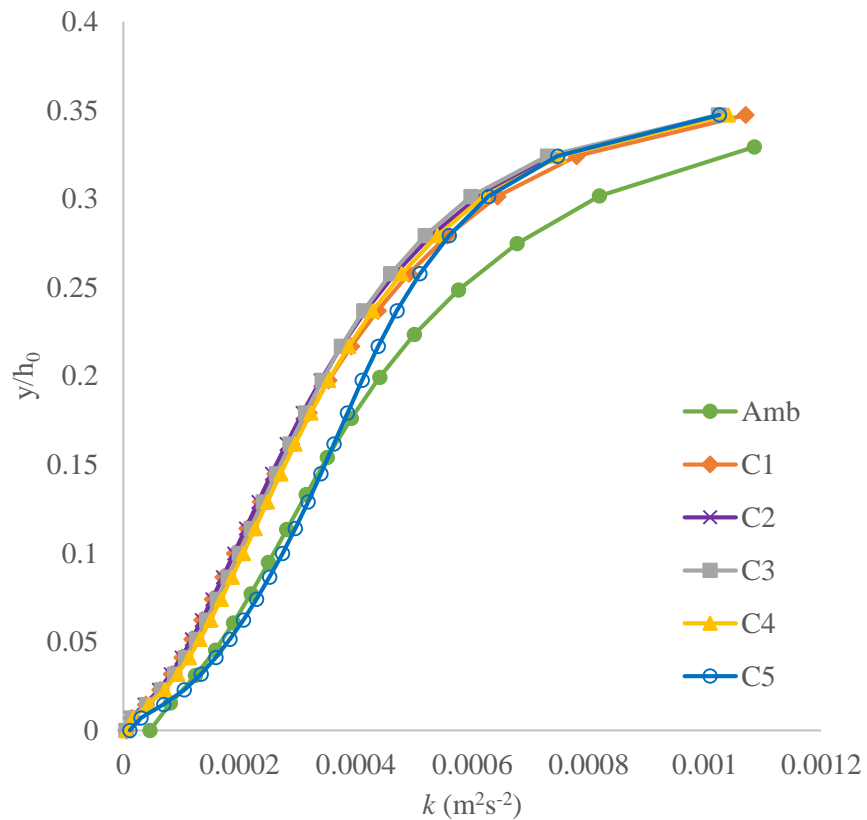
Figure 4.56: k values at z = 1205 mm

In the main channel, the value of k and/or TKE near the channel's bottom for configuration 5 is higher than others, while this phenomena is vice versa near the water surface. However, on the inclined bank the TKE for ambient flow has the highest value among them. It can be observed that there is a transition zone between main channel and bank slope, where the maximum value of TKE for different configuration will change. The vertical TKE profiles in the main channel are following similar trends as the Reynolds stress profiles. This is actually what is expected as mentioned before in Equation (2.16). The values of C_{TKE} of main channel at different levels are shown in Figure 4.57-4.62. It can be seen that an approximation of this parameter is around 0.3 for 200 to 600 mm away from vertical bank, however by approaching to inclined bank, C_{TKE} will be decreasing which is effected by the momentum exchange between main channel and inclined bank and the secondary current. Another outcome is that, while the vegetation density increasing the value of C_{TKE} in main channel will also increase at positions away from intersection of channel (Figure 4.57-4.59).
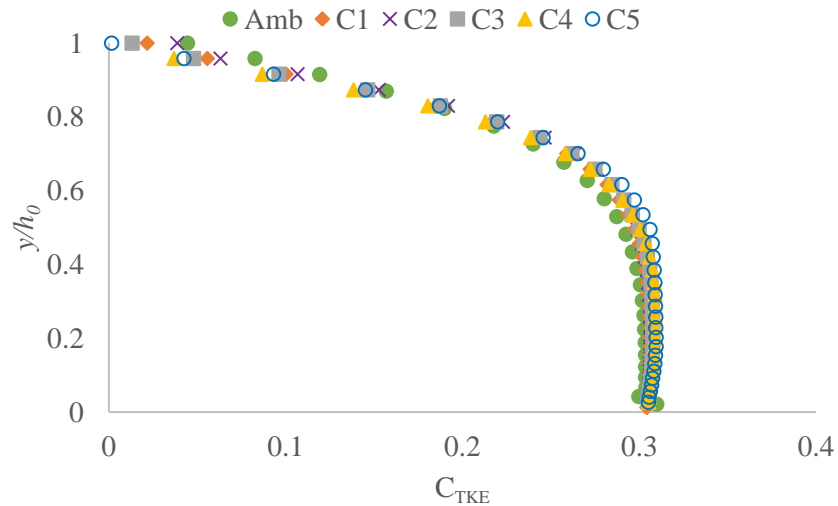

Figure 4.57: The magnitude of C_{TKE} at z = 200 mm
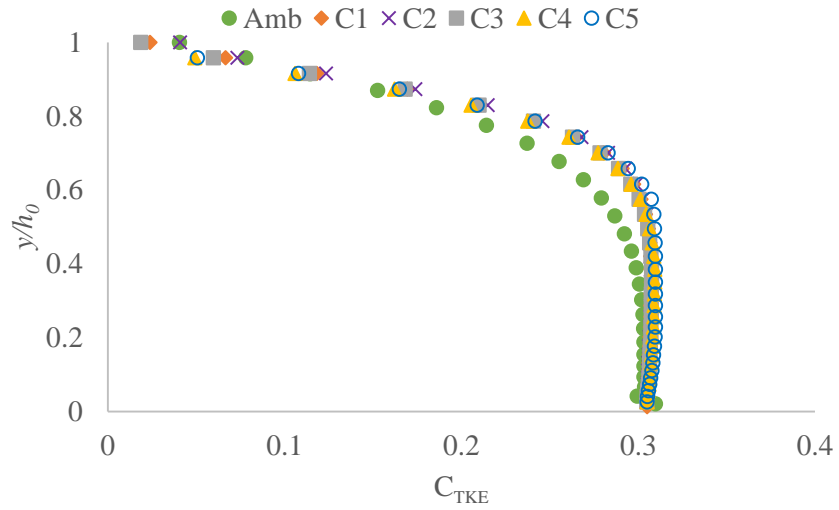
Figure 4.58: The magnitude of C_{TKE} at z = 400 mm
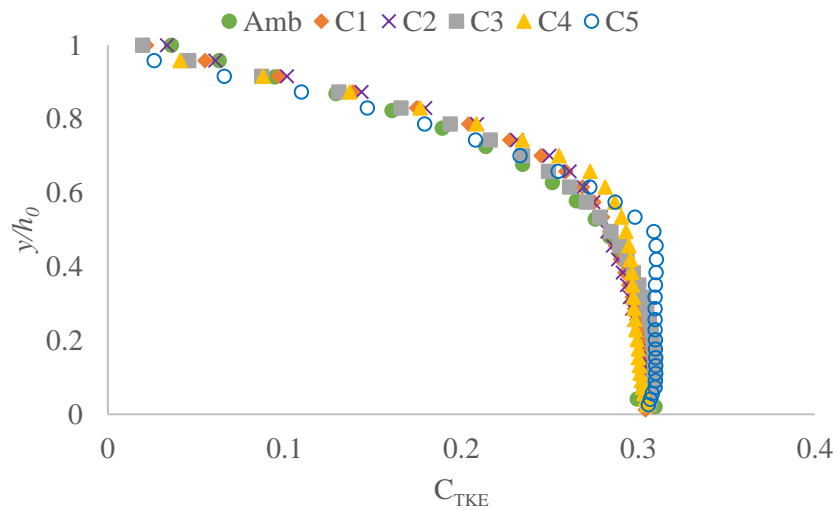
Figure 4.59: The magnitude of C_{TKE} at z = 600 mm
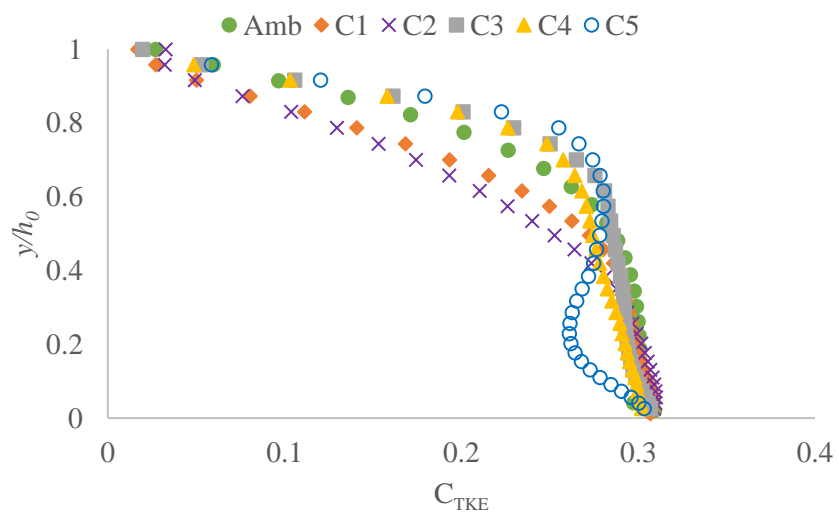
Figure 4.60: The magnitude of C_{TKE} at z = 750 mm
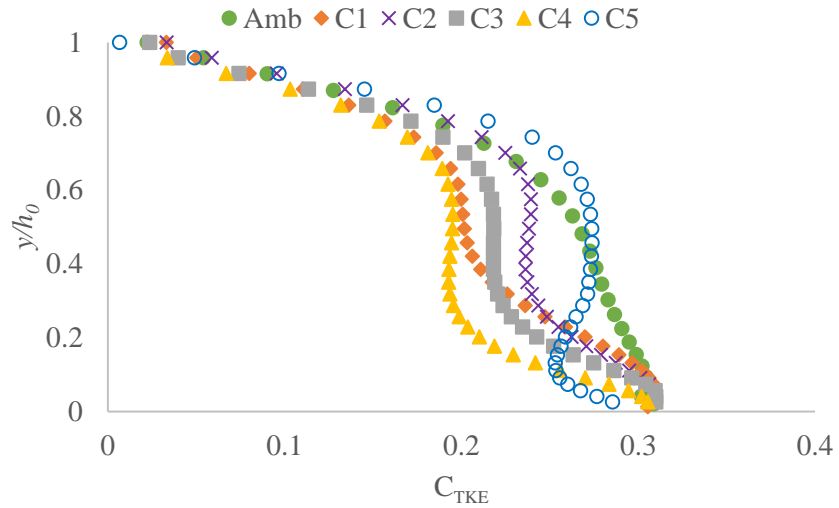
Figure 4.61: The magnitude of C_{TKE} at z = 850 mm
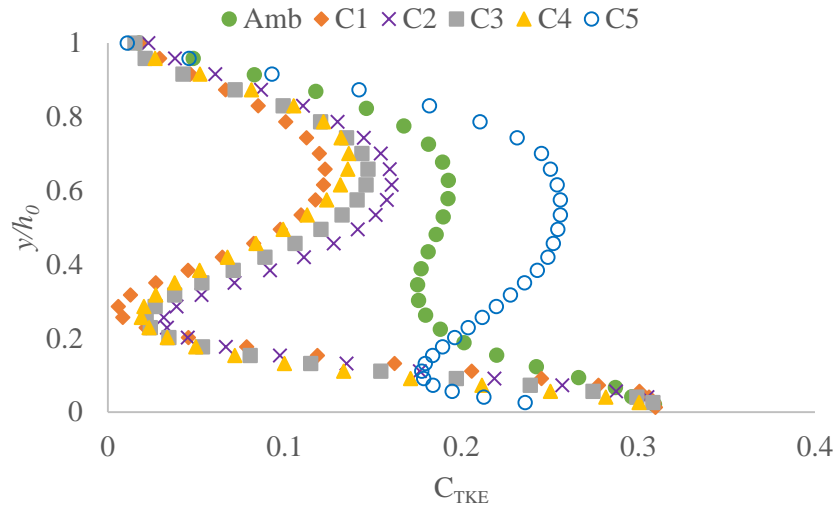
Figure 4.62: The magnitude of C_{TKE} at z = 900 mm

4.2.5 Analyzing the Secondary Current

Due to the increment in the density of vegetation cover on the inclined bank, an effective secondary current structure occurs in the channel. These secondary current structures are dramatically changing the behavior of the flow. The effect of these secondary currents is not dominantly affecting the flow at inclined bank. However, the effect is extremely complex and dominant at the vicinity of the interface of the main channel and the inclined bank. This secondary current therefore causes the distribution of streamwise and lateral velocity to be in complex form, as was described in previous

81

chapters. The vectors of secondary currents are given in Figure 4.63 in which arrows are showing the directions and the colors are defining the angle that arrows are having with flow direction.
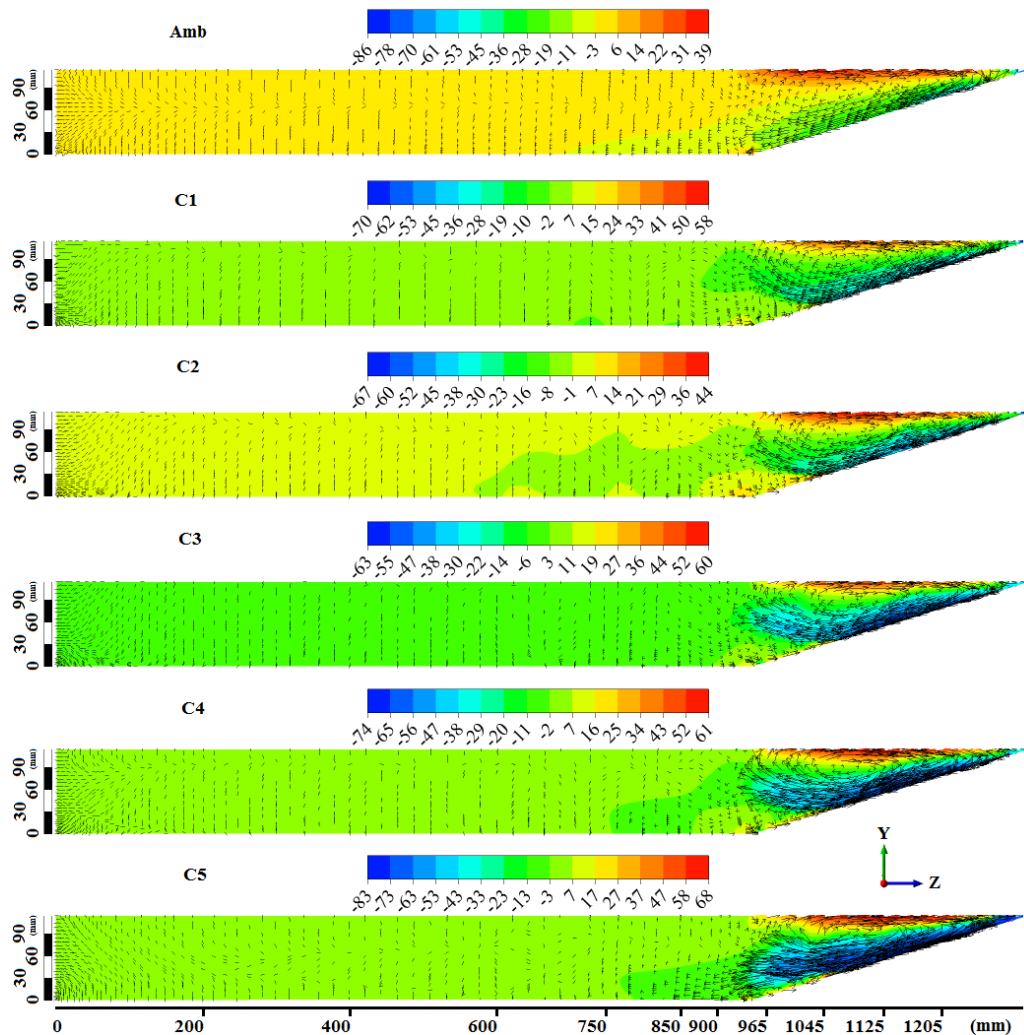
Figure 4.63: The vectors and angles (Degree) of secondary current

Observing the Figure 4.63, the secondary current angle will be increased with respect to increase of the vegetation density. Also, it shows that the linear configuration (C1, C3, C5) have more rate of change in secondary current angles, than staggered configurations (C2 and C4). However, this rate will decrease as the vegetation density increases.

Chapter 5

CONCLUSION

5.1 Conclusions

Computational hydrodynamic study was conducted by analyzing the turbulent flow structure, velocity profiles and the Reynolds shear stresses on an open channel in which one of the bank is vertical while the other was inclined and covered with rigid vegetation. The following statements summarize the major research findings while concluding the principal results of the computational analyses:

The RANS Simulation model is used in this study and the model provided reasonably good results for the streamwise velocity profiles, turbulence intensities, turbulent kinetic energy magnitudes and Reynolds shear stresses.

The vegetation coverage over the inclined riverbank increased the streamwise velocity in the main channel compared with the inclined bank surface. Velocity in the downstream direction decreased in the vicinity of riverbank/main channel interface and over the bank in all the configurations, however reduction in velocity did not result in a reduction in overall shear stress at the same region.

The increase of velocity in the main channel occurs nearly at the center of the main channel and the maximum velocity shifts towards the vertical river bank as long as the

density of the rigid vegetation increased (experiencing observations from configuration 1 to configuration 5)

Two maximum velocities are captured, one at the main channel and the other at the inclined bank which is the indication of the interface of flow between the main channel and the inclined bank.

Obviously the rigid vegetation elements over the inclined bank impacted the flow near the stream bank when compared with the ambient conditions. Surprisingly, the rigid elements generated velocity and shear stress distribution almost similar to the stream bank supporting the previous findings of the Valyrakis et al. (2015).

The Reynolds stresses was significantly effective on inclined bank, especially at ambient flow conditions, showing that the turbulence was generated even before the existence of rigid vegetation.

The turbulence intensity profiles within the rigid vegetation were high and reduced towards the main channel. In the main channel, the uniform turbulence intensity distribution within the depth of flow was experienced thus maximum turbulence intensity were occurring at almost all the depths of flow. On the other hand, the maximum turbulence intensity was occurring almost at the mid-depth of flow in the vicinity and above the inclined bank surface.

The momentum transfer along the interaction region between inclined bank and main channel was even available at ambient conditions due to the secondary currents. However, the momentum transfer increased as increasing the density of vegetation and

reaches to its maximum levels at configuration 5.

5.2 Recommendations for future studies

This study was conducted to improve the understanding of the rigid vegetation in the hydrodynamics of open channel flows by evaluating the effects of rigid vegetation on flow properties like velocity profiles, Reynolds shear stresses, turbulent intensities and the TKE. These analysis and results can be further treated in order to raise comments on the morphological changes that can occur due to the sediment transport and thus propose stream restoration plans especially for flood control analysis. On the other hand, already available model can be altered to obtain the effects of changes on the proposed model. These changes can be variable discharge, variable bank slopes and flexible vegetation above the inclined bank. Similar study can also simulate the super-critical flow conditions. By using the St. Venant equations in the simulations, unsteady flow conditions and variable bed morphology can be added to the future studies.

REFERENCES

Ackerman, J., & Okubo, A. (1993). Reduced mixing in a marine macrophyte canopy. *Functional Ecology*, 305-309.

Afzalimehr, H., Moghbel, R., Gallichand, J., & Jueyi, S. (2011). Investigation of turbulence characteristics in channel with dense vegetation. *International Journal of Sediment Research, 26*(3), 269-282.

Afzalimehr, H., & Subhasish, D. (2009). Influence of bank vegetation and gravel bed on velocity and Reynolds stress distributions. *International Journal of Sediment Research, 24*(2), 236-246.

Ansys, I. (2009). CFD 12.1 User Manual, Ansys: Inc.

Bathurst, J. C., Hey, R. D., & Thorne, C. R. (1979). Secondary flow and shear stress at river bends. *Journal of the Hydraulics Division, 105*(10), 1277-1295.

Bonakdari, H., Larrarte, F., Lassabatere, L., & Joannis, C. (2008). Turbulent velocity profile in fully-developed open channel flows. *Environmental Fluid Mechanics, 8*(1), 1-17.

Bradshaw, P., Cebeci, T., & Whitelaw, J. H. (1981). Engineering calculation methods for turbulent flow. *NASA STI/Recon Technical Report A, 82*, 20300.

Cameron, S., Nikora, V., Albayrak, I., Miler, O., Stewart, M., & Siniscalchi, F. (2013).

Interactions between aquatic plants and turbulent flow: a field study using stereoscopic PIV. *Journal of Fluid Mechanics, 732*, 345-372.

Cardoso, A., Graf, W. H., & Gust, G. (1989). Uniform flow in a smooth open channel. *Journal of Hydraulic Research, 27*(5), 603-616.

Carollo, F., Ferro, V., & Termini, D. (2002). Flow velocity measurements in vegetated channels. *Journal of Hydraulic Engineering, 128*(7), 664-673.

CFX, A. (2009). 12.1 Documentation Release 12.1 by ANSYS. *Inc., USA in November*.

Chao, W., Zheng, S.-s., Wang, P.-f., & Jun, H. (2015). Interactions between vegetation, water flow and sediment transport: A review. *Journal of Hydrodynamics, Ser. B, 27*(1), 24-37.

Choi, S.-U., & Kang, H. (2004). Reynolds stress modeling of vegetated open-channel flows. *Journal of Hydraulic Research, 42*(1), 3-11.

Cimbala, J. M., & Çengel, Y. A. (2008). *Essentials of fluid mechanics: fundamentals and applications*: McGraw-Hill Higher Education.

Coles, D. (1956). The law of the wake in the turbulent boundary layer. *Journal of Fluid Mechanics, 1*(02), 191-226.

Galperin, B., Kantha, L., Hassid, S., & Rosati, A. (1988). A quasi-equilibrium

turbulent energy model for geophysical flows. *Journal of the Atmospheric Sciences, 45*(1), 55-62.

Gambi, M. C., Nowell, A. R., & Jumars, P. (1990). Flume observations on flow dynamics in Zostera marina(eelgrass) beds. *Marine ecology progress series. Oldendorf, 61*(1), 159-169.

Hirschowitz, P., & James, C. (2009). Conveyance estimation in channels with emergent bank vegetation. *Water SA, 35*(5).

Hopkinson, L., & Wynn, T. (2009). Vegetation impacts on near bank flow. *Ecohydrology, 2*(4), 404-418.

Hu, X.-Y., Liu, B., Zeng, G.-M., Cheng, Y.-Z., & Li, D. (2008). Experimental study on effects of vegetation roughness on flow resistance of open channel. *Shuikexue Jinzhan/Advances in Water Science, 19*(3), 372-377.

Huai, W., Zeng, Y., Xu, Z., & Yang, Z. (2009). Three-layer model for vertical velocity distribution in open channel flow with submerged rigid vegetation. *Advances in Water Resources, 32*(4), 487-492.

Huang, P., Bardina, J., & Coakley, T. (1997). Turbulence Modeling Validation, Testing, and Development. *NASA Technical Memorandum, 110446*.

Jiménez, J. (2004). Turbulent flow over rough walls. *Annu. Rev. Fluid Mech.*, 173–196. doi: 10.1146/annurev.fluid.36.050802.122103

Klopstra, D., Barneveld, H., Van Noortwijk, J., & Van Velzen, E. (1996). *Analytical model for hydraulic roughness of submerged vegetation.* Paper presented at the Proceedings of the congress-international association for hydraulic research.

Liu, D., Diplas, P., Fairbanks, J., & Hodges, C. (2008). An experimental study of flow through rigid vegetation. *Journal of Geophysical Research: Earth Surface (2003–2012), 113*(F4).

Masouminia, M., Türker, U., & Fasihi, S. (2014). *Flow characteristics in 180 degree divergent bend.* Paper presented at the ACE 2014 -11th International Congress on Advances in Civil Engineering, Istanbul, Turkey.

Menter, F. R. (1994). Two-equation eddy-viscosity turbulence models for engineering applications. *AIAA journal, 32*(8), 1598-1605.

Neary, V. (2003). Numerical solution of fully developed flow with vegetative resistance. *Journal of engineering mechanics, 129*(5), 558-563.

Nepf, H. (1999). Drag, turbulence, and diffusion in flow through emergent vegetation. *Water Resources Research, 35*(2), 479-489.

Nezu, I., & Rodi, W. (1986). Open-channel flow measurements with a laser Doppler anemometer. *Journal of Hydraulic Engineering, 112*(5), 335-355.

Nikuradse, J. (1950). Laws of flow in rough pipes, Translation in National Advisory Committee for aeronautics: Technical Memorandum 1292. NACA, Washington,

p 62.

Perkins, H. (1970). The formation of streamwise vorticity in turbulent flow. *Journal of Fluid Mechanics, 44*(04), 721-740.

Petryk, S., & Bosmajian, G. (1975). Analysis of flow through vegetation. *Journal of the Hydraulics Division, 101*(7), 871-884.

Plew, D. R. (2010). Depth-averaged drag coefficient for modeling flow through suspended canopies. *Journal of Hydraulic Engineering, 137*(2), 234-247.

Prandtl, L. (1952). *Essentials of fluid dynamics: With applications to hydraulics aeronautics, meteorology, and other subjects*: Hafner Pub. Co.

Pujol, D., Colomer, J., Serra, T., & Casamitjana, X. (2010). Effect of submerged aquatic vegetation on turbulence induced by an oscillating grid. *Continental Shelf Research, 30*(9), 1019-1029. doi: 10.1016/j.csr.2010.02.014

Righetti, M. (2008). Flow analysis in a channel with flexible vegetation using double-averaging method. *Acta Geophysica, 56*(3), 801-823.

Sand-Jensen, K., & Pedersen, O. (1999). Velocity gradients and turbulence around macrophyte stands in streams. *Freshwater Biology, 42*(2), 315-328.

Shiono, K., & Knight, D. W. (1991). Turbulent open-channel flows with variable depth across the channel. *Journal of Fluid Mechanics, 222*, 617-646.

Simon, A., Bennett, S. J., & Neary, V. S. (2004). Riparian vegetation and fluvial geomorphology: problems and opportunities. *Riparian vegetation and fluvial geomorphology*, 1-10.

Soulsby, R., & Dyer, K. (1981). The form of the near-bed velocity profile in a tidally accelerating flow. *Journal of Geophysical Research: Oceans (1978–2012), 86*(C9), 8067-8074.

Stapleton, K., & Huntley, D. (1995). Seabed stress determinations using the inertial dissipation method and the turbulent kinetic energy method. *Earth Surface Processes and Landforms, 20*(9), 807-815.

Steffler, P. M., Rajaratnam, N., & Peterson, A. W. (1985). LDA measurements in open channel. *Journal of Hydraulic Engineering, 111*(1), 119-130.

Stone, B. M., & Shen, H. T. (2002). Hydraulic resistance of flow in channels with cylindrical roughness. *Journal of Hydraulic Engineering, 128*(5), 500-506.

Struve, J., Falconer, R., & Wu, Y. (2003). Influence of model mangrove trees on the hydrodynamics in a flume. *Estuarine, Coastal and Shelf Science, 58*(1), 163-171.

Thom, A. (1971). Momentum absorption by vegetation. *Quarterly Journal of the Royal Meteorological Society, 97*(414), 414-428.

Townsend, A. (1976). The structure of turbulent flow: Cambridge Univ. Press, New York.

Türker, U., Yagci, O., & Kabdaşlı, M. (2006). Analysis of coastal damage of a beach profile under the protection of emergent vegetation. *Ocean Engineering, 33*(5), 810-828.

Valyrakis, M., Liu, D., Mcgann, N. J., Turker, U., & Yagci, O. (2015). *Characterising the effect of increasing riverbank vegetation on the flow field across the channel*. Paper presented at the 36th IAHR World Congress, Netherlands.

Wilcox, D. C. (1988). Multiscale model for turbulent flows. *AIAA journal, 26*(11), 1311-1320.

Wilson, C. (2007). Flow resistance models for flexible submerged vegetation. *Journal of Hydrology, 342*(3), 213-222.

Wu, F.-C., Shen, H. W., & Chou, Y.-J. (1999). Variation of roughness coefficients for unsubmerged and submerged vegetation. *Journal of Hydraulic Engineering*.

APPENDIX

Appendix A: Velocity contours at cross-section placed 12 cm before last vegetation
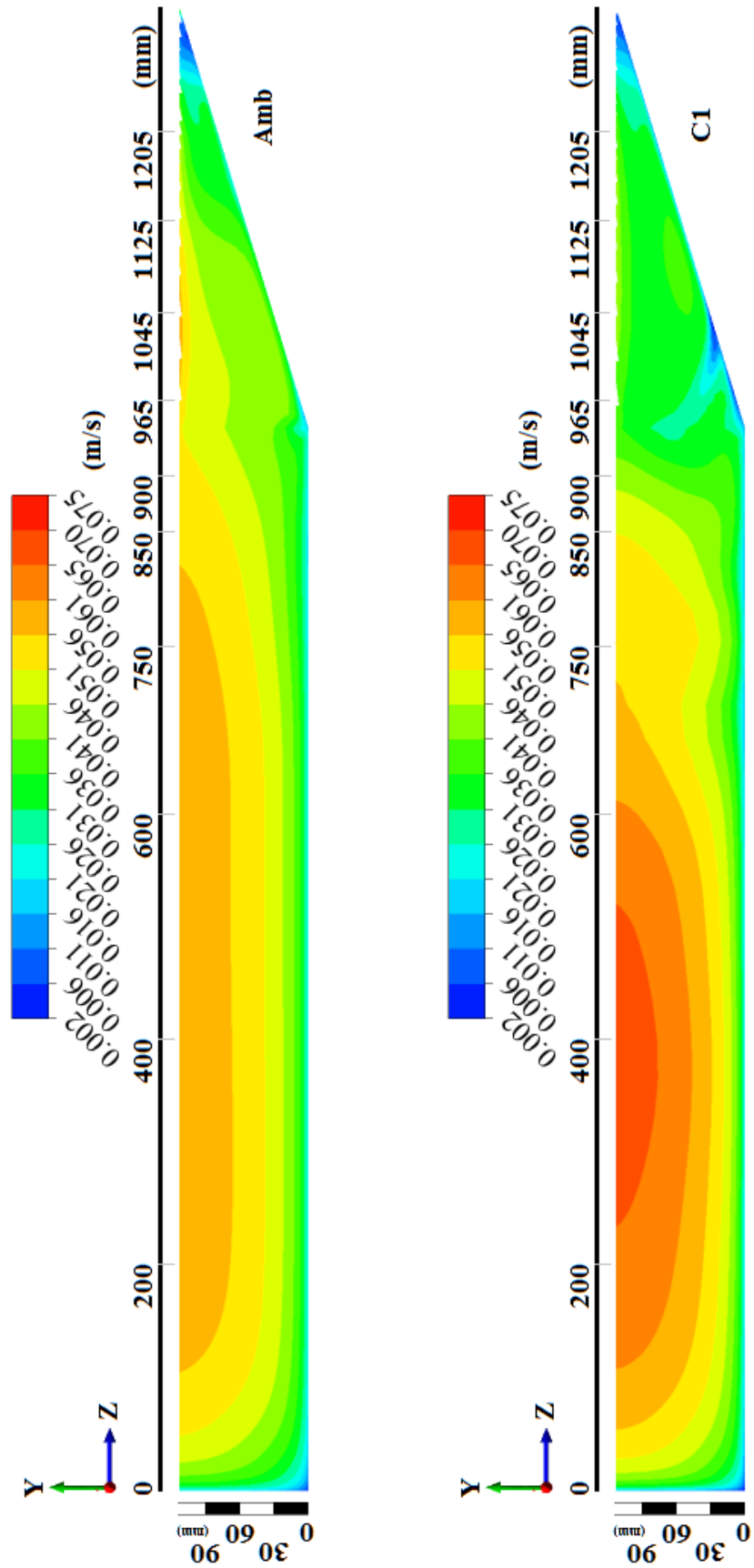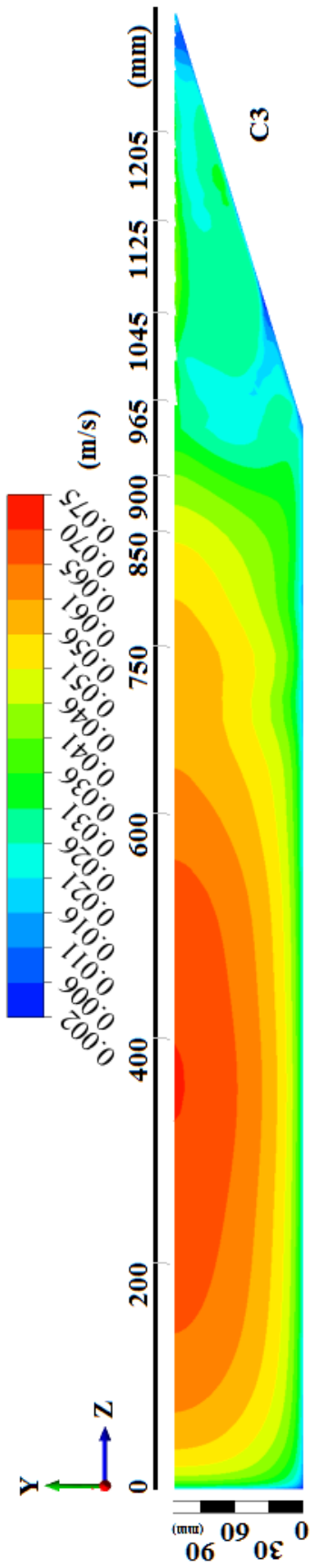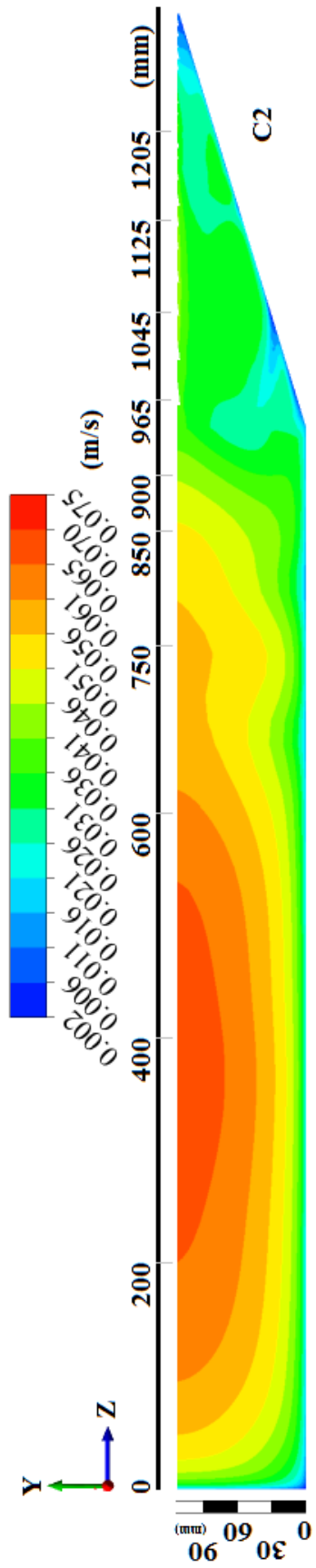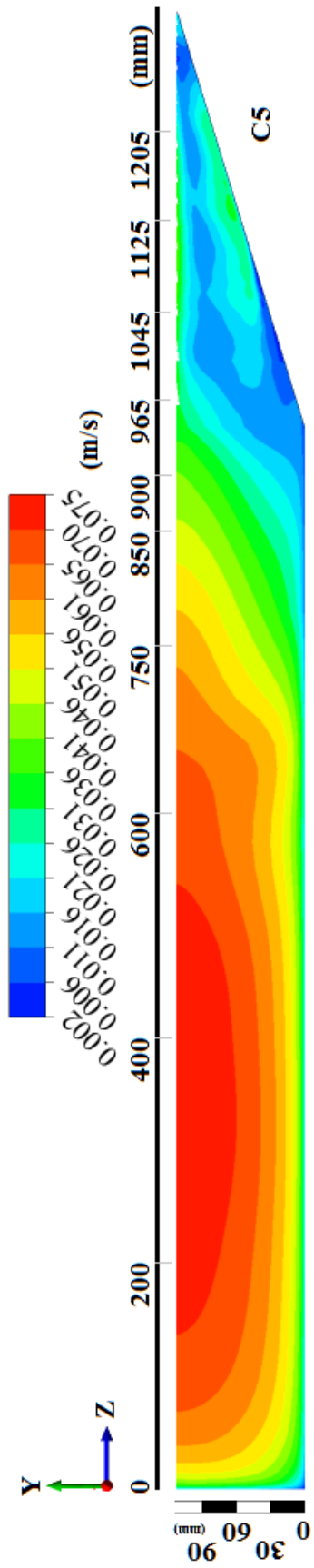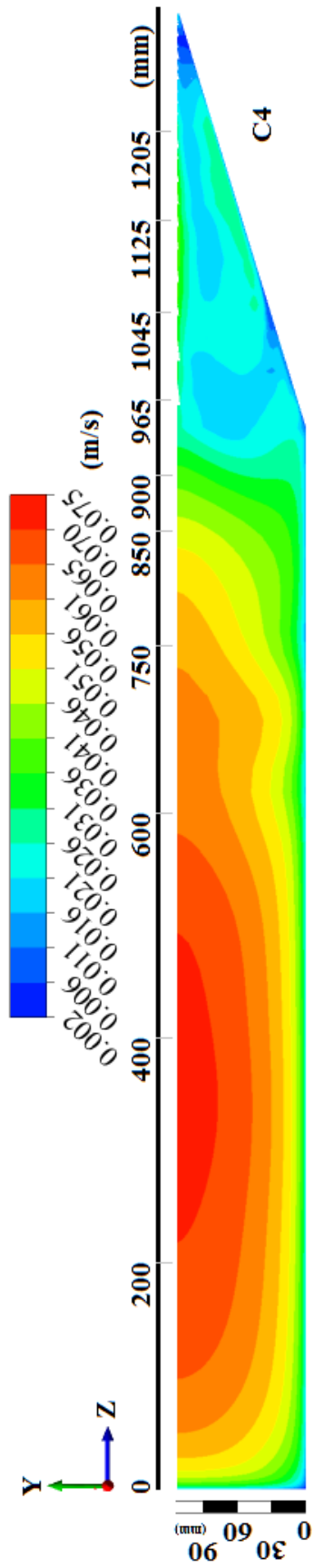
Appendix B: Magnitude of Reynolds shear stress at cross-section placed 12 cm before end of vegetation

C4

C5

(Pa)

(Pa)
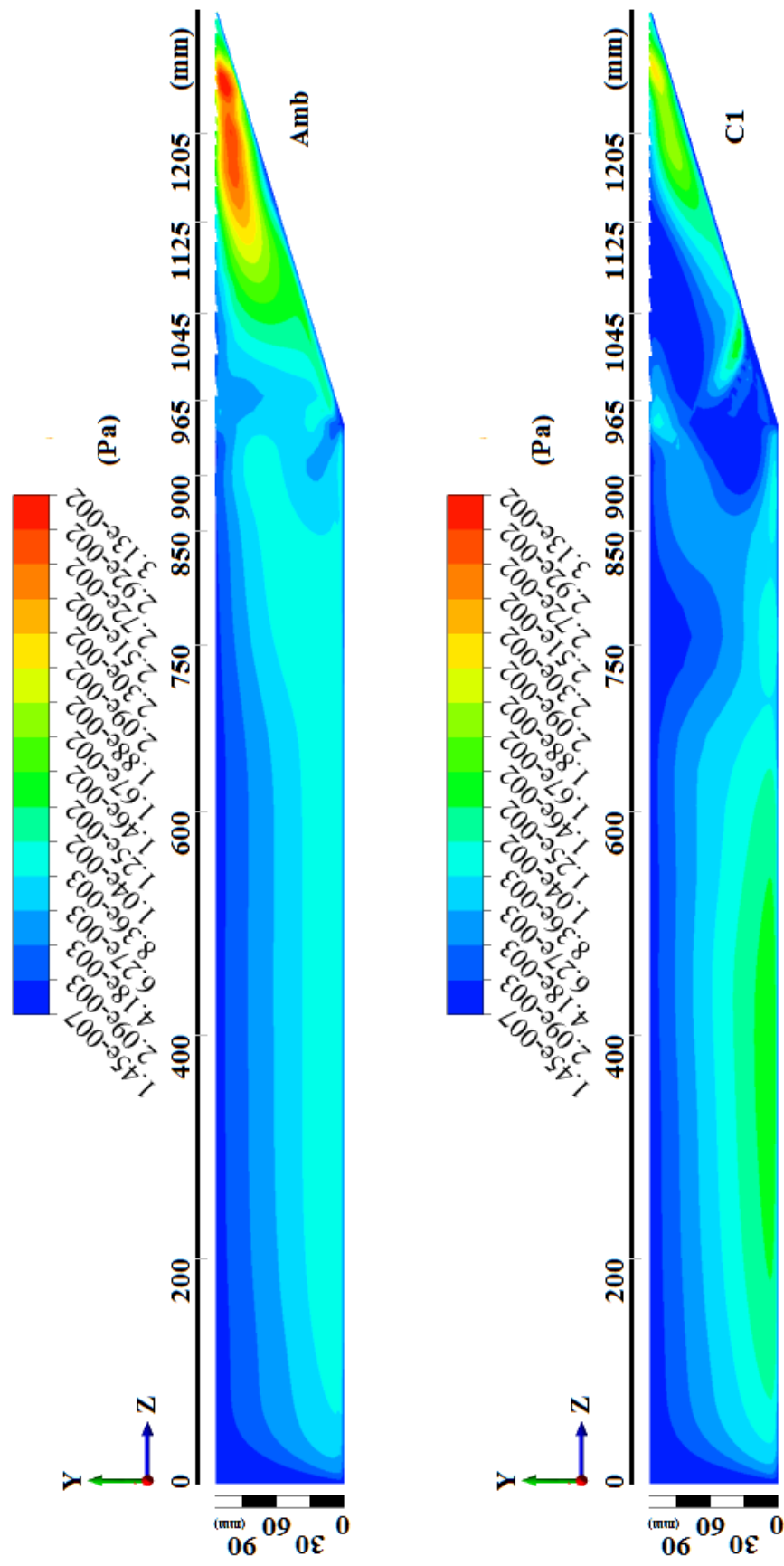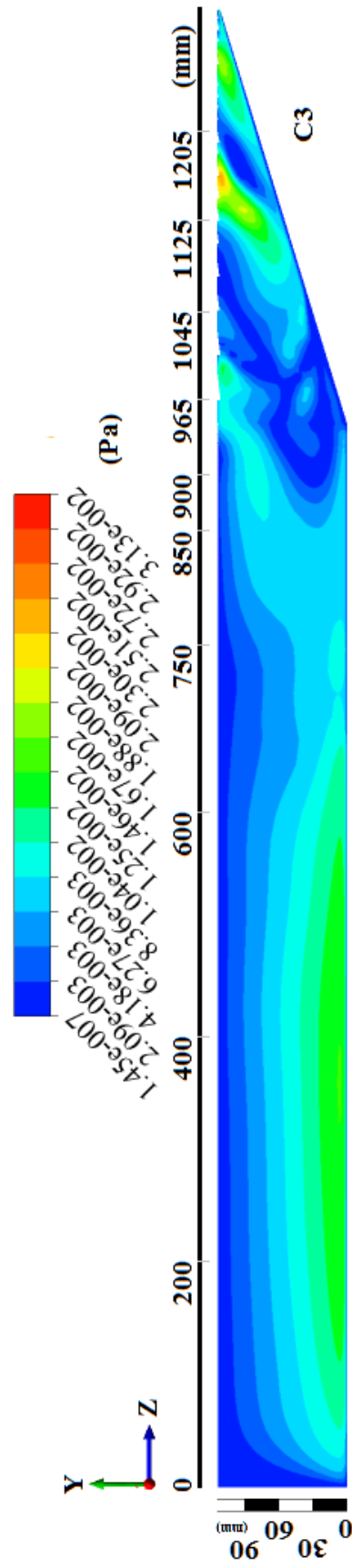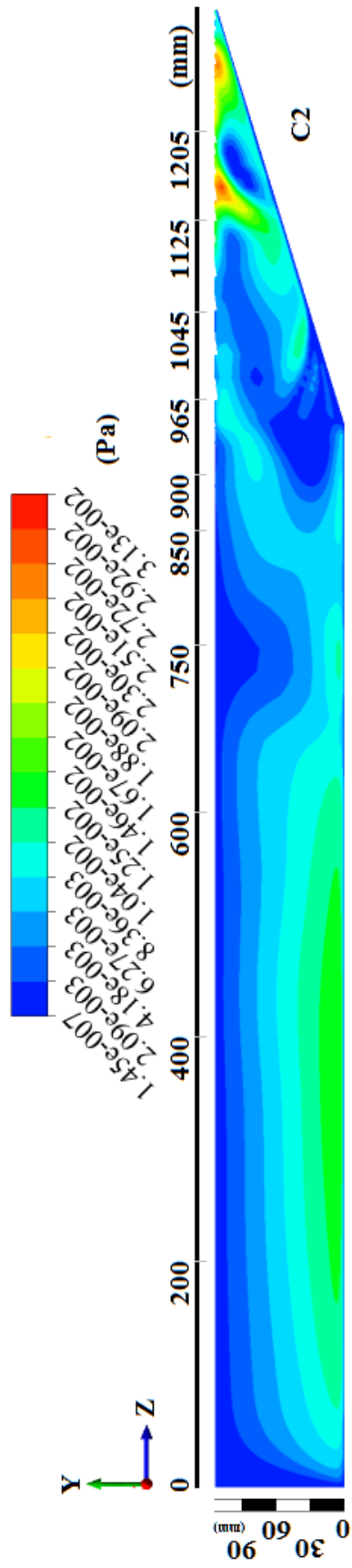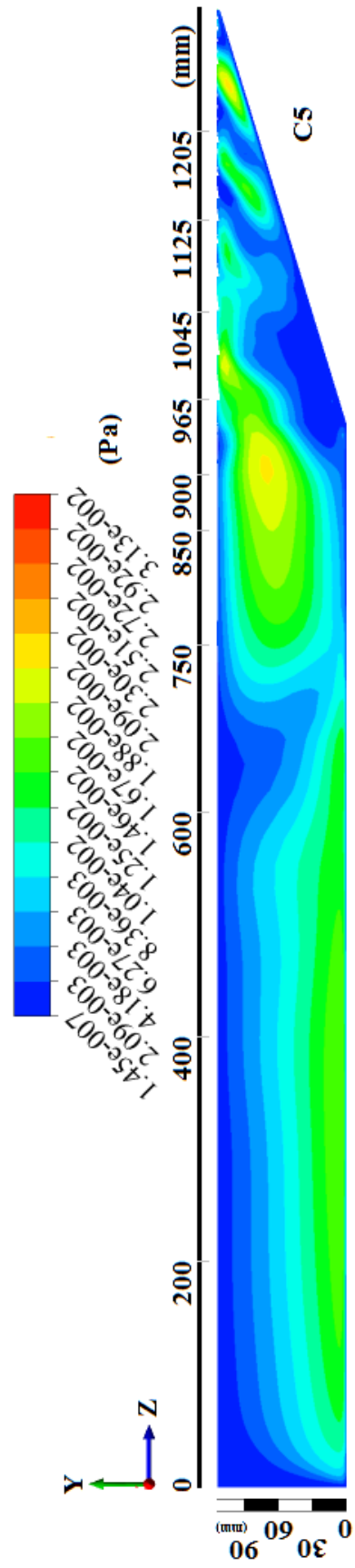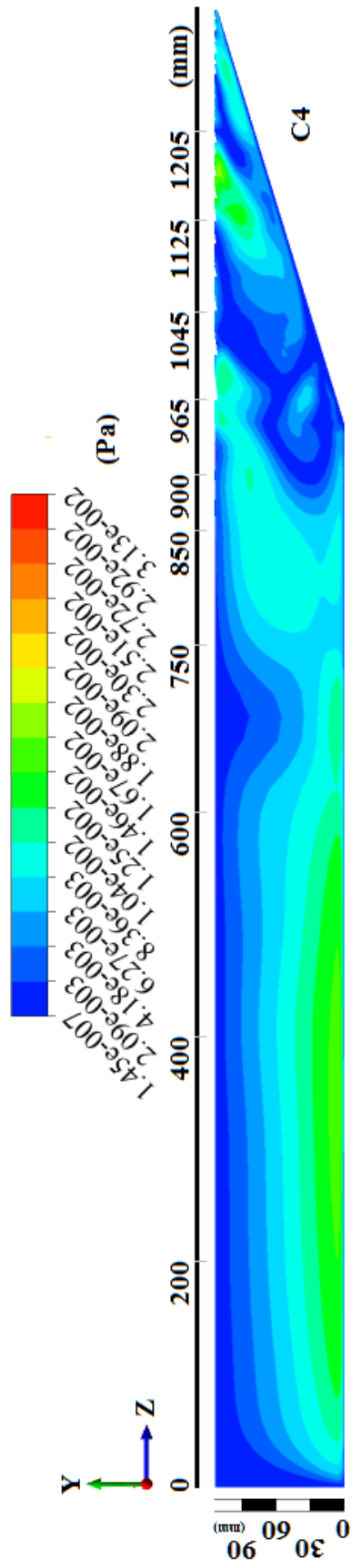
Appendix C: The vectors and angles (Degree) of secondary current